# Petrography, Geochemistry, and Stratigraphy of the Paleocene-Eocene Carbonate and Evaporite Deposits in the South of Iraq

---

A Thesis

Presented to

the Faculty of the Department of Earth and Atmospheric Sciences

University of Houston

---

In Partial Fulfillment of the Requirements for the Degree

of Master of Science

---

By

Zozan Abdlkhaliq Bazaz

December 2012

**Petrography, Geochemistry, and Stratigraphy of the Paleocene-Eocene Carbonate and Evaporite Deposits in the South of Iraq**

---

Zozan Abdlkhaliq Bazaz

APPROVED:

---

Dr. Henry Chafetz, Chairman

---

Dr. Ian Evans

---

Dr. George Grabowski

---

Dean, College of Natural Sciences and Mathematics

## ACKNOWLEDGMENTS

I want to extend my deepest thanks to my advisor, Dr. Henry Chafetz, for his advice and guidance. Dr. Chafetz spent an immense amount of time helping me to be a better geologist and writer. In addition, without his funding for the geochemical analyses, the course of my research would have been completed.

Dr. Ian Evans's remarks guided me in the very beginning of the research and better oriented me to make the best out of the research materials.

I would also like to thank ExxonMobil for providing the data set for this study. My co-advisor from ExxonMobil, Dr. George Grabowski, spent appreciable efforts to transfer the data as soon as practical, and he was available whenever I had questions.

My study in the United States would not have been possible without the sponsorship of the ExxonMobil Middle East and North Africa Scholarship Program. Thank you for giving me such a life opportunity. I am also thankful to the scholarship program administrator, the Institute of International Education, for its relentless work to make sure that international students get the utmost educational and cultural experience. My great thanks also goes to Dr. John Casey. His help to get me admitted at the University of Houston gave me a hand to take the first step in my academic journey.

Special thanks to Dr. Gao and Minako Righter (ICP-AES lab) and Carolina Muller (X-ray lab) for their assistance and guidance during samples preparation and analysis.

Finally, I would like to express heartfelt thanks to my parents. They made sure to call and encourage me. Their love, patience, and moral support were necessary to get me

through the most stressful times of this thesis. Thank you for implanting the value of education in my beloved siblings and me.

# Petrography, Geochemistry, and Stratigraphy of the Paleocene-Eocene Carbonate and Evaporite Deposits in the South of Iraq

---

An Abstract

Presented to

the Faculty of the Department of Earth and Atmospheric Sciences

University of Houston

---

In Partial Fulfillment of the Requirements for the Degree

of Master of Science

---

By

Zozan Abdlkhaliq Bazaz

December 2012

## Abstract

The Paleocene and Eocene carbonate and evaporite rocks in southern Iraq were deposited on a shallow carbonate platform that occupied the southwest margin of the Mesopotamian foreland basin. Tens of meters thick shallowing-upward cycles were identified based on the evaporite-rich carbonates representing cycle tops. The original depositional textures for the carbonates have been destroyed by pervasive dolomitization. The identified microfacies, after diagenetic overprint, are foraminiferal biodolomicrite, sparse peloidal and foraminiferal biodolomicrite, peldolomicrite, and peloidal and foraminiferal biodolosparite.

The Paleocene-Eocene dolomites have a wide spectrum of crystal sizes that range from micritic, aphanocrystalline, to 100 μm size crystals. The dolomite crystals are mainly planar-s to non-planar and they show syntaxial overgrowth cement in some horizons. Other diagenetic processes accompanying dolomitization throughout the section are allochem dissolution, evaporite precipitation and replacement, authigenic quartz precipitation, and pore-filling and -lining calcite and dolomite cementation.

This study also focused on documenting and evaluating the geochemical characteristics of the dolomites. X-ray analysis showed that dolomite is the dominant mineral in all of the representative microfacies. ICP-AES results indicate that the dolomites are nearly stoichiometric with the highest mole % $CaCO_3$ modal class between 50% and 51%.

The dolomites are associated with evaporites and yet have probably stabilized in contact with seawater or mixed meteoric and seawater rather than hypersaline seawater. This conclusion is based on their $Sr^{+2}$ and $Na^{+2}$ content (avgs. 102 and 600 ppm,

respectively). The Fe-enrichment in the dolomites (avg. 135 ppm) also indicates that dolomitizing fluids had a component of non-marine water. The wide range of the trace element values suggest that dolomitization had taken place in contact with fluids that had different chemistries and at different rock-water interaction ratios.

The dolomitization settings were enriched in organic carbon based on the highest modal class of $\delta^{13}C$ values between -6 and -7 ‰ PDB. Dolomitization in contact with meteoric water can be responsible for the dominantly negative $\delta^{13}C$ values. However, $\delta^{18}O$ values with their highest modal class between 0 and 2 ‰ PDB disagrees with this interpretation. Therefore, the $\delta^{13}C$ and $\delta^{18}O$ values are probably the result of dolomitization within sulfate-reducing bacterial zone.

## TABLE OF CONTENTS

## LIST OF FIGURES

## LIST OF TABLES

# CHAPTER 1 INTRODUCTION

Shallow water carbonate deposits have been continuously of interest to geoscientists because of their temporal and spatial distribution throughout the Earth's history. Geologists have studied shallow carbonate rocks from outcrops and the subsurface in order to understand their physical, chemical, and biological properties. Ancient shallow carbonate deposits trap some of the biggest extractable hydrocarbon resources in addition to hosting Pb and Zn ores (Pratt et al., 1992). The control of environmental parameters on depositional processes and type of sediments in shallow carbonate settings makes ancient deposits a valuable proxy for studying paleo-environment conditions. Moreover, shallow water carbonate facies promptly respond to changes in the seawater level, chemistry, living organism, etc., that makes the study of these deposits relevant to all of the disciplines dealing with the planet Earth.

Evaporite rocks are usually associated with shallow water carbonates deposited in arid and semi-arid environments. The presence of evaporites can highly influence the facies succession and diagenetic patterns. Moreover, the mineralogy and sedimentary attributes of evaporite deposits can provide valuable information with regard to the physiography of a carbonate-evaporite depositional setting (Warren and Kendall, 1985; Kendall, 1992).

Regardless of the platform morphology, i.e., shelf, ramp, etc., the dominant facies succession observed in both modern and ancient shallow water carbonates is vertically shallowing-upward facies succession, commonly referred to as shallowing-upward sequences or cycles (Wilson, 1975; James, 1984; Hardie, 1986). The reason behind the

shallowing-upward pattern is mainly attributed to the abundance of sediments to fill accommodation space that in turn results in decreasing bathymetry. On the other hand, deepening-upward sequences are also documented in the rock record despite the arguments about their genesis (Fisher, 1975; Satterley and Brandner, 1995). Evaporite deposits are also interpreted in terms of upward changes in mineralogy that are controlled by water salinity, and freshening- and -brining-upward are equivalent terms to the carbonates deepening- and shallowing-upward cycles, respectively (James and Kendall, 1992).

The shallow water on the platform during deposition of the carbonates makes these deposits prone to multiple episodes of diagenesis from fluctuations in relative sea level. Alterations of carbonate cements and grains are common syn- and post-depositional diagenetic processes and petrographic analysis is a fundamental approach to identify diagenetic patterns (Bathurst, 1975). Similarly, the geochemistry of carbonate deposits is also altered during different phases of diagenesis, and based on the chemistry of diagenetic fluids, mineralogy, elemental content, and isotopic ratios, geochemical changes occur to different degrees (Allan and Mathews, 1977; Brand and Veizer, 1981).

This study is focused on determining the petrographic and geochemical characteristics of the Paleocene-Eocene carbonate and evaporate rocks in southern Iraq that were deposited on a shallow water carbonate-evaporite platform. For better understanding of the depositional environments, paragenesis, and stratigraphic sequence, petrographic analyses of thin sections were conducted to distinguish rock types, microfacies, vertical facies succession, and diagenetic fabrics. Moreover, distinctive microfacies types were subject to geochemical analyses to identify their mineralogy

(aragonite, high-magnesium calcite [HMC], low-magnesium calcite [LMC], and dolomite), major and trace element content ($Ca^{2+}$, $Mg^{2+}$, $Sr^{2+}$, $Na^{2+}$, $Fe^{2+}$, and $Mn^{2+}$), and $\delta^{13}C$ and $\delta^{18}O$ values. The combination of petrographic and geochemical analyses has significant implication for understanding the development of the stratigraphic sequence.

**1.1 Study Area and Tectonics**

The study area is located within the vicinity of Basra (or Al Basrah) city in the south of Iraq (Fig. 1), and the data set utilized in this study comes from oil and gas wells of southern Iraqi fields (Fig. 2). The wells penetrated the Paleocene-Eocene intervals that are overlain by the younger Tertiary and Quaternary deposits. The Paleocene-Eocene carbonates and evaporites in southern Iraq were deposited on a shallow and widespread carbonate platform (most likely a carbonate ramp) sitting on the southwest flank of the northwest-southeast trending Mesopotamian foreland basin (Sharland et al., 2001; Jassim and Budday, 2006).

The incipient Mesopotamian foreland basin formed during the Late Cenomanian-Early Turonian when microcontinents separated from the Arabian Plate in Late Tithonian and collided with the fore-arc ridge of the intra-oceanic subduction zone. Compression resulted from diachronous collisions and led to ophiolite obduction in the form of thrust sheets that were emplaced on the north and northeastern margin of the Arabian Plate, and the consequent load generated by the ophiolite thrust sheets formed the foreland basin (Fig. 3a) (Jassim and Budday, 2006).

During the Palecene and Eocene, the main tectonic activities were the continuous subduction of the last remnants of the Neo-Tethys beneath Eurasia, and the continental

collision between the Arabian Plate and central Iran corresponds with the closure of the Neo-Tethys Ocean (Fig. 3b) (Sharland et al., 2001; Jassim and Budday, 2006).

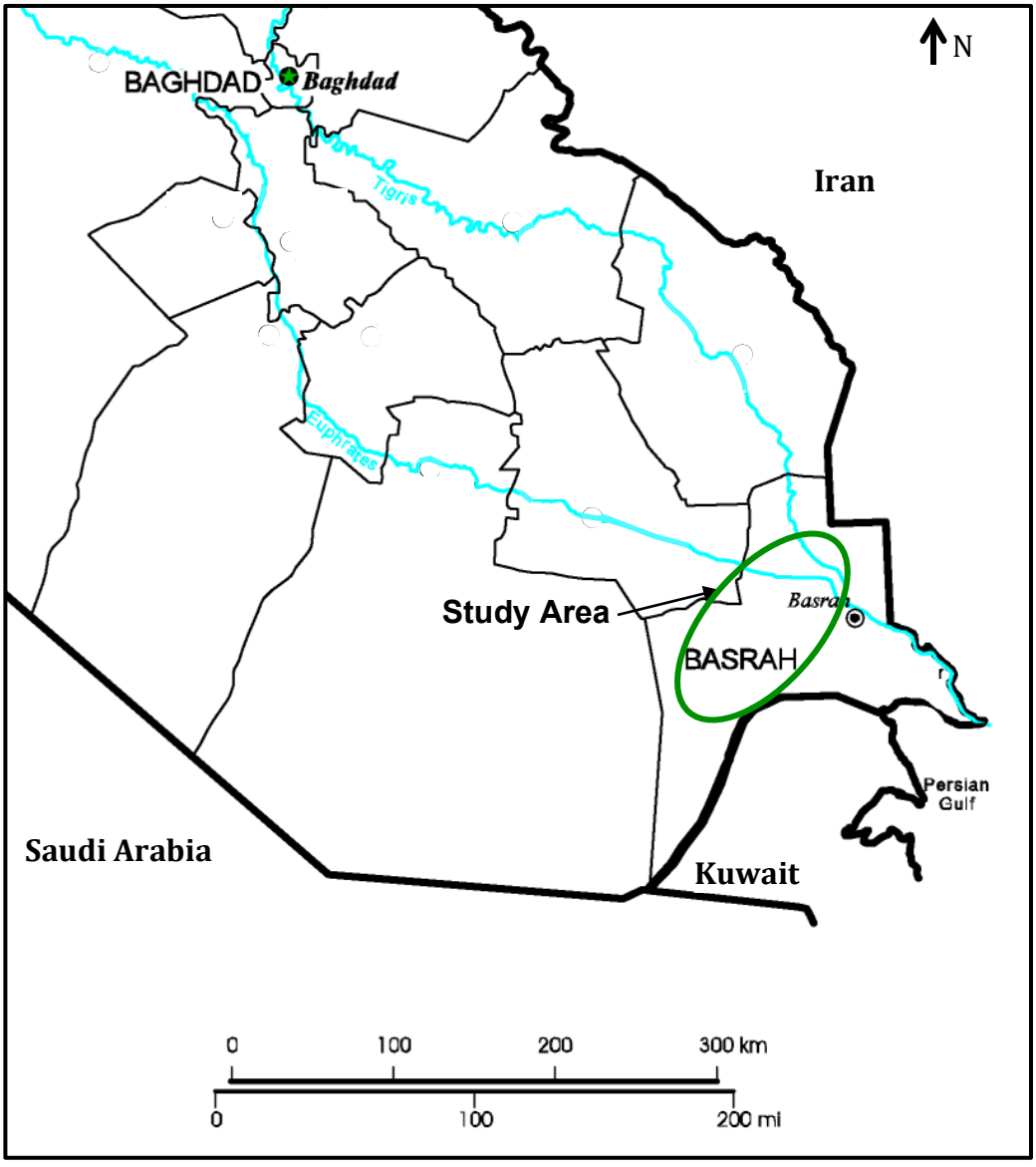


**Figure 1** Study area location (modified from www.globalsecurity.org).

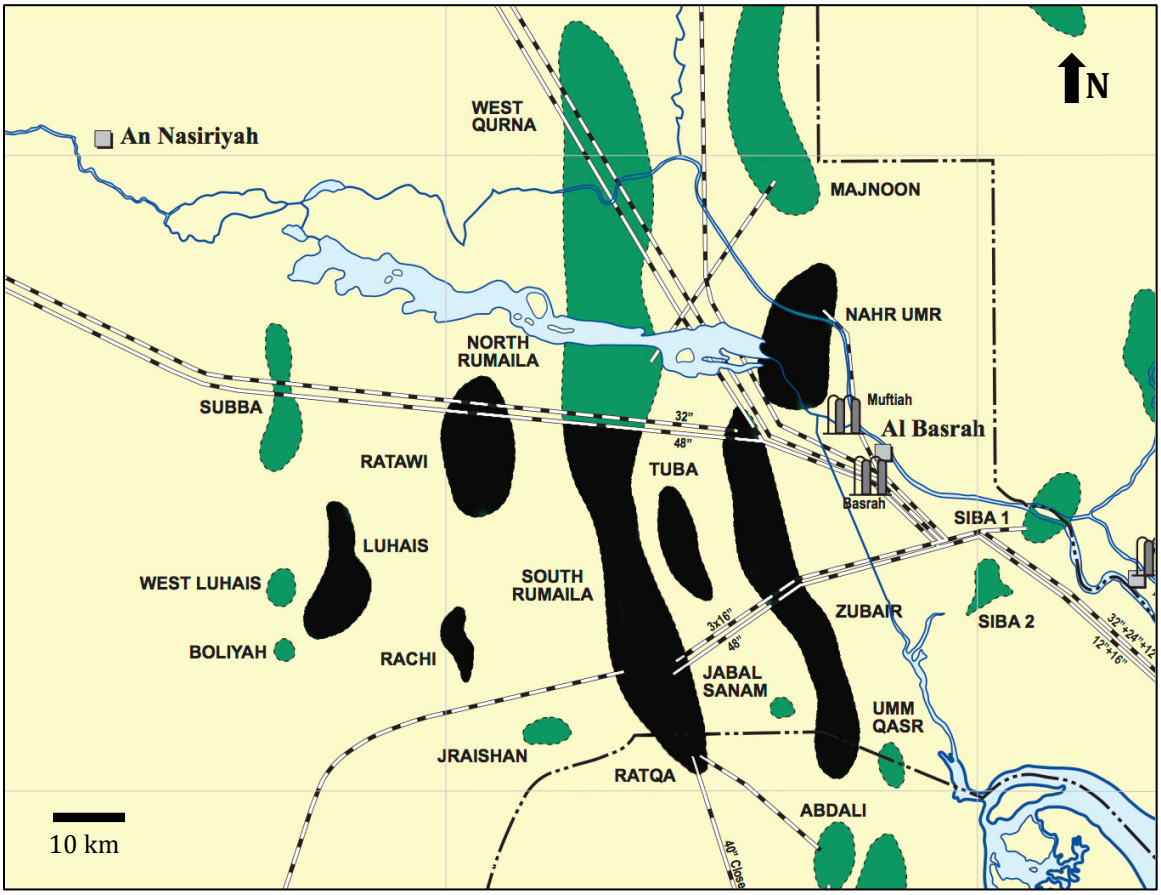


**Figure 2** Oil and gas fields in southern Iraq included in this study (modified from Iraq Field Atlas, 2003).

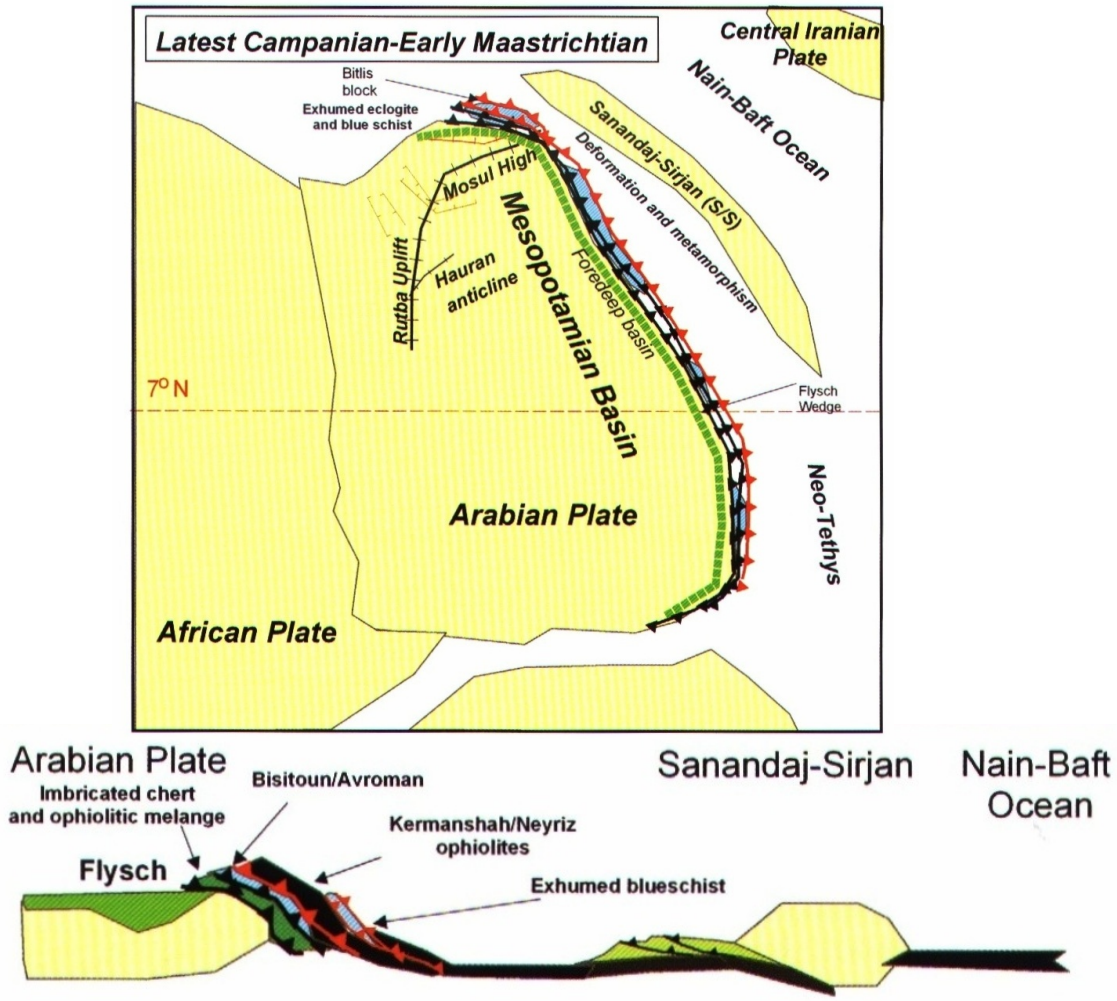


**Figure 3a** Tectonic maps and schematic cross-sections for the Arabian Plate during the Late Cretaceous showing ophiolite obduction and formation of foreland basin (from Jassim and Budday, 2006).

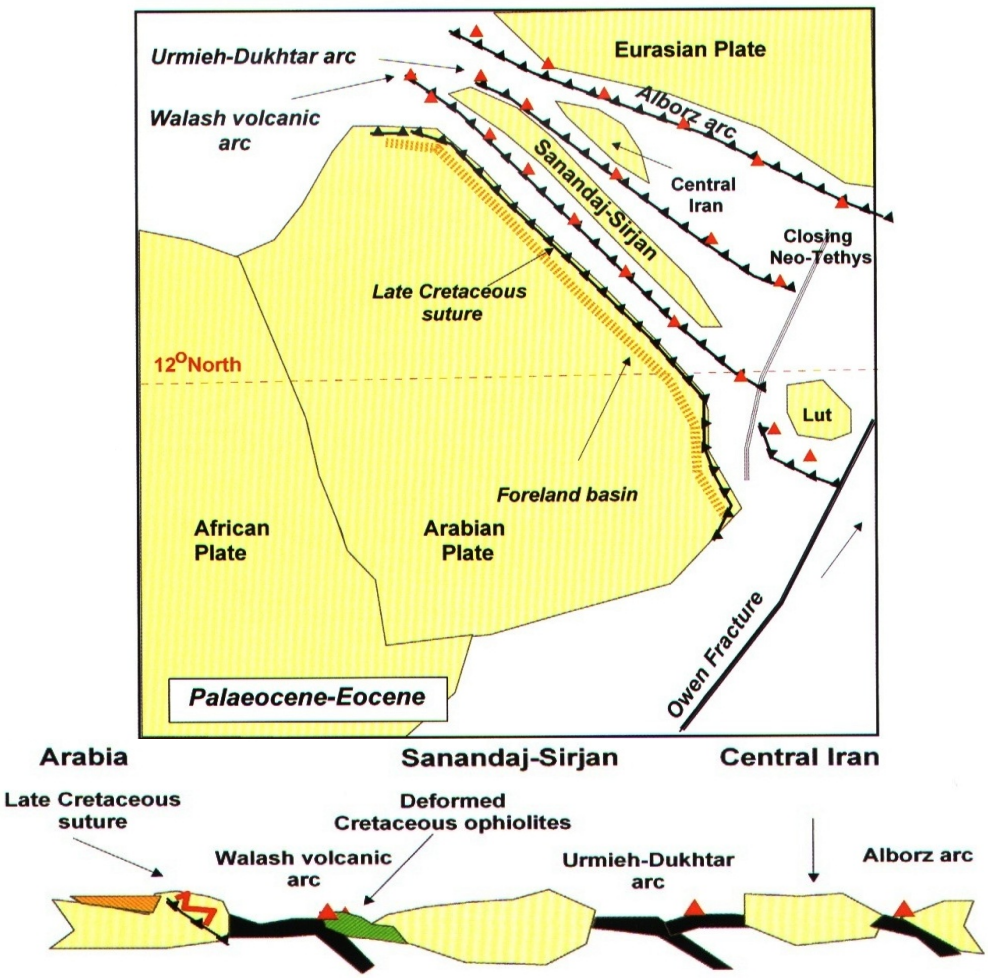


**Figure 3b** Tectonic maps and schematic cross-sections for the Arabian Plate during Paleocene-Eocene showing the closure of Neo-Tethys with continuous subduction (from Jassim and Budday, 2006).

The onset of the continental collision and closure of the Neo-Tethys Ocean are not clearly dated. Jassim and Goff (2006) proposed that continental-to-continental collision and final closure of the Neo-Tethys took place during Paleocene-Eocene and they suggested age refinement, whereas Homke et al. (2009) reported ages for the Arabian Plate and central Iran collision from Eocene to Late Miocene. The sum of Paleogene-Neogene convergent tectonics along the north and northeastern Arabian Plate margin and central Iranian Plate resulted in the formation of the present day Zagros fold-and-thrust belt, and the remnant of the Mesopotamian foreland basin is currently represented by the Persian (or Arabic) Gulf foreland basin as shown in Figure 4 (Jassim and Goff, 2006; Homke et al., 2009).

The main tectonic units of the Arabian Plate are: the Precambrian shield, stable shelf, unstable shelf, and Zagros suture. All of the tectonic units are present in Iraq except the Precambrian shield. Basement-deep transverse and longitudinal fault systems cut through all of the tectonic units. Jassim and Budday (2006) established the regional tectonic framework of Iraq in 1987, and they divided each unit into zones and subzones based on their geological and geomorphological characteristics. The boundaries separating zones and subzones (Fig. 5) were modified by Jassim and Budday (2006).

The study area lies within Zubair subzone that is part of the bigger Mesopotamian zone; a zone characterized by subsurface arches and antiforms damped at the surface by the Quaternary cover. The Mesopotamian zone has experienced subsidence since the Late Permian, yet the structural pattern of the Zubair subzone is shaped by the underlying basement through N-S trending folding and faulting developed by the late Nabitah Orogeny. It is bounded by basement transverse faults in its northern and southern parts.

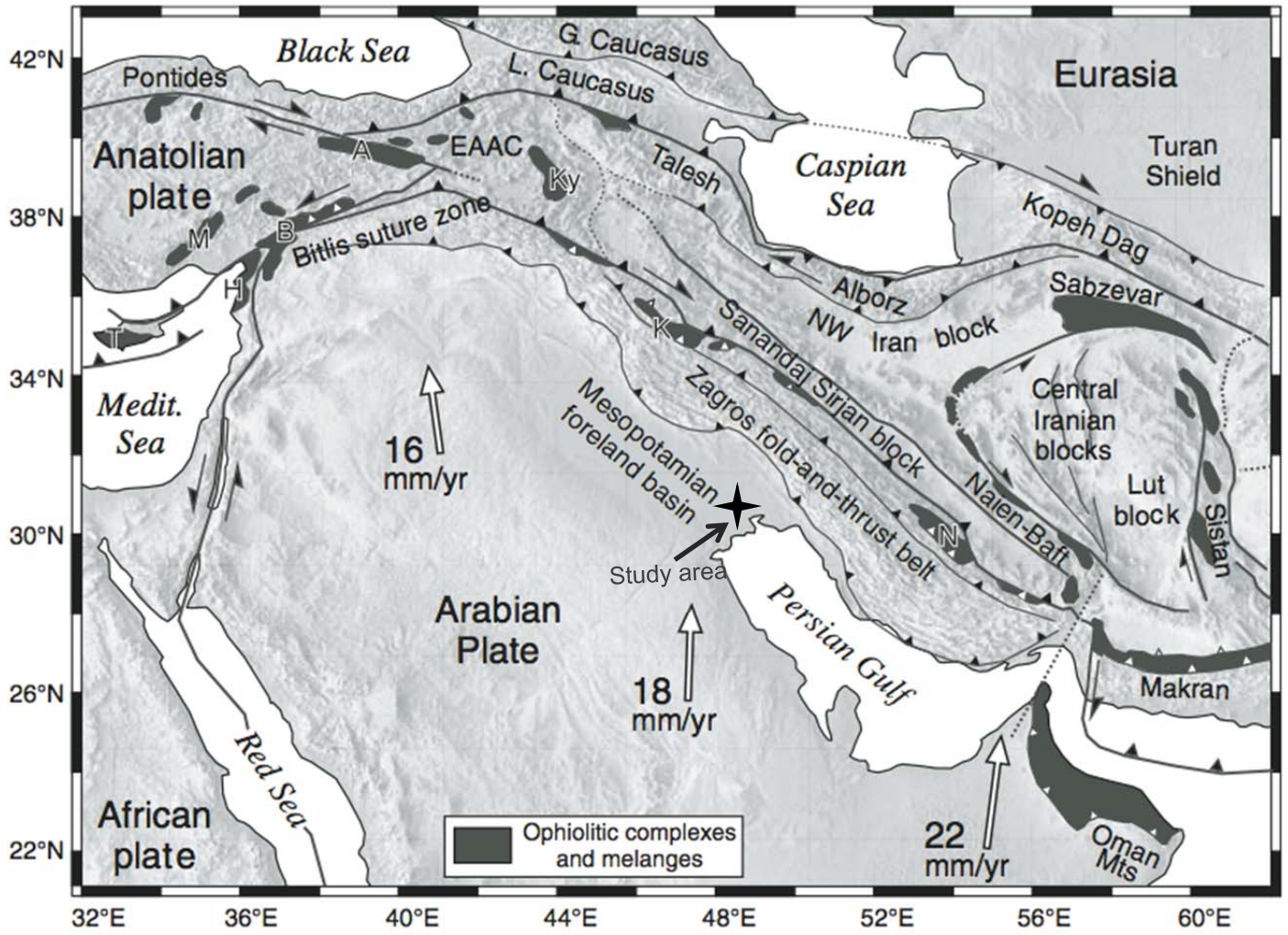


**Figure 4** The present day tectonic and structural elements of Arabian-Eurasian collision zone (from Homke et al., 2009).

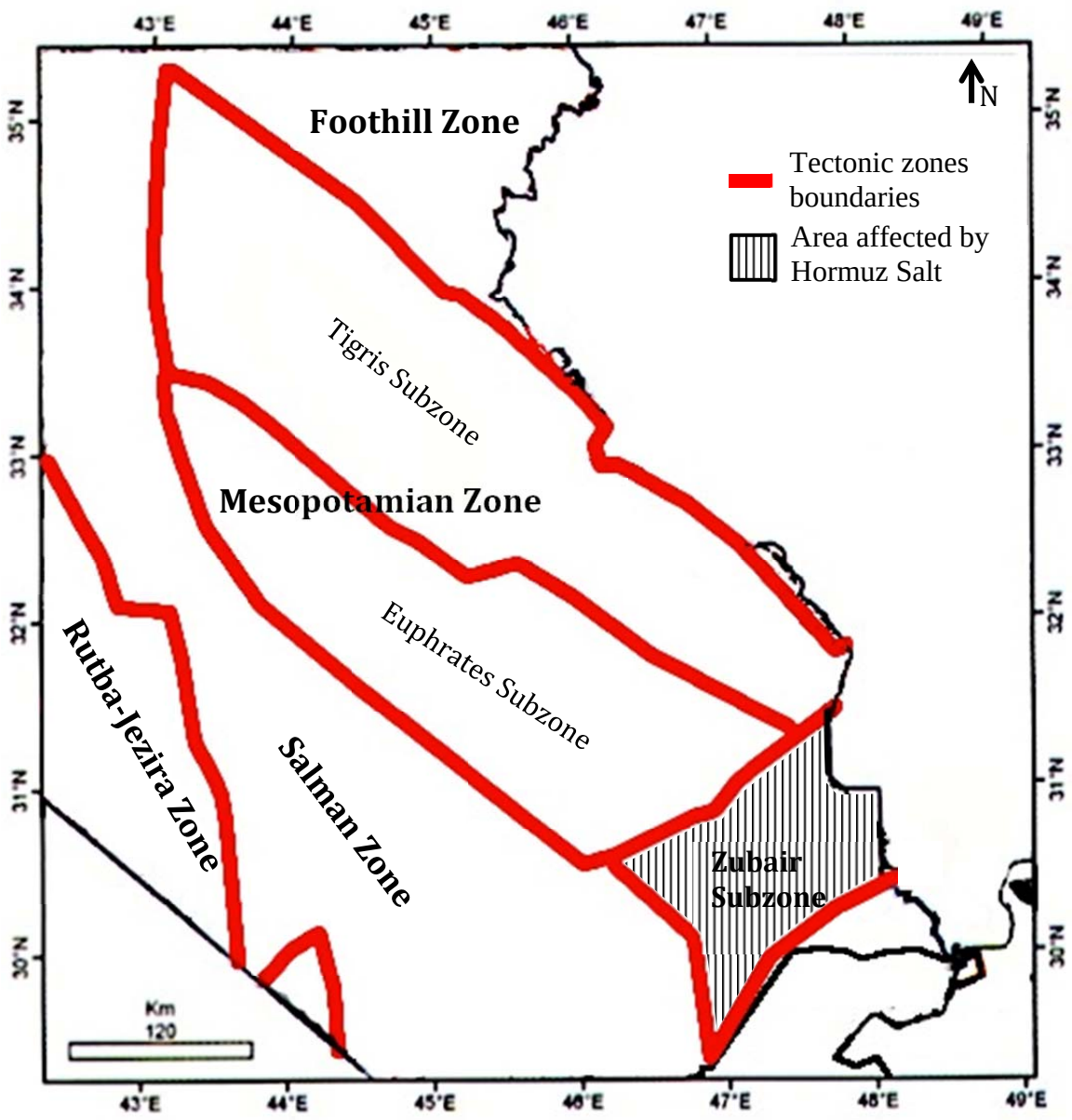


**Figure 5** Map showing the study area represented by the Zubair subzone. Note that the Zubair subzone is the only zone affected by Hormuz Salt (from Jassim and Goff, 2006).

Structures within the Zubair subzone went through tectonic reactivation phases during the Permo-Carboniferous, Mesozoic, and Tertiary, in addition to structural movements caused by the Infra-Cambrian salt (Jassim and Budday, 2006). Based on the regional tectonic history, the influence of structural dynamics on the deposition of Paleocene-Eocene deposits was inevitable.

## 1.2 Stratigraphy

The stratigraphic development of the Paleocene-Eocene rocks in the north and northeast margin of the Arabian Plate is broadly described by Alsharhan and Narin (1995) to have resulted from two regressional events separated by a transgressional event with the latter being a period of quiescent paleogeographic conditions. Beginning in Early Paleocene, a major transgression restored the shallow marine carbonate depositional environment over a plate-wide erosional hiatus that resulted from the short term Maastrichtian-Danian regression. This hiatus is absent in the Ras al Khaimah basin in northern United Arab Emirates and Zagros basins in southeast Iran. In Late Eocene-Oligocene, another regressional event took place that exposed most of the carbonate platforms and marks the top of the Paleogene rocks.

The stratigraphy of Paleocene-Eocene rocks in southern Iraq was first described by Owen and Nasr (1958) based on data derived from oil and gas wells drilled within Basra province and Kuwait. The strata were named the Hasa Group and divided into three formations based on their lithostratigraphic and biostratigraphic characteristics. These formations are the Umm Er Radhuma, Rus, and Dammam formations.

The ages of the formations are controversial (e.g., Sharland et al., 2001, Jassim and Budday, 2006, Liu et al., 2006). Formation ages used in this study are obtained from an unpublished report by Liu et al. (2006; ExxonMobil Exploration Company) in which the ages were determined using nannofossils as well as planktonic and benthic foraminifera. Moreover, ages assigned by previous workers were taken into consideration while preparing the biostratigraphic report that will be utilized in this study. Another advantage of using ExxonMobil's ages is that the study is based on samples from the

wells included in this thesis study, so the formations' contacts should correspond with their age determinations.

The three formations representing the Paleocene-Eocene in the study area are lithostratigraphically correlatable with strata in Saudi Arabia, Kuwait, and Qatar (Fig. 6). Yet, the thicknesses change and lateral and vertical variations in lithofacies are encountered. Moreover, their ages do not match because of erosion and non-depositional processes acted differently across the broad spatial distribution (Alsharhan and Narin, 1995). These formations have been studied from outcrops and wells and are described below.

### 1.2.1 The Umm Er Radhuma Formation (Paleocene to Early Eocene)

The Umm Er Radhuma Formation was named from a water well in the Emm Er Radhuma area, in Saudi Arabia. The dominant lithofacies described from wells in Kuwait and southern Iraq are dolomitic, marly, and anhydritic limestones (Owen and Nasr, 1958). In southern Iraq, the thickest section (570 m in wells) of the Umm Er Radhuma Formation is encountered near the Shat Al Arab River within the Mesopotamian zone. The formation laterally passes into the open marine Aliji Formation at its north and northeast boundary, and pinchs out on structural highs, or laterally passes to the phosphatic Akashat Formation at its west and northwest boundary (Fig. 7) (Jassim and Budday, 2006). The sections included in this study come from the wells Zubair No.1 and Nahr Umr No.1 with the measured thicknesses being 440 and 415 m, respectively. The Umm Er Radhuma Formation includes shallow water carbonate and evaporite facies that were deposited in a shallow lagoon and sabkha environments (Jassim and Budday, 2006).

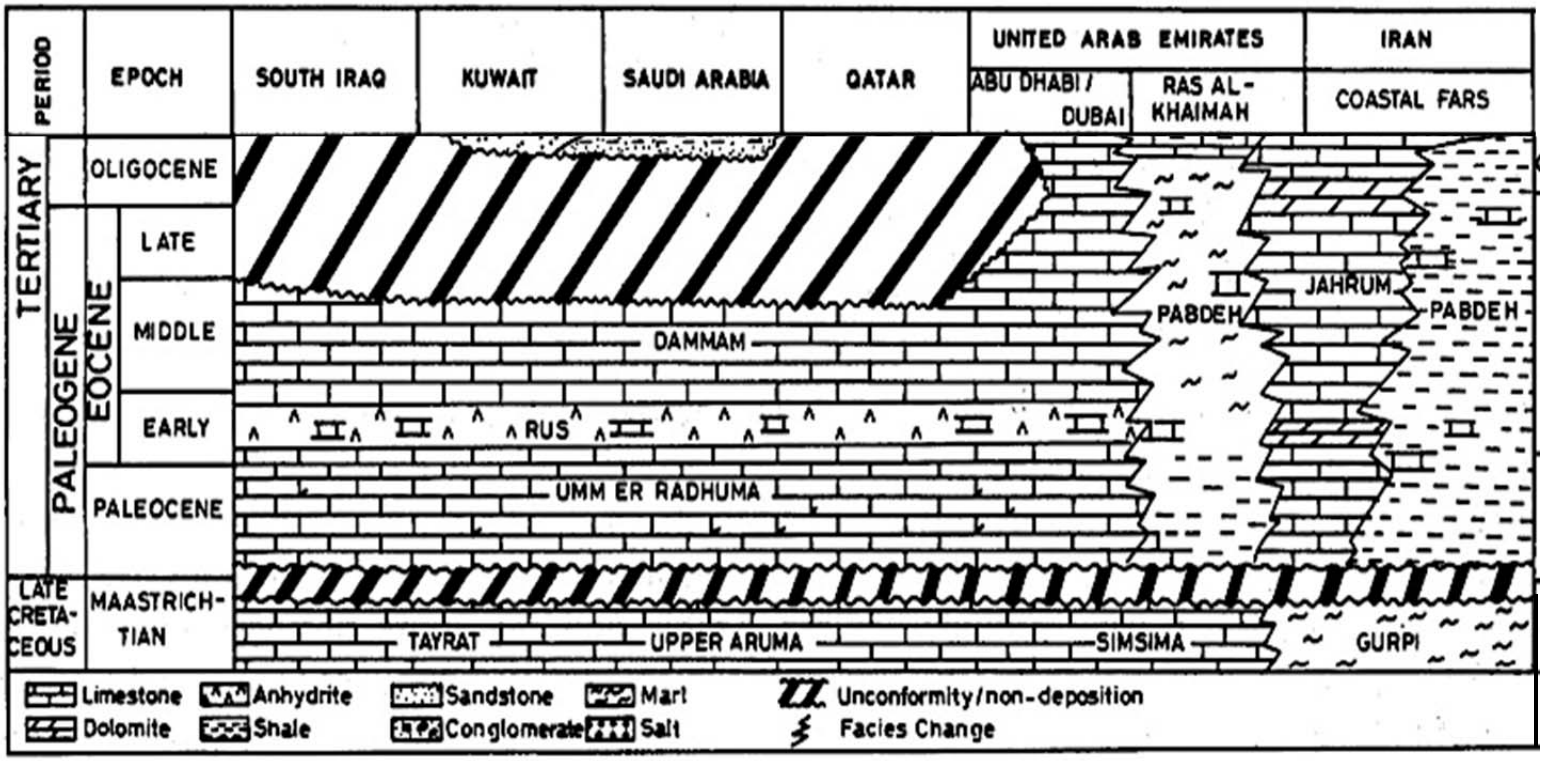


**Figure 6** Paleogene lithostratigraphic chart showing the distribution of the three formations in this study across the Arabian Plate (modified from Alsharhan and Nairn, 1995).

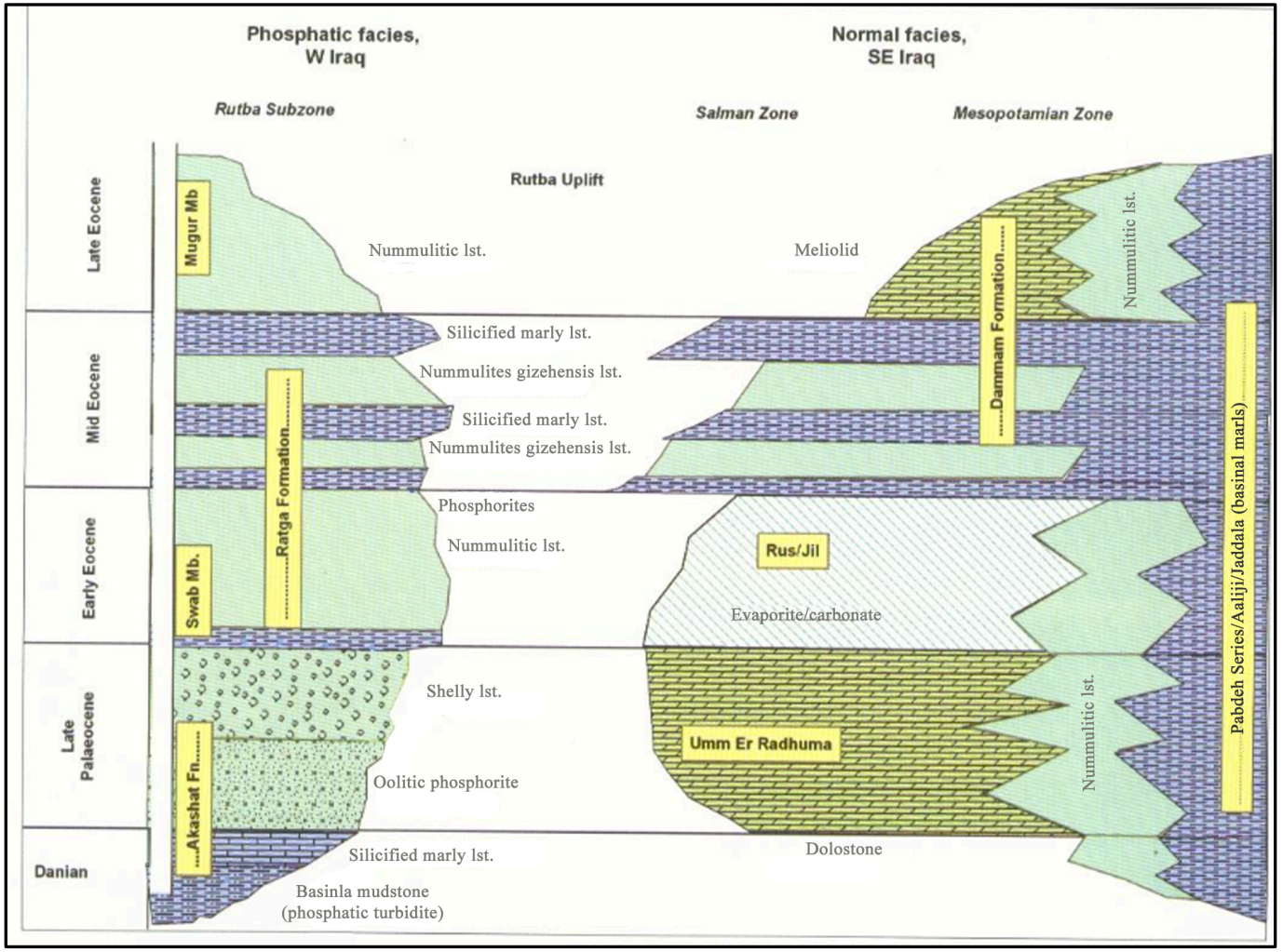


**Figure 7** Stratigraphic correlation for Umm Er Radhuma, Rus, and Dammam formations in southern Iraq with the phosphatic formations in western Iraq (from Jassim and Goff, 2006).

Different ages have been assigned to the formation based on the location of the studied sections. Jassim and Budday (2006) suggest that the Umm Er Rhaduma age might be limited to the Paleocene in southern Iraq based on outcrop studies of the topmost beds. However, the nature (i.e., conformable, disconformable, and gradational) of the upper contact with the Rus Formation changes between localities, and the same situation exists for the erosional lower contact. Therefore, Paleocene to Early Eocene age is assigned here based on biostratigraphic data from Zubair No.3 well in the south of Iraq (Liu et al., 2006).

### 1.2.2 The Rus Formation (Early to Middle Eocene)

The type locality of the Rus Formation is on the southeastern flank of the Damam dome at Jebel Umm Er Rus in Saudi Arabia, and its subsurface reference section is in Zubair No. 3 well, southern Iraq. It is represented predominantly by thick and massive anhydrite that includes layers of unfossiliferous limestones interbeded with a few blue marl and shale beds (Owen and Nasr, 1958). The Rus Formation overlies the Mesozoic and lower Cenozoic carbonate platforms on the Arabian Plate in the subsurface, except on paleogeographic highs where it is mostly removed by erosion and/or karst collapses formed during the Middle Pleistocene wet climatic times (Steinhauff et al., 2011).

The Rus Formation is combined with the upper Um Er Radhuma Formation and the lower Dammam Formation in some locations because of the gradational changes in lithofacies, but it is clearly distinguished in the subsurface between Takhadid-Qurna and Al Batin transverse faults in southern Salman and Mesopotamian zones (Fig. 8) (Jassim and Budday, 2006). The measured thickness in Zubair No.1 well is 112.5 m, however the

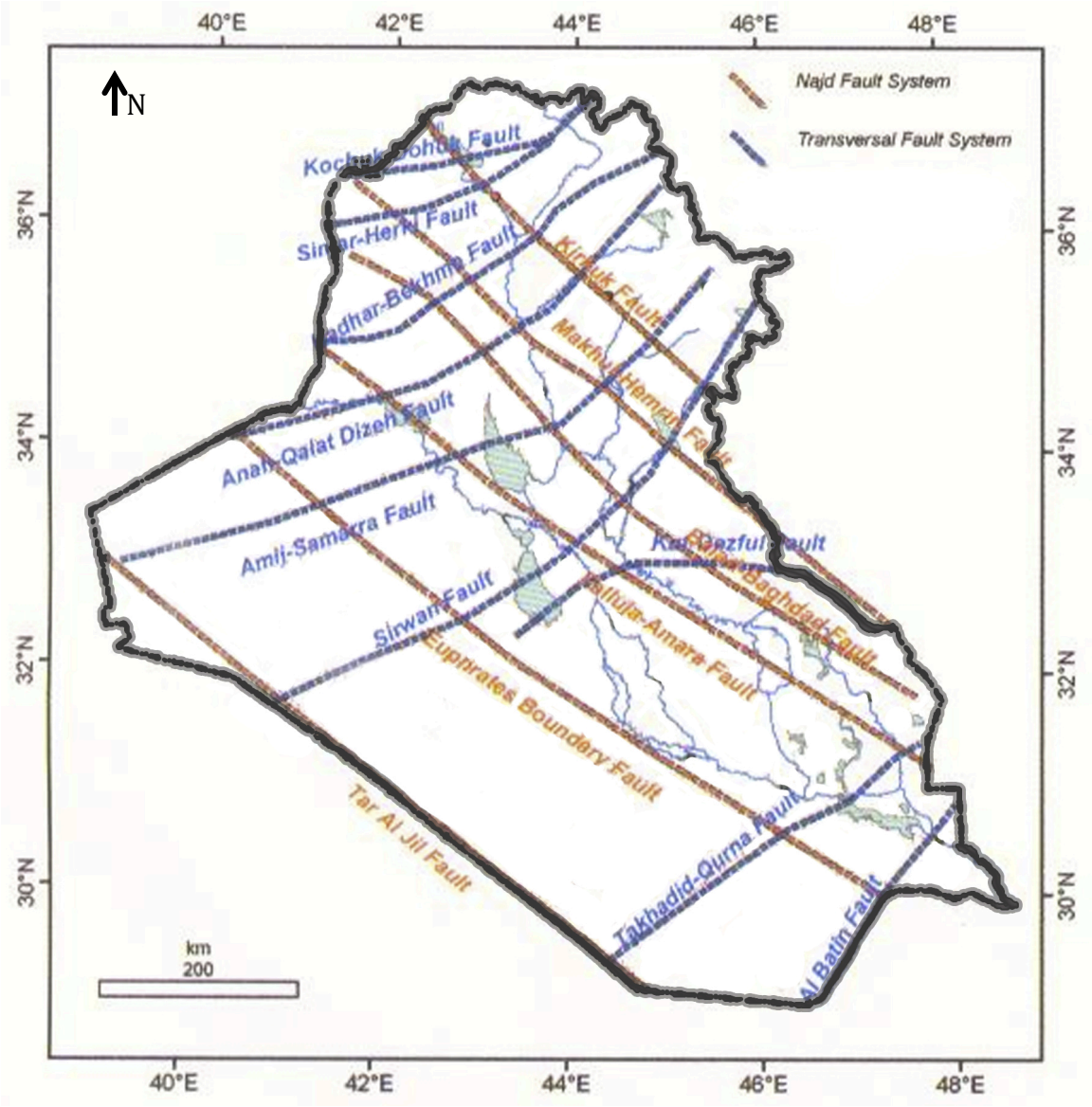


**Figure 8** Structural map showing the study area bounded by Takhadid-Qurna and Al Batin transverse faults and Euphrates longitudinal fault (from Jassim and Goff, 2006).

formation is not found in the Nahr Umr No.1 well because it laterally pinches out in the deeper platform areas to the east.

An Early to Middle Eocene age is given to the Rus Formation based on data from wells Zubair No. 1 and 3, although its age is controversial because of the time-transgressive nature of the basal unit. The formation can be as old as Late Paleocene in some locations on the platform (Liu et al., 2006).

### 1.2.3 The Dammam Formation (Middle and Upper Eocene)

The Dammam Formation crops out on the rim of Dammam dome in Saudi Arabia, and its reference subsurface section in Basra and Kuwait areas comprises whitish-gray, porous, dolomitized limestones, soft chalky limestones, and nummulitic limestones (Owen and Nasr, 1958). In southern Iraq, the Dammam Formation is restricted to Euphrates and Zubair subzones of the Mesopotamian zone, and the southern part of Salman zone (Jassim and Budday, 2006). The thicknesses of the sections included in this study are 217 and 280 m measured from the wells Zubair No.1 and Nahr Umr No.1, respectively.

Spatial and temporal changes in the Dammam Formation lithofacies are easily observed and several formal and informal units have been proposed based on outcrop and well sections (Jassim and Buday, 2006). The formation mostly contains whitish grey dolomitized nummulitic and milliodal limestones that were deposited in restricted lagoon and open marine environments.

The Dammam Formation is unconformably overlain by the Ghar Formation, and its lower part has a diachronous depositional pattern, yet based on fossils recovered from

Zubair No.1 and 3 wells, Middle to Early Eocene age is given to the formation (Liu et al., 2006)

### 1. 3 Paleoclimate

The differences in the facies and sediment content of modern carbonate-evaporite platforms based on climatic conditions are well documented, and both depositional and diagenetic trends are highly influenced by climatic zone conditions (James and Kendall, 1992; Tucker, 1993; Kuznetsov, 2006). On a global scale, the Paleogene Period represents a greenhouse interval that is characterized by the pronounced Paleocene-Eocene Thermal Maximum (PETM) documented in deposits across relatively wide and shallow continental shelves and in deep oceanic settings (Sluijs et al., 2008).

One of the important events in the Early Cenozoic is the rising of both temperature, 4 to 5 °C in the tropics, and calcite compensation depth (CCD) that reached <2 km during the Paleocene-Eocene Thermal Maximum (Zachos et al., 2005). This was followed by a long pattern of cooling well documented in the Late Eocene to Early Oligocene strata that corresponded with ≈ 1 km deepening of CCD (Allen and Armstrong, 2008). Furthermore, both oceanic and atmospheric $CO_2$ reservoirs and $pCO_2$ went through marked changes during the Paleogene (Higgins and Schrag, 2006). Whereas the causes of these events are controversial and are not the subject of this study, their effects are important because the mineralogy (Given and Wilkinson, 1987) and isotopic composition (Zachos et al., 2001) of sedimentary carbonates that are controlled by them.

Throughout the Paleogene, shallow water covered most of the Peri-Tethyan areas providing favorable conditions for the development of shallow carbonate platforms (Fig. 9) at low latitudes and warm temperature waters. These conditions also boosted the growth of the carbonate-building nummulitid foraminiferans that are a major facies

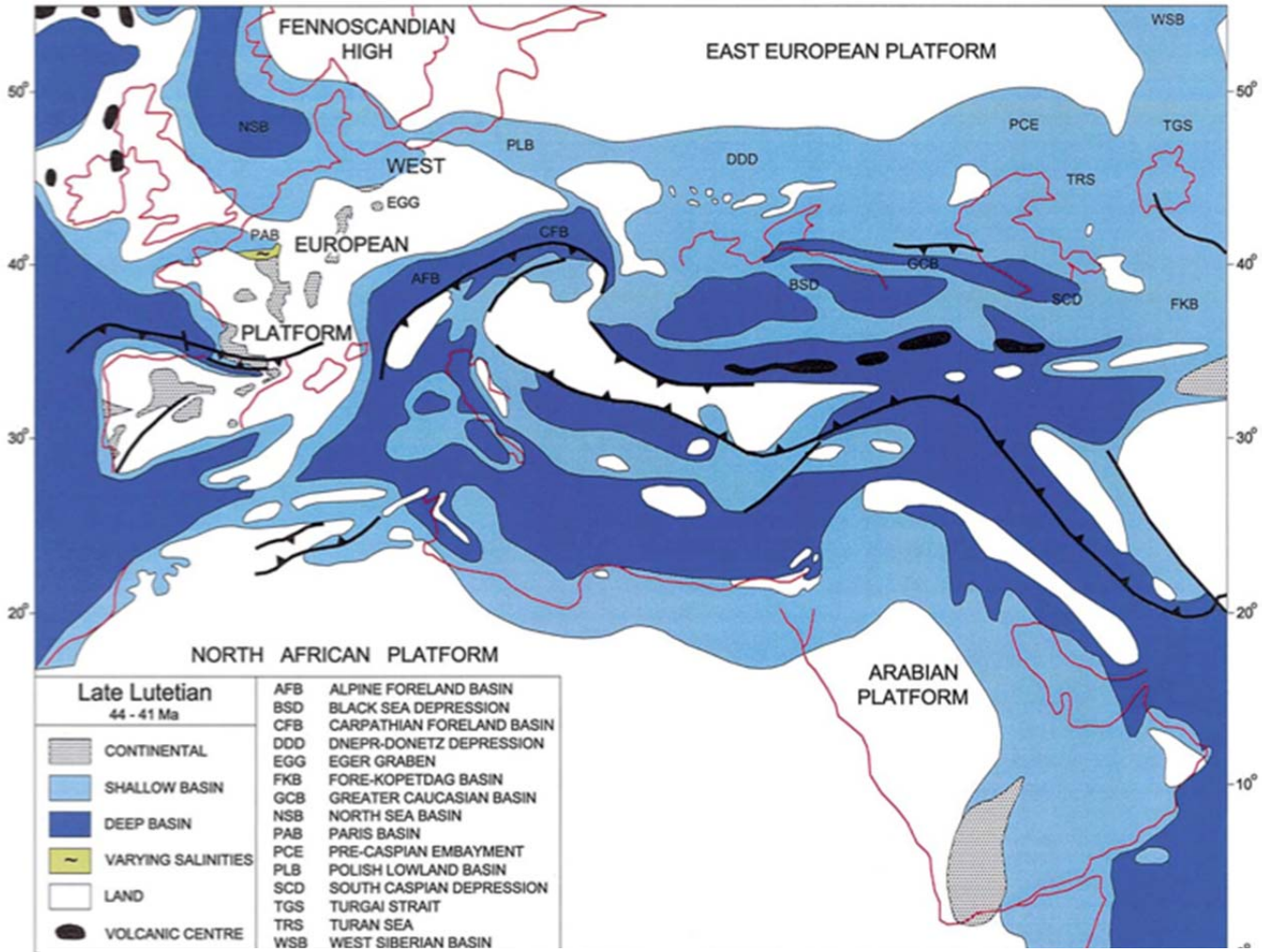


**Figure 9** A generalized map showing the distribution of the Peri-Tethys platforms during the Paleogene. Shallow platforms are colored in light blue (from Meulenkamp and Sissingh, 2003).

component in Paleogene carbonates (Philip, 2003). Regarding the paleoclimate of the study area during the Paleogene, the Arabian Plate occupied a low latitude northern hemisphere position in the 20-25°C isotherms, and the Paleocene-Eocene carbonate platform was developed within an arid to semi-arid climate (Golonka, et al 1994; Dull, 2004). Data from the Kuwait/Basra area show that carbonate-evaporite deposits dominated the Arabian Plate from the Middle Permian onward (Beydoun, 1998), and the depositional setting was represented by a shallow northeastern shelf of the plate that extended at times for 2000 km in width (Murris, 1980).

# CHAPTER 2 METHODS

## 2.1 Data Description

The data set used in this study is provided by ExxonMobil and it includes electrical well logs, thin sections, and well cuttings. The well logs are measured from the wells Zubair No.1 and 3, Nahr Ummr No.1 and 3, South Rumaila No.34, Ratawi No.1, Rachi No.1, and Luhais No.1 (fields including these wells are shown in Fig. 2). The well logs are spontaneous potential and resistivity and do not therefore show systematic patterns with changes in lithofacies, as they respond to changes in permeability that is controlled by diagenesis rather than the original depositional texture or a particular lithofacies. However, the tops and bottoms of the evaporitic Rus Formation can be identified from the well logs through the irregular and high amplitude response. Some of the major kicks in the logs can be traced between two adjacent wells. However, the absence of similar patterns within a number of adjacent wells makes the well logs useless to construct a sub-formation regional correlation of stratigraphic units bounded by major surfaces like exposure surfaces and maximum transgression surfaces. Therefore, the use of the well logs is limited to represent the regional correlation for the Um Er Radhuma, Rus, and Dammam Formations.

The thin sections in this study come from the Nahr Ummr No.1 and Zubair No.1 wells. Thin sections representing the Rus Formation are restricted to the basal carbonate part of the formation in Zubair No.1. The rest of the section in Zubair No.1 is made up of anhydrite and the formation is absent in Nahr Ummr No.1.

The thin sections are mainly prepared from cuttings, except for a few intervals where the samples are from cores. The cuttings are sub-angular granules, and there are around 3-5 particles in each thin section. There were no reports enclosed with the thin sections explaining the bases for selecting the particles. Therefore, it is assumed that the particles in each thin section represent the dominant facies of the drilled intervals. Cuttings were collected from Nahr Umr No.1 well and preserved in small paper bags with their depth interval indicated. The majority of the sample bags contain around 20 g of cuttings with particles ranging from medium sand to pebble sizes.

**2.2 Petrography**

A standard petrographic study was conducted on the thin sections from Nahr Ummr No.1 (500 thin sections) and Zubair No.1 (160 thin sections) wells in order to observe the microfacies of the Umm Radhuma and Dammam Formations. Depositional environments were inferred from microfacies interpretation based on the types of allochems, micrite versus sparite abundance, and presence of evaporite minerals. Textural modifications that resulted from diagenetic alterations were also examined for both allochems and matrices.

Two major difficulties were associated with the petrographic study. First, because each thin section was prepared from 3-5 cutting particles rather than a rock slice, not all of the grains have the same thickness and this made it difficult to identify some characteristics, e.g., birefringence and grain fabric in some thin sections. Secondly, a single thin section in some cases includes two different rock types (e.g., dolomite and dolomicrite). The latter problem regularly takes place where there is a change in facies.

However, the actual rock type and vertical sequence (e.g., coarsening and/or fining-upward) can be recognized after examining a number of successive thin sections.

The petrographic study was conducted using Nikon model LV100POL microscope with a mounted camera connected to a computer. Photomicrographs were taken for distinctive microfacies and diagenetic patterns. Imaging software NIS-Elements F2.30 is associated with the microscope.

Distinctive microfacies were repeatedly observed during the petrographic study in different horizons. These microfacies include dolomite with different textures, dolomitic mudstone, and mudstone. In order to determine the depositional and diagenetic settings associated with these microfacies, geochemical analyses were conducted. Since time and budget ceilings did not allow running geochemical analyses for these rocks in all of the horizons, petrography was used to decide on the intervals to be analyzed and best represent these distinctive microfacies. Moreover, given that the hydrochemistry of the world ocean was not constant during the Paleogene, the samples for geochemical analyses were not exclusively chosen based on their petrographic characteristics, but also based on stratigraphic position. Thus, petrographic and geochemical aspects were both considered.

**2.3 Sample Preparation for the Analyses**

A total of twenty-six whole-rock samples were chosen from the cuttings of the Nahr Umr No.1 well for mineralogical, elemental, and isotopic analyses. X-ray diffraction, inductively coupled plasma-atomic emission spectrometry (ICP-AES), and carbon and oxygen isotopes mass spectrometry were the methods used to obtain the sum

of the geochemical characteristics. Since clay-size rock powder is needed for all the analyses, around 5-7 g of rock particles were picked from each sample bag. Some of the sample bags contain minor amounts of particles showing different color and texture. Whereas this may have resulted from the presence of different lithofacies within the 3 m sampling intervals, or cuttings were mixed during the drilling, particles of the dominant rock type were picked for the analyses. This procedure agrees with petrographic examination in which the microfacies were interpreted based on the dominant type of particles. In addition, when the particle size was between medium- to coarse -grain size, cuttings were put in a petri dish and particles were picked using a tweezers under a binocular microscope.

It is not unusual for drilling mud to become consolidated on the surface of cutting particles if the cuttings are not washed after recovering them from shale shaker. Therefore, to avoid contamination, all of the picked particles were submerged in water for a day, then washed and rinsed in e-pure water and kept in an oven for a day at 100 °C.

A crust of bitumen covered some of the cutting particles (Fig. 10), so a special treatment procedure was followed. The cuttings were ground to a fine sand size using a ceramic mortar and pestle, and then they were put in round bottom flask that was filled with Dichloromethane. The flasks were put in a sonicator water bath for 30 minutes, and after that, the samples were filtered and washed with methanol and e-pure water. The samples were kept in an oven for a day at 100°C to dry.

Eventually, all the rock samples were ground to a fine powder and each was homogenized using a ceramic mortar and pestle. One gram of the rock powder was put in

vials and sent to the University of Michigan Isotope Laboratory, and the remaining powder was kept in vials for XRD and ICP-AES analyses at the University of Houston.

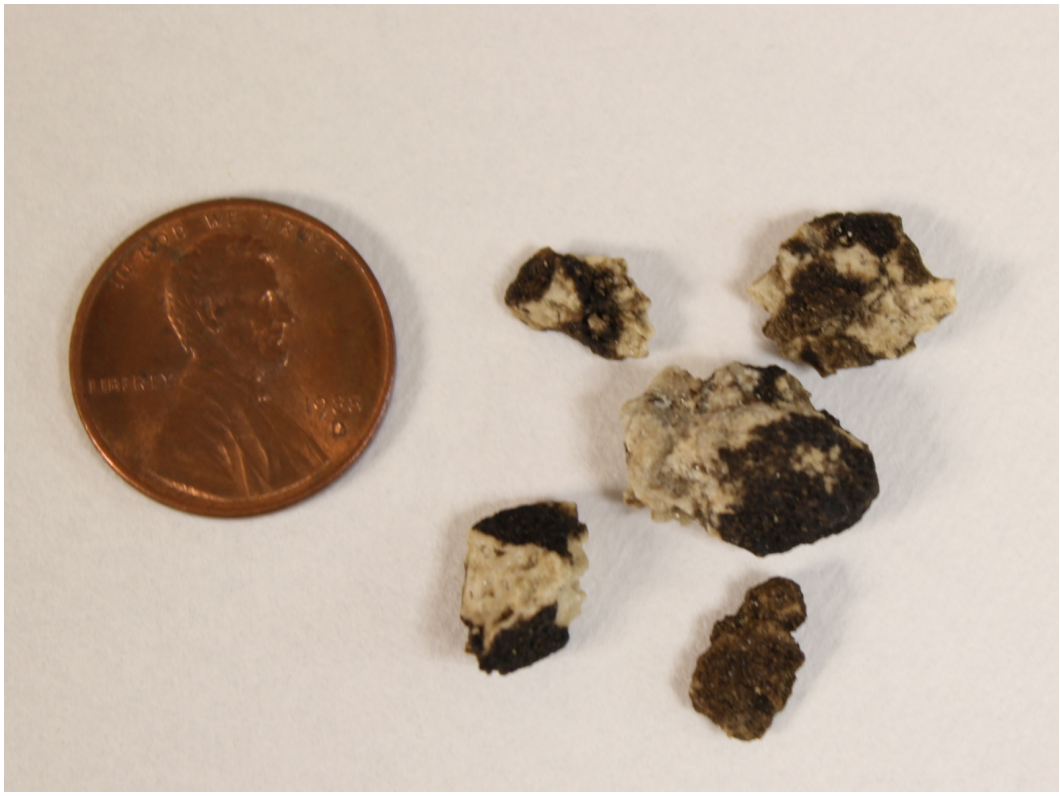

**Figure 10** Cutting sample from Nahr Umr No.1 well with bitumen crust covering them.

## 2.4 X-ray Diffraction Analyses

Previous studies of the mineralogical composition of Paleocene-Eocene carbonates have been made in Saudi Arabia, Qatar, and Oman (e.g., ÇaĞtay, 1990; Alboukhary and Alsharhan, 1998; Holail et al., 2005; Hersi, 2011). No geochemical studies have been published about the Paleogene carbonates in southern Iraq. X-ray diffraction is a quick method to determine the mineralogical composition from a small amount of whole rock powder.

To avoid powder agglutination and remove volatiles, adequate amounts of powder were put in an oven at 110°C overnight. Plastic X-ray sample holder was used, and the sample powder was flattened using a slide glass (Fig. 11). In order to monitor any drift in the machine, a pure quartz sample, a laboratory standard, was analyzed between every 3 samples. The X-ray diffraction analysis was conducted in the Texas Center for Superconductivity at the Universioty of Houston using Siemens D-500 Diffractometer with Cu-K $\alpha$ radiation. The machine was set to scan 2θ from $5^{o}$ to $65^{o}$ with step size of $0.03^{o}$ at the rate of 1 step/second. Tube current and voltage were set to 40 mA and 30 kV.

The X-ray diffraction analysis was conducted to qualitatively determine the carbonate, evaporite, and clay minerals, and to chose the analytical procedures for stable isotope spectrometry and ICP-AES that vary based on mineralogical composition.

The mineralogy of carbonate rocks can be subject to multiple phases of diagenetic alteration, and X-ray is commonly used to identify carbonate minerals. Major peaks for the analyzed samples were interpreted using the X'Pert HighScore Plus software, and major dolomite peaks are predominantly represented in the samples. The mineral

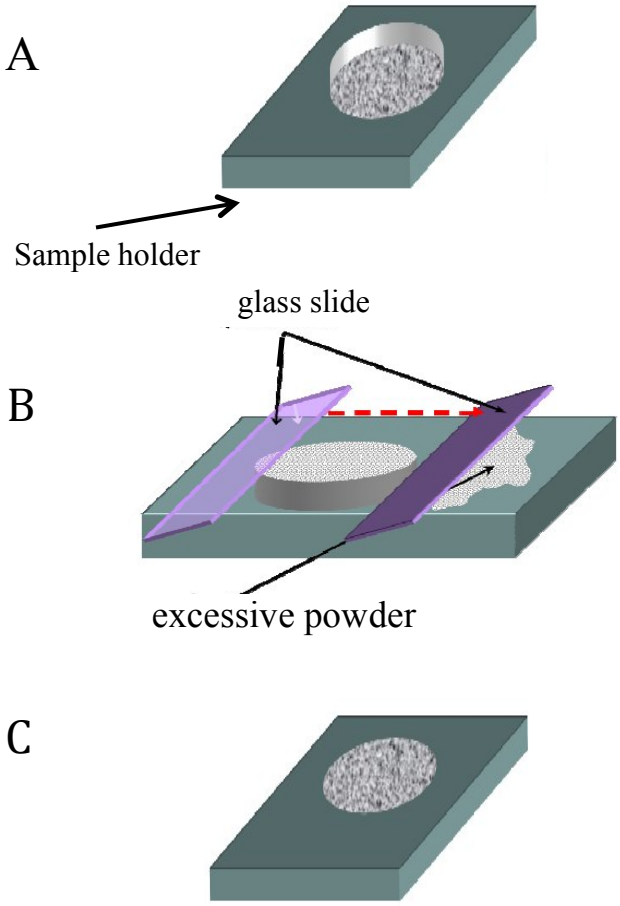


**Figure 11** Diagram showing the procedure for filling the XRD plastic sample holder with rock powder: (A) Empty sample holder, (B) filling sample holder, (C) filled sample holder (modified from www2.arnes.si).

dolomite is stoichiometric with mole % Ca:Mg of 1:1. However, X-ray data for Phanerozoic dolomites all over the North America show non-stochimetric dolomite with mole % $CaCO_3$ range from 48 to 57. Two well defined modes at 51 % $CaCO_3$ (nearly stoichiometric dolomite) and 55 % $CaCO_3$ (distinctly calcian dolomite) were observed (Sperber et al., 1984). The d104 peak is used to determine mole % $CaCO_3$ (Lumsden, 1979) and mole % $MgCO_3$ (Goldsmith et al., 1961). The quantitative application of X-ray data has several shortcomings resulting from errors in both peak intensity and area. One of the major problems is the preferred orientation of the sample powder that results in different peak intensities for each sample depending on their orientation (Reeder and Sheppard, 1984). In addition, heterogeneous particle size and structural damage to mineral crystals from grinding can alter peak intensities at different scales (Gavish and Friedman, 1973). Another systematic error is caused by the changes in lattice spacing due to the substitution of other cations for $Ca^{2+}$and $Mg^{2+}$, particularly $Fe^{2+}$ and $Mn^{2+}$ cations (Goldsmith and Graf, 1958).

The degree of order in dolomites is another important mineralogical characteristics that can be studied using X-ray analysis. A well-ordered dolomite is made up of cation layers of calcium and magnesium alternating with each other with $CO_3$ layers in between them. The degree of order was attained from the ratio of the 015 peak intensity to the 110 peak according to Goldsmith and Graff's (1958) method. The degree of order is related to stoichiometry and crystal size, that is, the more ordered dolomite, the more stoichiometric and bigger the crystal size (Sperber et al., 1984). Because measuring the mole % for $CaCO_3$ and $MgCO_3$ is prone to systematic and analytical errors mentioned above, the X-ray analyses results were qualitatively interpreted to provide an

initial idea about the mineralogical content, and the concentration of the major elements (Ca and Mg) were measured by ICP-AES.

### 2.5 Major and Trace Element Analyses

The diagenetic effects on the Paleocene-Eocene carbonate rocks were observed from petrographic examinations. Therefore, twenty-six samples with distinctive petrographic texture were chosen for elemental analysis to find the chemical attributes of different microfacies. The concentration of major ($Ca^{2+}$ and $Mg^{2+}$) and trace ($Sr^{2+}$, $Na^{2+}$, $Fe^{2+}$, and $Mn^{2+}$) elements were measured by ICP-AES. The sample solution preparation method was modified from Smith (1994) and Xia (1995) that were established to analyze REE in igneous rocks.

Rock powders prepared earlier (see section 2.2) were heated in an oven overnight at 110°C to remove volatiles. To avoid contamination, all of the of the plastic wares used during the analyses were submerged in a glass beaker filled with 8 N nitric acid and put on a hot plate for 24 hours at 100°C, after that, the plastic wares were rinsed with e-pure water and stored in zipper plastic bags. For each sample, 0.2 g of sample powder was dissolved in 100 ml 1 N trace metal grade hydrochloric acid. Each sample was dissolved in Teflon beakers with a magnetic stirrer for 30 minutes. The solution was filtered, and filter paper was rinsed with e-pure water 3 to 4 times. All of the solution was collected in Teflon beakers and put on a hot plate until all of the water was evaporated and a crust formed. Once a crust formed, 100 ml of 2 N nitric acid was added to a beaker in order to digest the crust and make the final solution for instrumental analysis. The solution had

been stored in polyethylene bottles, and was used for $Sr^{2+}$, $Na^{2+}$, $Fe^{2+}$, and $Mn^{2+}$ elements analyses with dilution factor of 1:500.

Solution for major ($Ca^{2+}$ and $Mg^{2+}$) elements analyses was prepared by mixing 5 ml of the trace elements solution with 95 ml of 2 N nitric acid. The solution was stored in polyethylene bottles, and ready for analyses with dilution factor of 1:10,000.

The sample solutions for both major and trace elements were analyzed using Thermo Jarrel-Ash Atom Scan 25 Inductively Coupled Plasma – Atomic Emission Spectrometer in the Earth and Atmospheric Sciences Department at the University of Houston. Elemental abundance is reported in parts per million (ppm) representing the average of four sequential measurements. Procedure blanks were prepared and analyzed for each element to determine contamination that may have taken place during solution sample preparation. In addition, during the analysis of each element, a standard for the same element was analyzed between every three sample measurements. The standard measurements were used as quality control to correct for machine drift. The precision based on relative standard deviation percentage was <1.7% $Ca^{2+}$, <1.3% $Mg^{2+}$, <2.7% $Sr^{2+}$, <1.9% $Na^{2+}$, <5% $Fe^{2+}$, and <3% $Mn^{2+}$.

**2.6 Oxygen and Carbon Stable Isotope Analyses**

Isotopes are atoms of an element with dissimilar physical properties that resulted from atoms having the same number of protons but a different number of neutrons. The difference in the number of neutrons results in a range of atomic masses from light to heavy, and an accumulation might lose light or heavy isotopes during physical, chemical, and biological processes (Hoefs, 1997).

The isotopic composition for a mineral precipitating from a solution in equilibrium depends on the fractionation factor, which is a representation of isotope exchange during the reaction, and it is expressed by the equation:

$$\alpha_{\text{product-reactant}} = R_{\text{product}} / R_{\text{reactant}}$$

where $R_{product}$ is the ratio of the heavy (rare) to the light (common) isotopes in the product and $R_{reactant}$ is the ratio of the heavy (rare) to the light (common) isotopes in the reactant (Friedman and O'Neil, 1977).

Oxygen and carbon isotopic compositions are measured based on the ratio of the less abundant isotope to the more abundant one, $^{18}O/^{16}O$ for oxygen and $^{13}C/^{12}C$ for carbon. These measurements are reported relative to standards, which is the difference between the sample and a standard (δ value), in parts per thousand (‰). The δ, or delta value is expressed as:

$$\delta_{sample}=(R_{sample} - R_{standard} / R_{standard}) \times 1000$$

where R is the isotopic ratio, that is, $^{18}O/^{16}O$ for oxygen and $^{13}C/^{12}C$ for carbon. Two standards are available for the isotopic ratio of oxygen; the Standard Mean Ocean Water (SMOW) and Vienna PeeDee Belemnite (VPDB). The standard isotopic ratio of oxygen in water is 0.0020052 SMOW, and 0.0020671 VPDB in sedimentary carbonates. The values of oxygen standards can be converted using the equation (Anderson and Arthur, 1983):

$$\delta^{18}O_{SMOW} = 1.03086\ \delta^{18}O_{VDPB} + 30.86$$

On the other hand, the standard of the carbon isotope ratio in the sedimentary carbonates is 0.011237 VPDB.

Dolomite is the main mineral in all of the carbonate samples in this study. The isotopic composition of oxygen in dolomites depends on the isotopic composition of the diagenetic fluid and ambient temperature during dolomitization. At low rock-water interaction ratio, the oxygen isotope ratio of replaced carbonates is considered to have minimum influence on the oxygen isotope ratio in the produced dolomite because the high volume of seawater required during dolomitization. The diagenetic fluid can be a mixture of different waters (i.e., mixed fresh and seawater, hypersaline water, etc.), and $\delta^{18}O$ for a dolomite sample may indicate a certain diagenetic setting (Land, 1983). Temperature highly controls the value of oxygen isotope in dolomite by altering the value of the fractionation factor ($\alpha$) between dolomite and water (Matthew and Katz, 1977). Based on $\alpha_{\text{dolomite-water}}$ values obtained from high temperature experiments, there is around 15 °C range of uncertainty in temperature for a given $\delta^{18}O_{water}$, and around 4‰ range of uncertainty in $\delta^{18}O_{water}$ for a given temperature; in addition, the range of $\delta^{18}O$ dolomite and $\delta^{18}O$ calcite is from about 3‰ to 4‰ at 25°C when of calcite and dolomite coexist in the same rock (Land, 1983).

In contrast, temperature has minor control on the fractionation factor of carbon isotopes in dolomite. The significant parameters are both the mineralogy and $^{13}C/^{12}C$ of the original carbonate and $^{13}C/^{12}C$ of dolomitizing fluid. The low $CO_2$ content in diagenetic fluids compared to $CO_2$ content in carbonate rocks results in minor change in $\delta^{13}C$ in dolomites formed from carbonate replacement. However, terrestrial diagenetic fluids are enriched in organic carbon sourced partially from atmospheric $CO_2$ and more importantly from water percolating through $CO_2$-rich soil horizons. Organic carbon is

enriched in $^{12}C$, thus if organic carbon-rich fluids are incorporated in the solid-solution reaction which leads to dolomitization, the dolomite will have a low $\delta^{13}C$ value (Allan and Mathews, 1982). In general, organic-rich sediments are depleted in $^{13}C$ because $^{12}C$-rich carbon dioxide is a byproduct of bacterial processes and decarbolyxation. Yet, bacterial fermentation can result in $^{13}C$-rich $CO_2$ because of the large fractionation with bacterial methane (Irwin et al., 1977).

Biologically precipitated calcium carbonates are also subject to dolomitization, and because the original carbon and oxygen isotope composition is an important parameter, it is necessary to mention the variation in the carbon and oxygen isotope composition for different calcareous organisms and species caused by the "vital effect". Oxygen and carbon isotopic fractionations are different during processes such as photosynthesis, respiration (Swart, 1983), and rapid growth rate (Ziveri et al., 2003). Therefore, different calcareous organisms produce a wide range of isotopic compositions (Fig. 12). Dolomites with different $\delta^{13}C$ and $\delta^{18}O$ values are produced as a result of the type of dolomitized skeletal sediments, or if the isotopic composition of diagenetic fluid is altered by interaction with dissolved skeletal grains.

In addition to the factors mentioned above, the ocean water has gone through changes in its carbon and oxygen isotopes throughout the Phanerozoic. In relation to this study, the Paleogene Period witnessed major excursions in $\delta^{13}C$ and $\delta^{18}O$ values contemporaneous with major climatic changes (Zachos et al., 2001; Higgins and Schrag, 2006). Phanerozoic $\delta^{13}C$ values in most marine carbonates range from -2‰ to +2‰ PDB (Brand and Veizer, 1981), and $\delta^{18}O$ values are closer to 0‰ with about ±1‰ if marine carbonate is precipitated in equilibrium with seawater (Hoefs, 1997). Veizer and Hoefs

(1976) found that $\delta^{13}C$ and $\delta^{18}O$ values for both limestone and dolomite become lower with increased age. In addition to the type of diagenetic fluid and precursor carbonates, these secular variations are important when oxygen and carbon isotope data are interpreted.

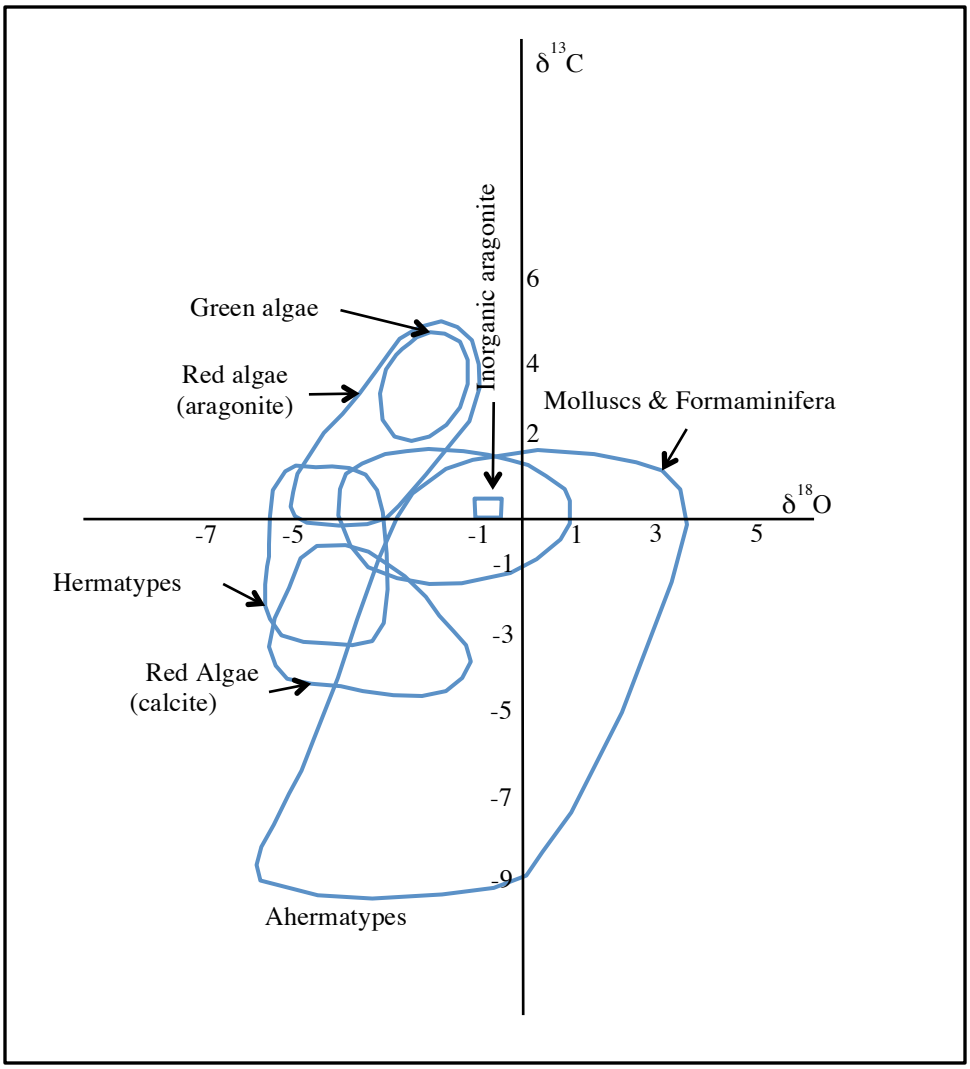


**Figure 12** $\delta^{13}C$ and $\delta^{18}O$ values of different groups of calcareous organism measured from pristine samples from Swart (1983) after Keith and Weber (1965), Weber and Woodhead (1970), Land et al. (1977), Emiliani et al., (1978), and Swart and Coleman (1980).

The isotopic analysis was performed at the University of Michigan Stable Isotope Laboratory. Carbonate powder samples weighing a minimum of 10 micrograms were placed in stainless steel boats. In order to remove volatile contaminants and water, samples were roasted at 200° C in a vacuum for one hour. Samples were then reacted at 77° ± 1°C with 4 drops of anhydrous phosphoric acid for a total of 12 minutes. The reaction took place inside individual borosilicate reaction vessels in a Finnigan MAT Kiel IV preparation device coupled directly to the inlet of a Finnigan MAT 253 triple collector isotope ratio mass spectrometer. NBS 18 and NBS 19 standards were used to correct $O^{17}$ data for acid fractionation and source mixing by calibration to a best-fit regression line. Data are reported in ‰ (parts per thousand) notation relative to VPDB. Different carbonate powder standards are analyzed on daily bases in the lab to monitor the precision and accuracy of data. At least four standards are reacted and analyzed daily. Measured precision is maintained at better than 0.1 ‰ for both carbon and oxygen isotope compositions.

# CHAPTER 3 PETROGRAPHY

## 3.1 PETROGRAPHY

A standard petrographic study was carried out to identify the microfacies for a total of 650 thin sections. The thin sections are from the wells Nahr Umr-1 (500 thin sections) and Zubair-1 (150 thin section). The distance between the two wells is 40 km (Fig. 13), and their stratigraphic correlation is shown in figure 14.

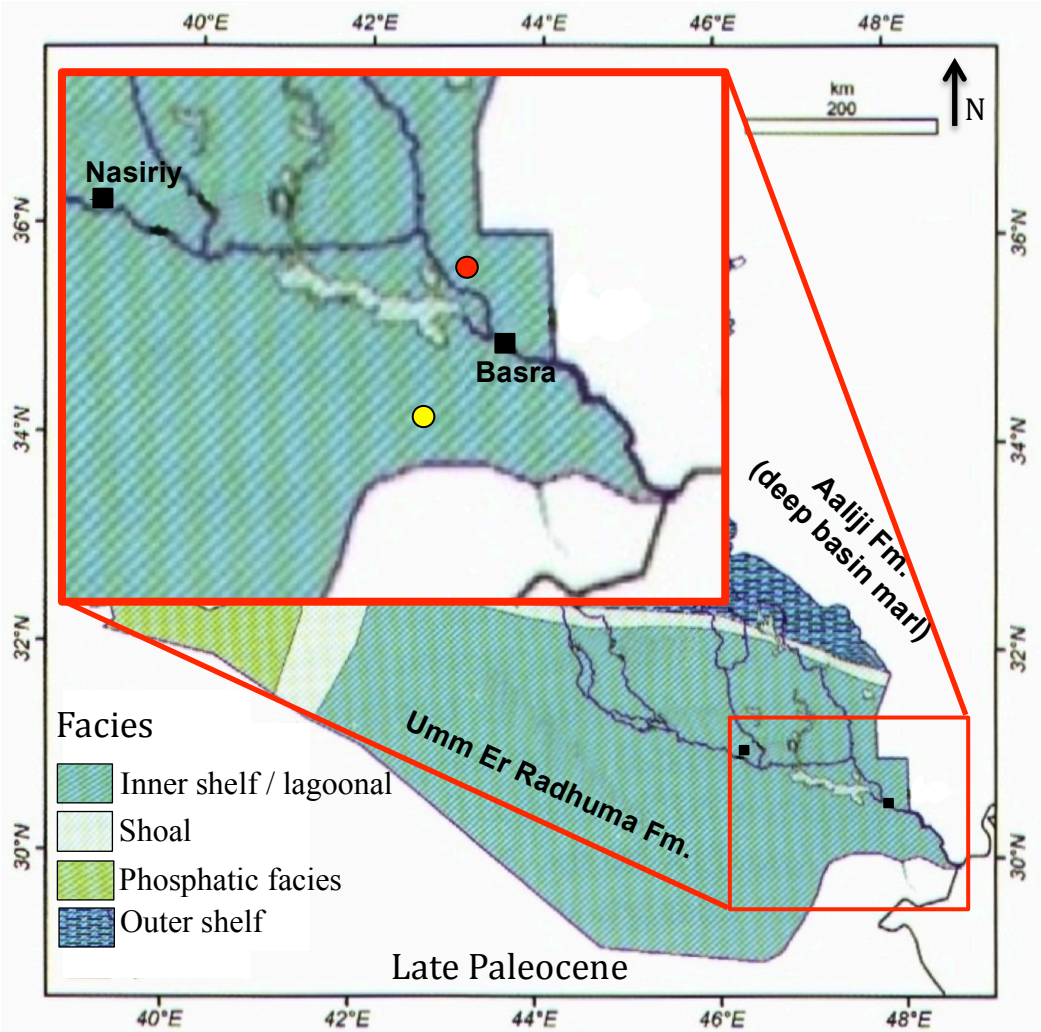


**Figure 13** The locations of Zubair No.1 (yellow circle) and Nahr Umr No.1 (red circle) wells plotted on the Late Paleocene paleofacies map (modified from Jassim and Budday, 2006).

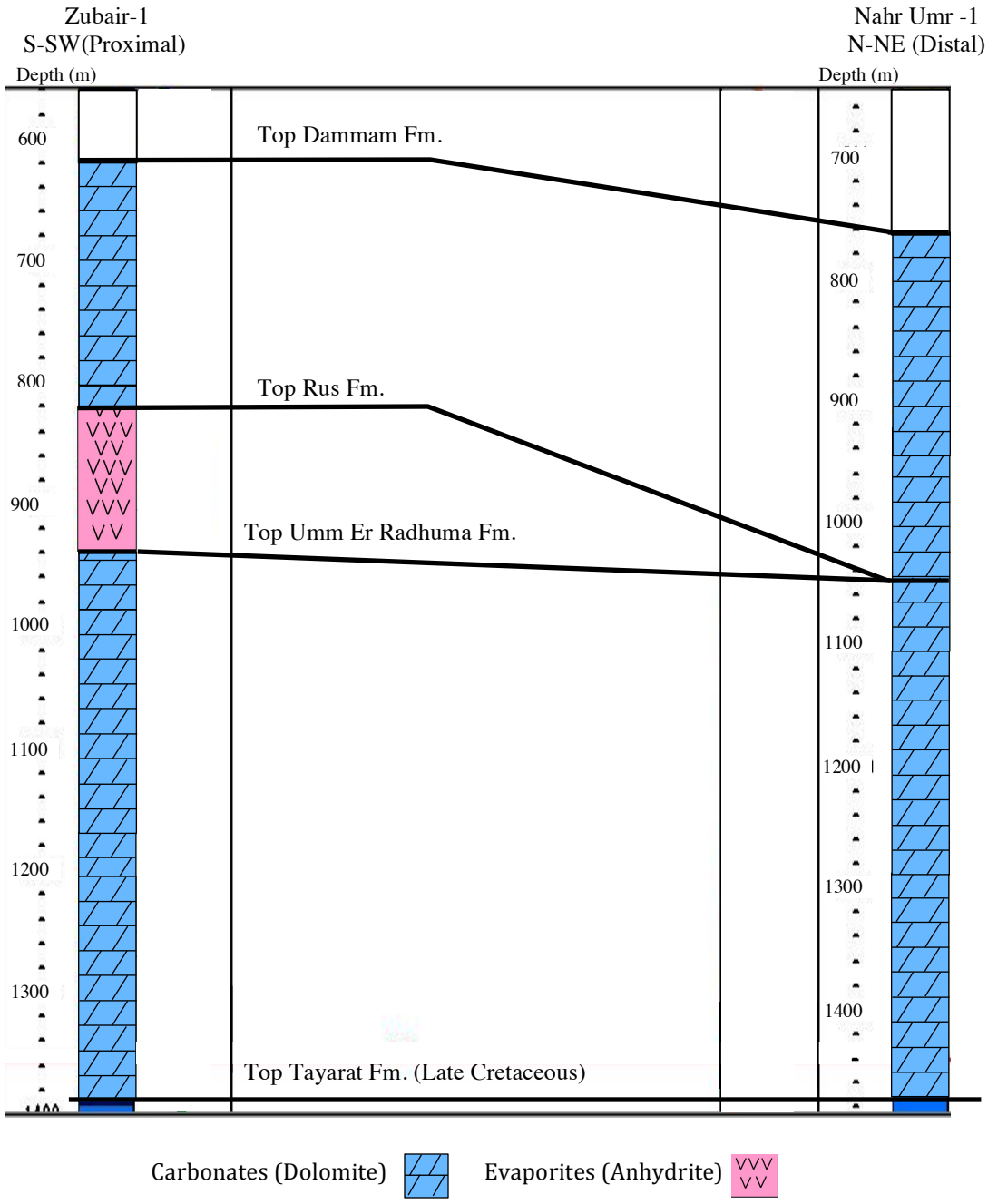


**Figure 14** Stratigraphic correlations between Zubair No.1 and Nahr Umr No.1 wells.

The petrographic attributes for the Paleocene-Eocene carbonate interval, in general, do not exhibit variation in terms of the types of allochems, matrices, and diagenesis. The whole section is dolomitized based on the geochemical analyses for a suite representative of the microfacies. The pervasive and non-mimetic dolomitization has frequently obliterated all of the primary depositional features in most of the section. Thus, seldom are the precursor allochems preserved. The identified allochems are forams and peloids as seen in the incompletely altered samples.

Foraminiferal biodolomicrite (Fig. 15), peldolosparite (Fig. 16), and peloidal dolomite (Fig. 17) are the main types of microfacies that give clues about the original depositional textures. The identification of the original depositional texture is obstructed by dissolution of the allochems and dolomitization of the matrices throughout most of the section. A broad spectrum of allochem-rich to allochem-sparse rocks is the result of variations in the original allochem content and degree of diagenetic alteration. The allochems are mostly held together by micrite size grains, early marine cementation of the allochems was observed only in a few thin sections.

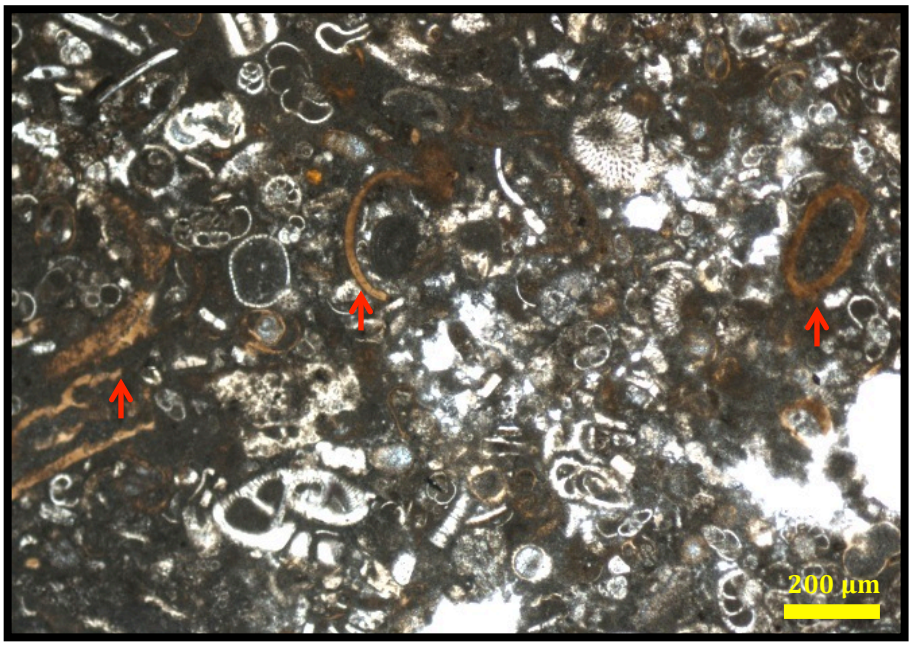


**Figure 15** Photomicrograph of a packed foraminiferal biodolomicrite showing the dominance of rounded calcareous grains, mostly forams. The brown grains (red arrows) are probably phosphatic grains (plain light).

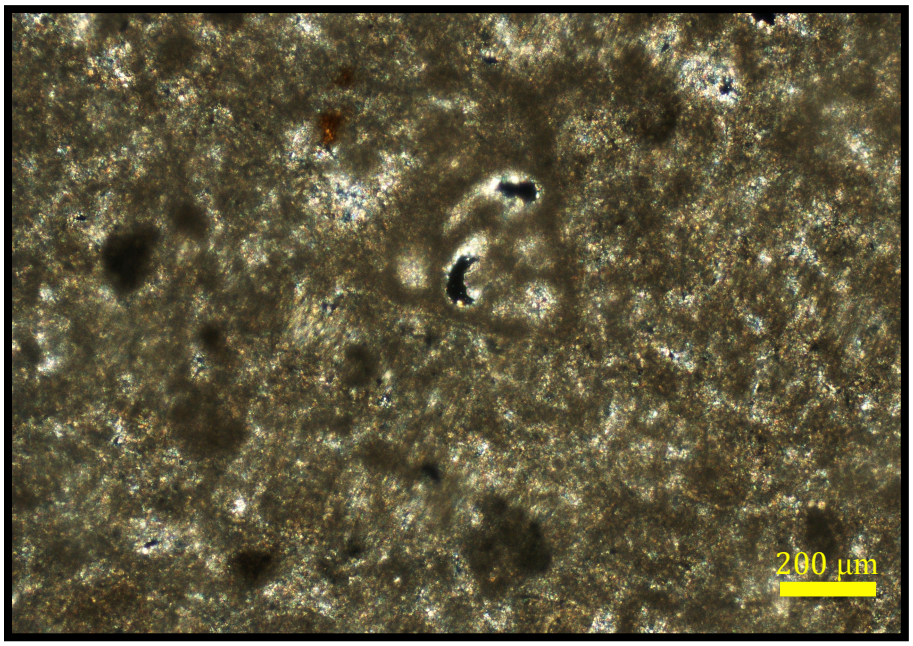


**Figure 16** Photomicrograph for a peldolosparite showing a micritized fossil grain. The matrix is represented by pellets and very finely crystalline dolospar (cross nicols).

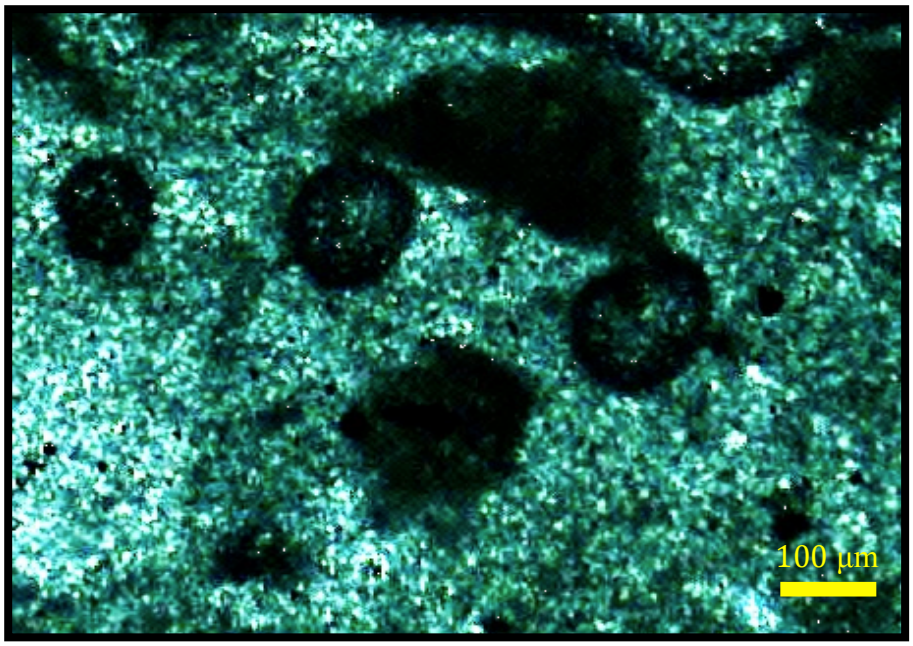


**Figure 17** Photomicrograph for a peloidal dolomite (plain light).

The grain size varies significantly. Foram grains range from tens of microns in diameter to grains large enough to be observed with the naked eye. The variation in grain size is related to the difference in foram taxa. The foram grains are mostly observed based on the presence of moldic pores (Fig. 18) and micritic shells (Fig. 19). The peloids, in contrast, have grain sizes as small as tens of microns but never exceed 500 µm (Fig. 17). The size variation is also the result of different cross-sections through the allochems.

Packed peloidal and foraminiferal biodolomicrite and packed foraminiferal biodolomicrite are more abundant in the distal to the paleoshoreline Nahr Umr No.1 well than the proximal Zubair No.1 well where diagenesis, probably by meteoric water, leached allochems.

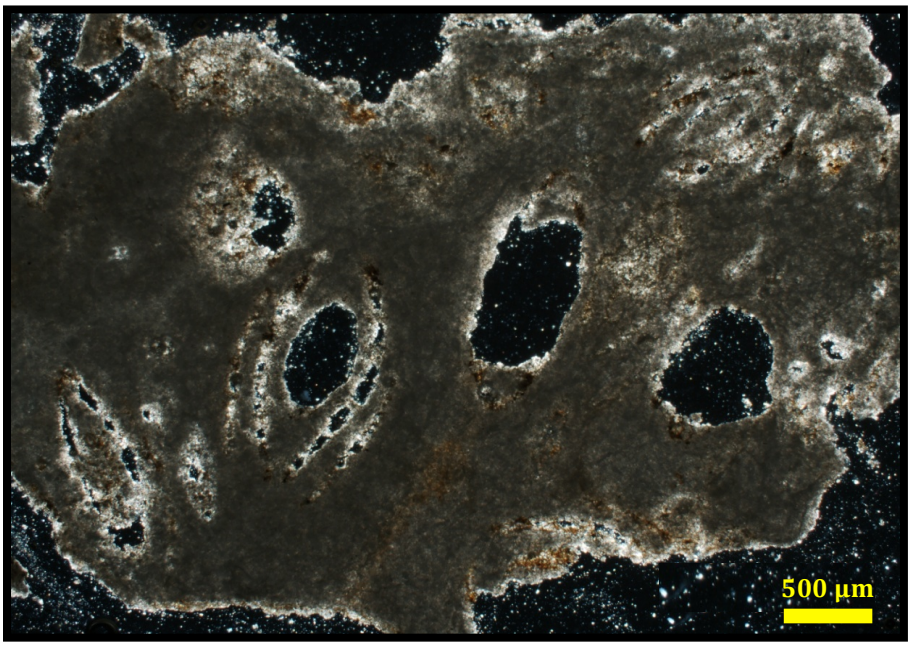


**Figure 18** Photomicrograph of foraminiferal biodolomicrite. The microfacies type was inferred based on moldic pores (cross nicols).

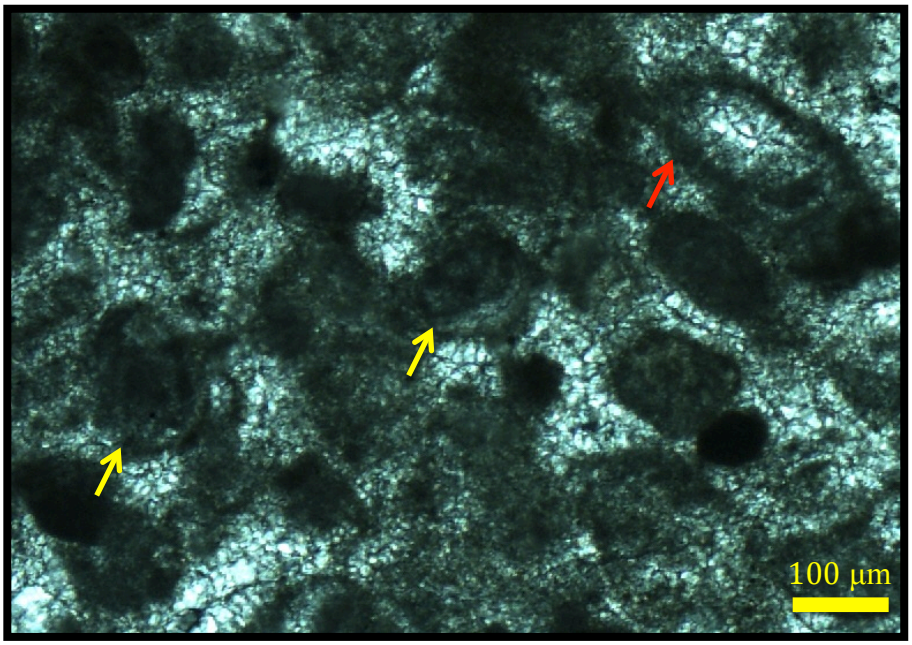


**Figure 19** Photomicrograph of dolomitized peloidal and foraminiferal dolosparite. The foram grains are barely recognized (yellow arrows). The red arrow points to what looks like micritic envelopes (cross nicols).

Where there are no skeletal grains in dolomicrite, a few peloids were commonly observed; however, pure dolomicrite was also observed in some intervals. Rounded pores filled and/or lined with very fine spar crystals were also observed in this microfacies (Fig. 20). Porosity is generally low in this type of microfacies and the pore geometry does not give clues about the preexisting grains.

Dolomicrite is a common microfacies. The crystals for this type of microfacies are aphanocrystalline, i.e., unresolvable under microscope, but 5-10 μm equant crystals are commonly observed within the dolomicrite microfacies (Fig. 21). The rocks show different colors under reflected light (e.g., white, grayish-white, brownish-white, and reddish-white).

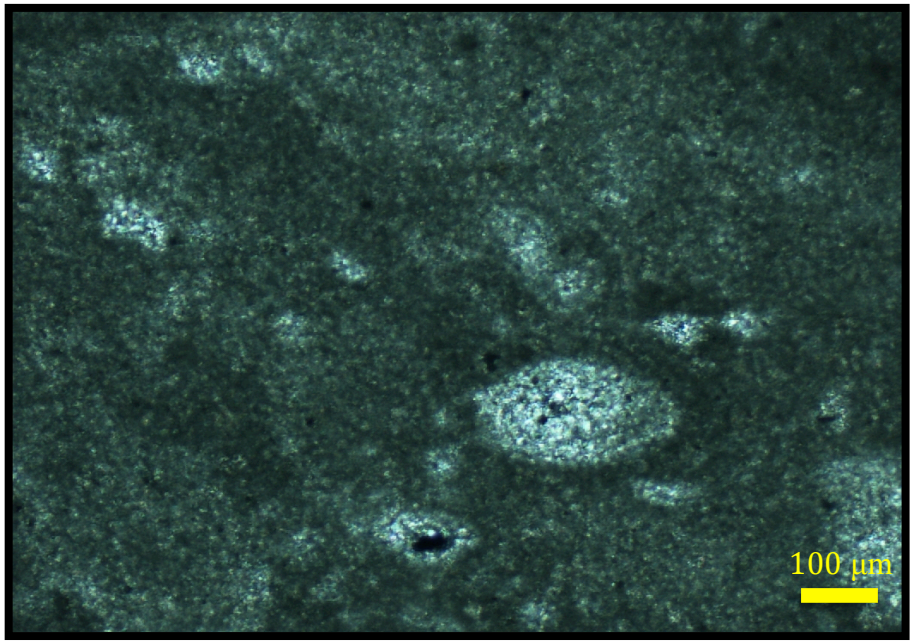


**Figure 20** Photomicrograph for dolomicrite microfacies (cross nicols)

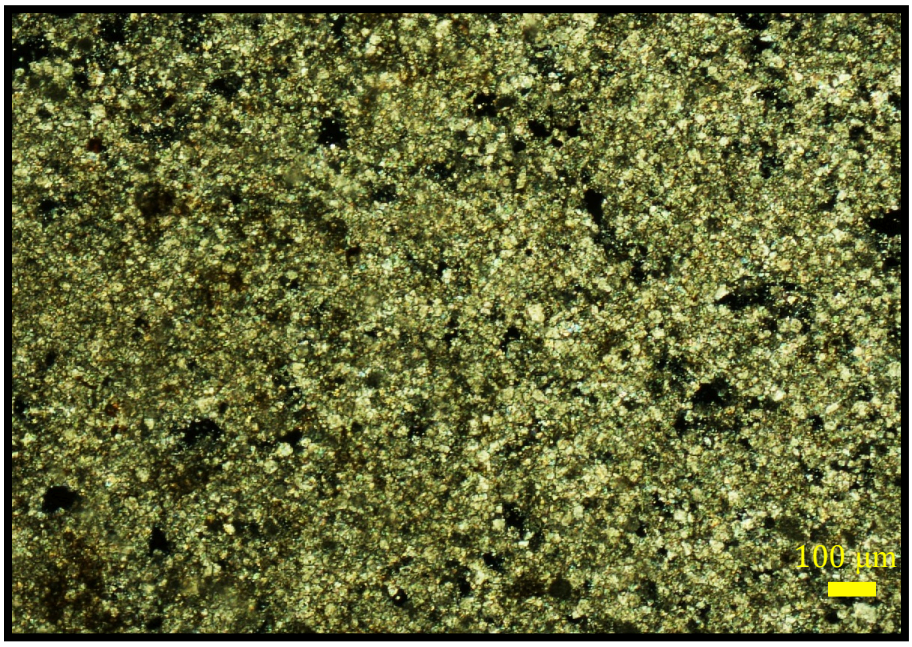


**Figure 21** Photomicrograph for dolomicrite (cross nicols)

Non-carbonate grains within the Paleocene-Eocene section in the two wells included in this study are evaporites and quartz. The evaporite minerals within carbonate matrices are mainly gypsum and anhydrite. They occur as nodules, pore filling crystals, clustering crystals, and replacive crystals (Fig. 22, 23, and 24). Radiating anhydrite crystals are around 300 µm long, and the size of replacive and nodular evaporites highly varies with no regular size because they occupy pores tens of microns in diameter or occur as single grains with size of a few millimeters.

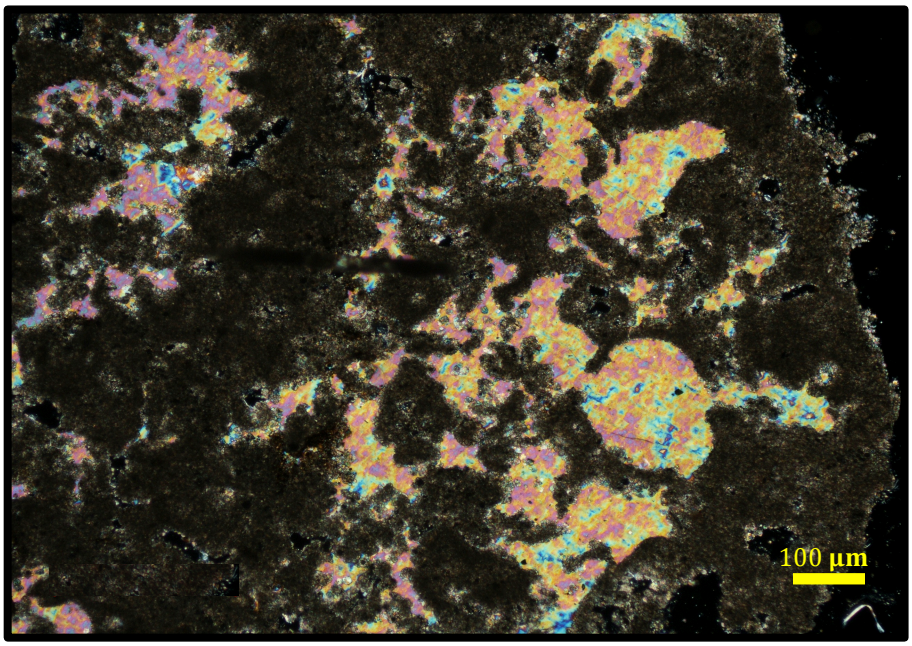


**Figure 22** Anhydrite nodules in dolomicrite (cross nicols).

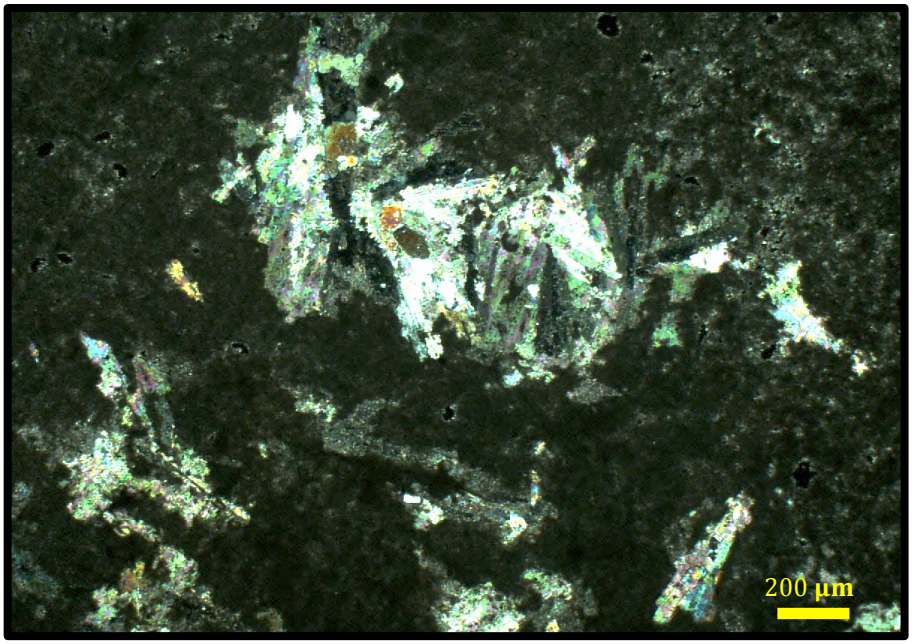


**Figure 23** Radiating anhydrite crystals embedded in dolomicrite (cross nicols).

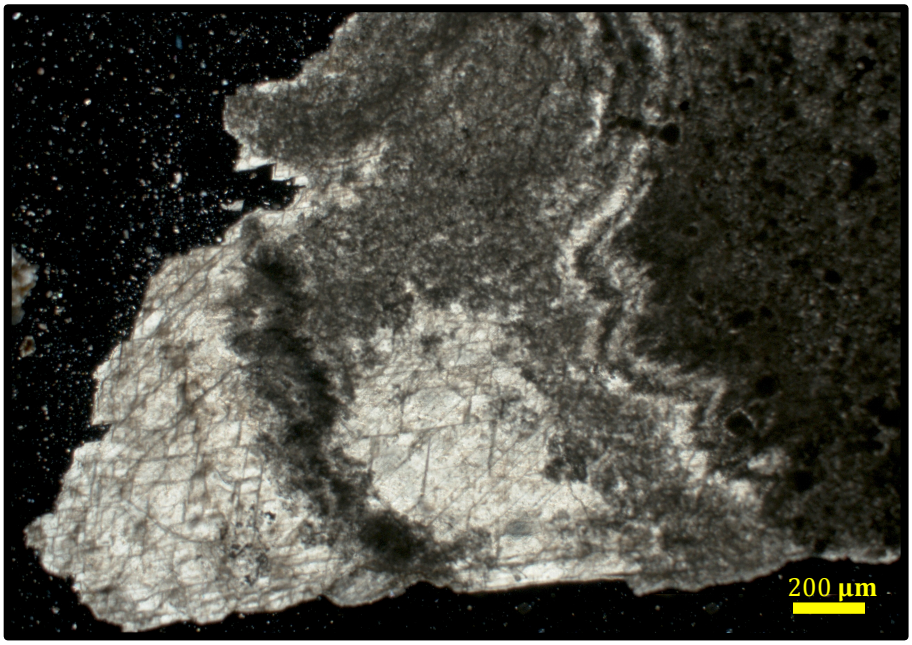


**Figure 24** A photomicrograph showing the replacement of micrite by gypsum (cross nicols).

Quartz crystals were also observed within the carbonate rocks. Authigenic quartz crystals clustering in voids occur in many horizons in Umm Er Radhuma and Dammam Formations. The crystals are subhedral to anhedral and range from 20 to 250 µm (Fig. 25). Quartz crystals show well-developed faces toward free void space, but in general, crystal faces are obliterated because of competition for growth space (Fig. 25). Growth zonation also characterizes the well-developed void filling crystals. The high birefringence of some of the quartz crystals is the result of anhydrite remnants and thicker than normal thin section (Scholle and Ulmer-Scholle, 2003), yet authigenic quartz crystals with typical quartz birefringence also exist (Fig. 26).

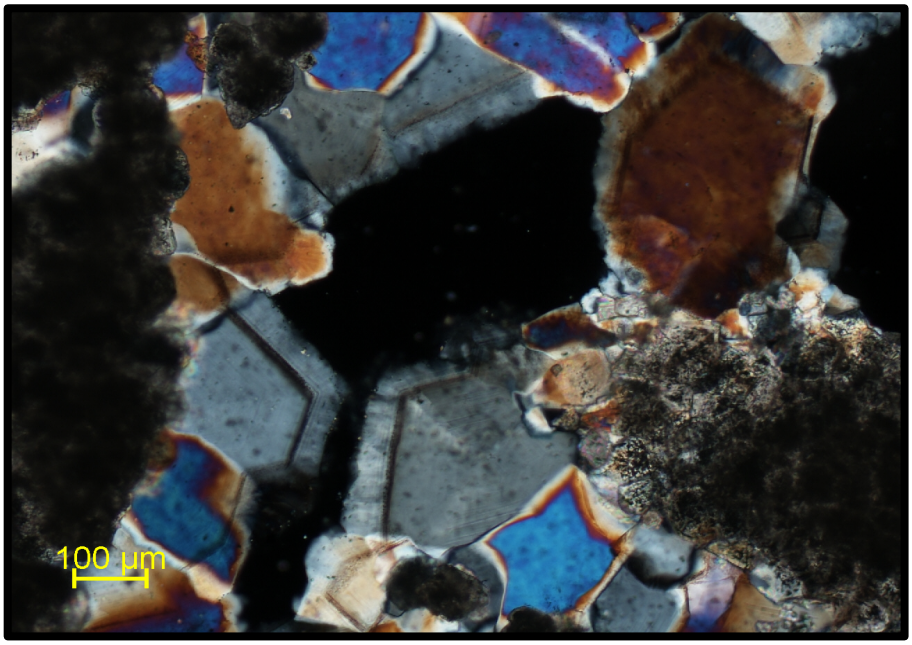


**Figure 25** Photomicrograph of authigenic quartz that precipitated in voids in the dolomite. Notice the well-developed crystal faces and growth zonations (red arrow) where growth space is available. The high birefringence is the result of remnants of anhydrite (cross nicols).

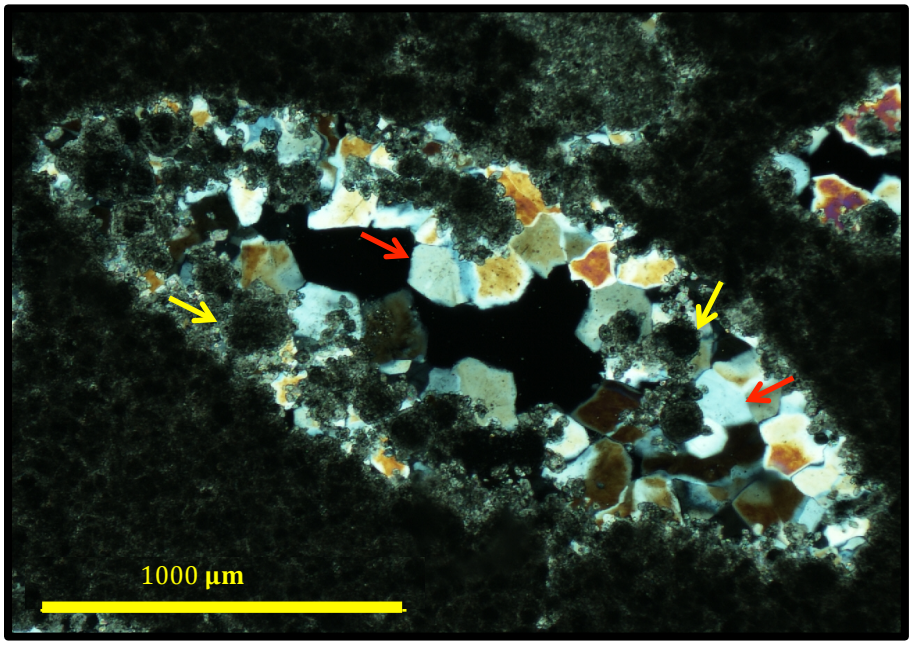


**Figure 26** Photomicrograph of authigenic quartz that precipitated in a moldic pore. The foggy grains (yellow arrows) are remnant dolomite rhombs. Some of the authigenic quartz crystals show normal (red arrows) birefringence in this photomicrograph (cross nicols).

### 3.1.1 Diagenesis

Lithification of carbonate sediments can be early diagenetic processes. Foram and peloid grains throughout the Paleocene-Eocene section are mostly held together by micrite. Isopachous fibrous, bladed, and acicular marine cements are absent within the entire carbonate section, except for a few thin sections from the upper part of Dammam Formation in which isopachous prismatic to equant cement surrounds micritized forams and peloids (Figs. 27 and 28). The crystal size for the equant and prismatic cement is between 5 to15 µm, and surround the whole grain.

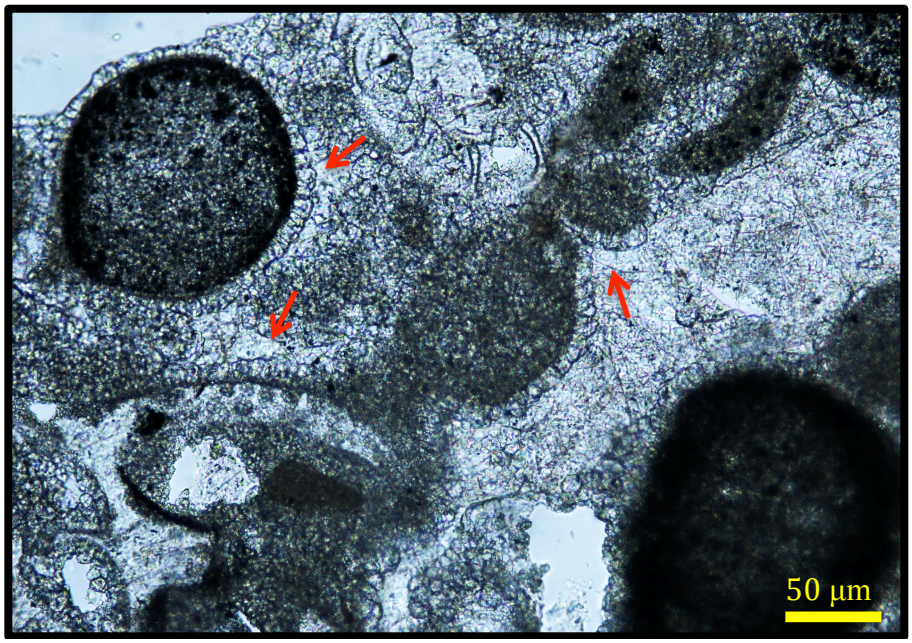


**Figure 27** Photomicrograph showing the isopachous prismatic to equant cement (red arrows) surrounding peloids and micritic relics of fossils (plain light).

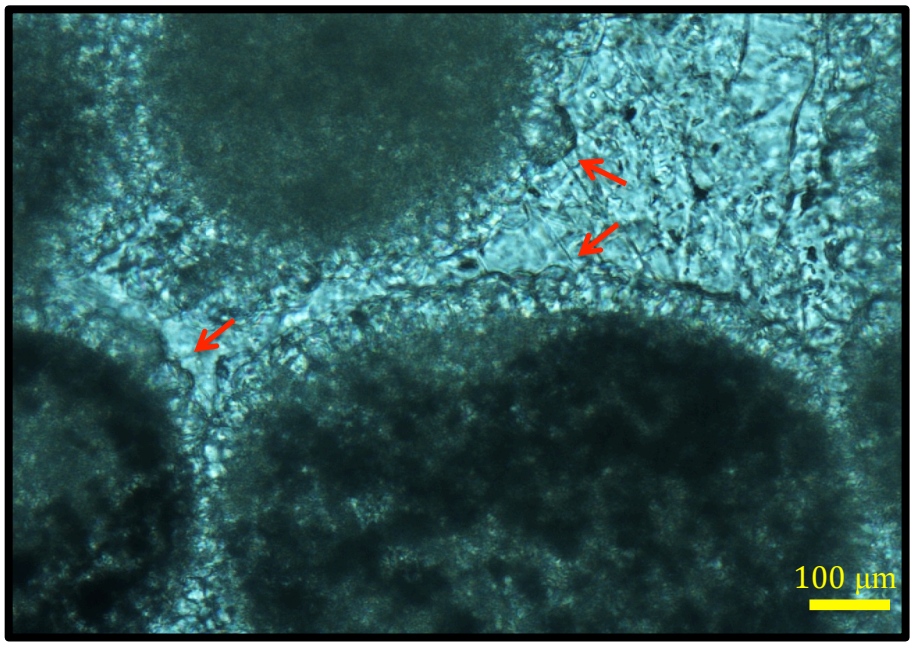


**Figure 28** Photomicrograph showing the isopachous prismatic to equant cement (red arrows) surrounding peloids (plain light).

Destructive diagenetic processes like dissolution and dolomitization are dominant throughout the carbonate section. Thus, it is possible that early allochem-coating cements were destroyed during later diagenesis.

Pore-filling and -lining calcite cements are common types of cement within the entire Paleocene-Eocene section (Fig. 29). The cement crystals are anhedral to subhedral with a broad range of crystal sizes from a few microns to a couple hundred microns. In some thin sections, blocky calcite cement occupies big voids with crystal size around 1000 µm and show growth zonation (Fig. 30).

The presence of pore-filling and -lining calcite cements is not restricted to a particular microfacies or stratigraphic section. They occupy pores in the different dolomites. In addition, the calcite cement does not appear to have replaced the

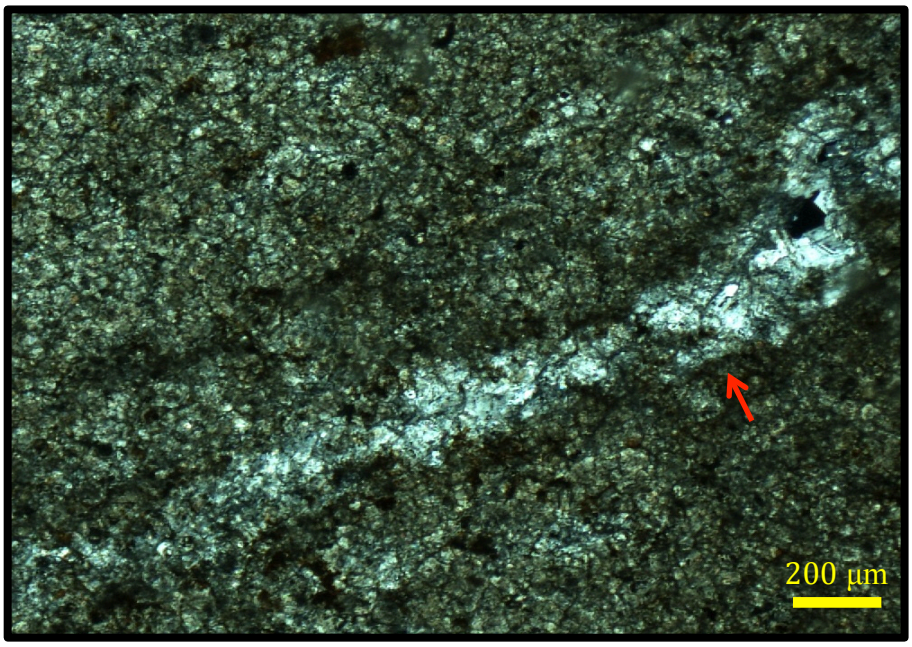


**Figure 29** Photomicrograph showing pore-filling spar (red arrows) within a non-planar finely crystalline dolomite (cross nicols).

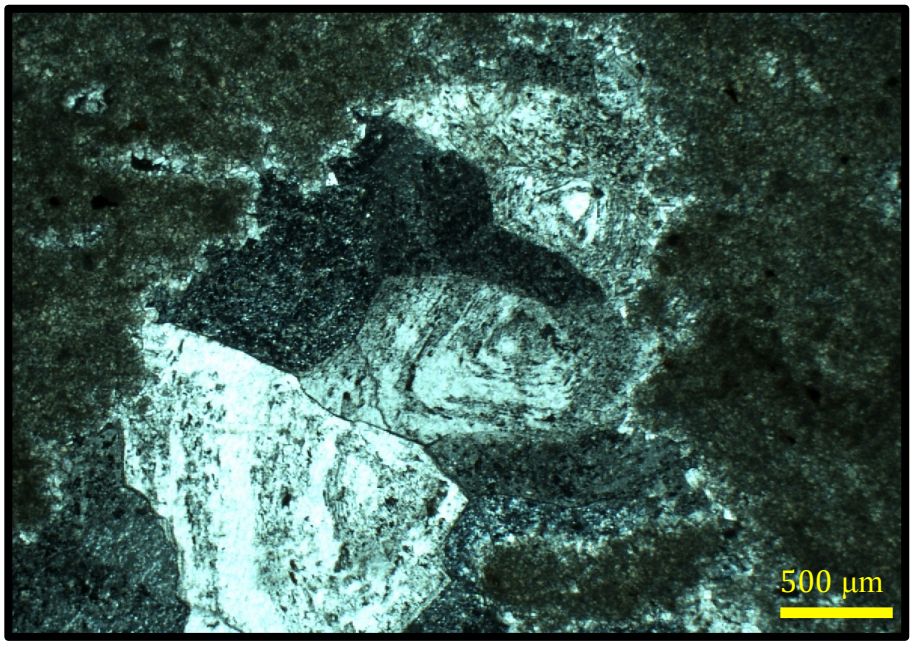


**Figure 30** Photomicrograph of big blocky spar cement filling big voids of a non-planar finely crystalline dolomite. Notice the inclusion-rich zonation within the spar crystals (cross nicols).

precursor grains because the cements generally grow on the inner side of the pore wall toward the center of the intraparticle porosity. Petrographic examination of this cement type suggests that it precipitated during the last phase of diagenesis based on three observations. First, the spar crystals did not replace the pre-existing grains, but they grow on the pore walls. Second, spar crystals never show dissolution features, which implies that they were in equilibrium with last type of diagenetic fluid. Third, the calcite crystals fill or line some of the pores of the pervasively dolomitized rocks.

As mentioned above, forams and peloids were the only observed types of allochems in the Paleocene-Eocene section within the study area. Selective dissolution of calcareous grains is of one the common types of diagenesis observed throughout the carbonate interval and produces moldic porosity. Although it is difficult to know the type of the leached grains, it is believed that the spherical and oval pores were produced from the dissolution of fossils, mainly foraminifera. This assumption is based on two observations. First, when the fossils are preserved, oval and spherical forams, like nummulites and miliolids, and gastropods dominate the entire Paleocene-Eocene interval (Fig. 15). These are also the fossil types of the Paleogene rocks within the study locations (Ziegler, 2001, Jassim and Budday, 2006; Liu et al., 2006) Secondly, relics of the ultrastructure of leached fossils can be identified where the rock is not intensively altered by other aspects of diagenesis, particularly dolomitization (Fig. 18).

The original presence of allochems has significance with regard to the original depositional texture, and it is critical in studying the depositional pattern. Therefore, microfacies were interpreted based on the absence versus presence of moldic pores of the

leached allochems. Moldic porosity is also a result of dissolution of gypsum and anhydrite nodules (Choquette and Pray, 1970), and a micritic limestone formerly rich in evaporite nodules versus one formerly rich in fossils has a completely different implication for interpreting the environment of deposition. The interpretation was made based on the observed evaporite versus fossil relics within a short stratigraphic succession of thin sections in addition to pore size and shape.

The foram grains show micritic shell outlines in many samples (Figs. 31 and 32). The micritic foram relics are valuable because they aided the interpretation of the original depositional texture that is repeatedly hampered by dissolution and/or dolomitization.

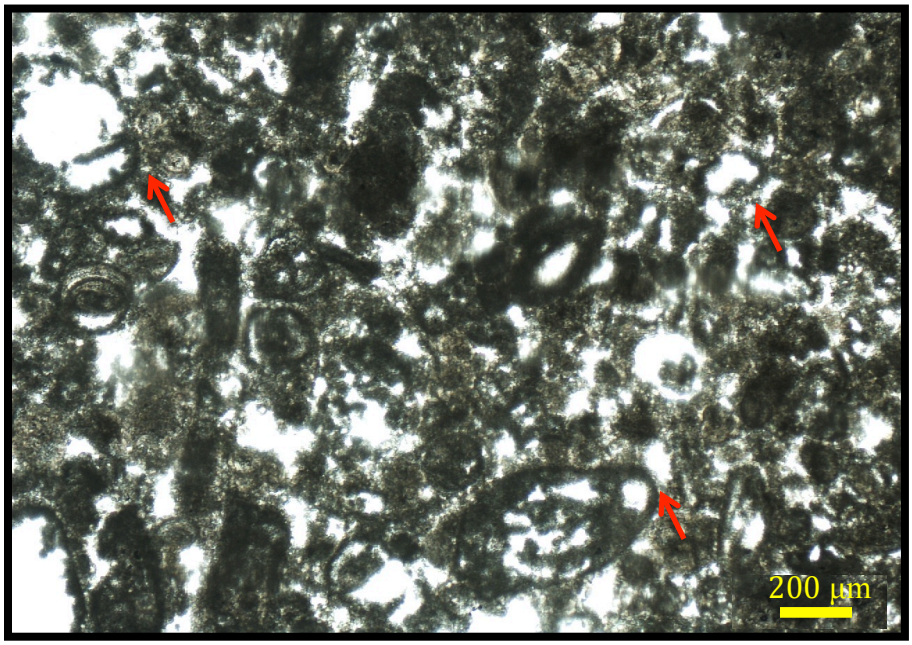


**Figure 31** Photomicrograph for a packed peloidal and foraminiferal biodolosparite showing the micritic outline of the forams (red arrows). Some of the grains show dissolution feature (plain light).

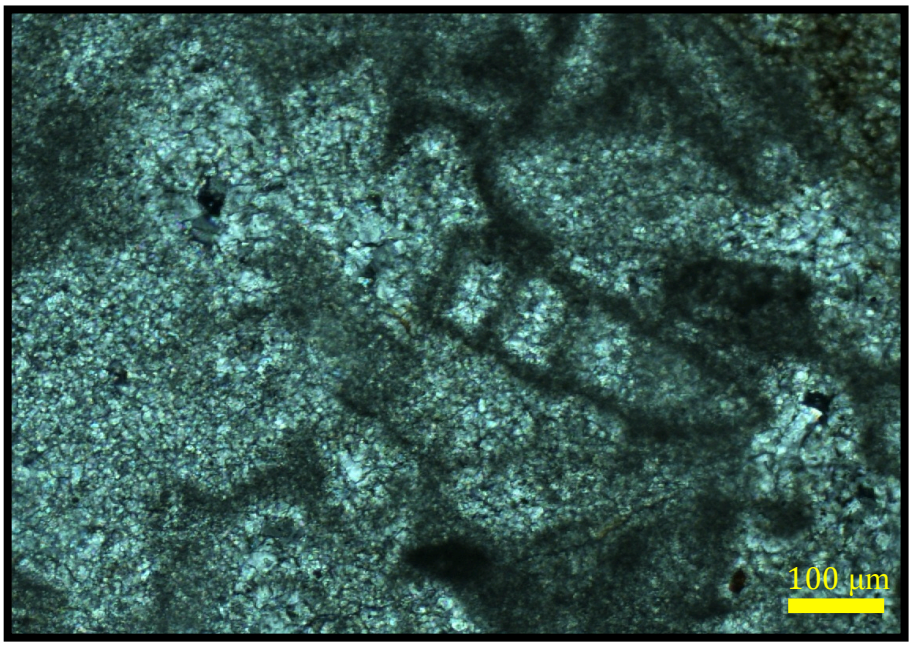


**Figure 32** Photomicrograph for a dolosparite showing the micritic outline of the foram grain (cross nicols).

The presence of micrite around skeletal grains and micritic relics can be the product of micro-borings filled with micrite, or remnants of aragonite and high-Mg calcite cement. No boring features were identified during the basic petrography. Early cementation of carbonate grains by aragonite and microcrystalline high-Mg calcite is common on protected platforms at low latitudes (Tucker and Bathrust, 1990).

The presence of micrite around the skeletal grains, whether it was formed through cementation or micritization, in the dolomitized rock suggests that this process was an early diagenetic one. This is another line of evidence supporting the interpretation that deposition took place in the marine phreatic zone (Longman, 1980).

Later diagenesis included the dissolution of skeletal grains that most probably took place under the influence of meteoric water. Replacement, recrystallization, and neomorphism of unstable marine micrite are also induced by meteoric water.

Anhedral to subhedral spar crystals up to 10 µm (Figs. 33) were assumed to be recrystallized or neomorphic micrite based on petrographic examination. However, geochemical analyses for this microfacies show that it is all dolomite. Dolomite is also the major mineral in the samples of micritic microfacies.

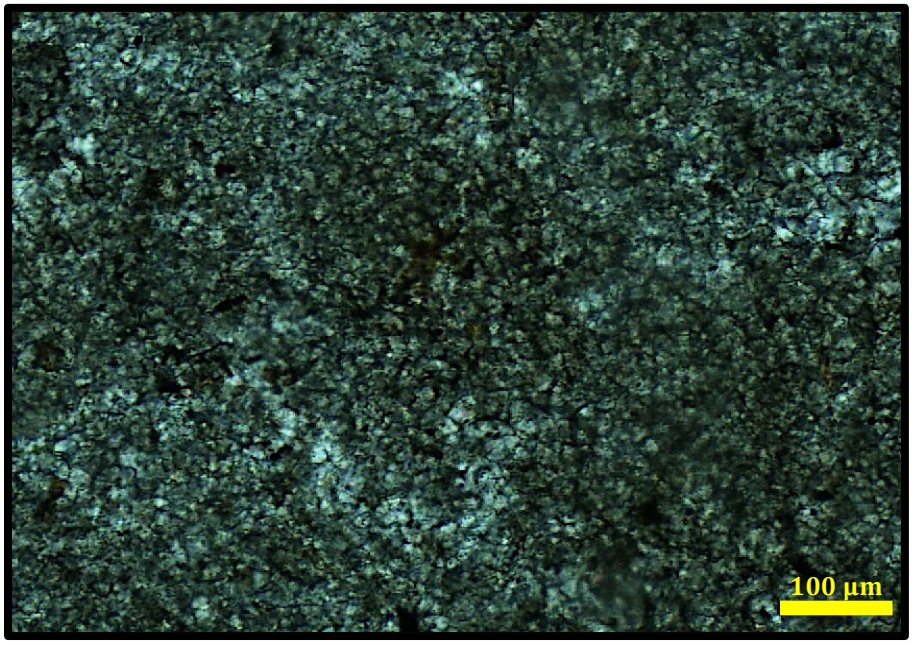


**Figure 33** Photomicrograph for very finely crystalline dolomite. Note that some of the dolomite crystals have identifiable crystals (cross nicols).

Other types of diagenesis are authigenic quartz precipitation, evaporite precipitation, and replacement of carbonates by evaporites.

Silica precipitation is also a significant type of diagenesis. Authigenic quartz is exclusively associated with dolomite facies with sparse anhydrite and gypsum content, and it most commonly occupies vugs and moldic pores in some thin sections (Fig. 34).

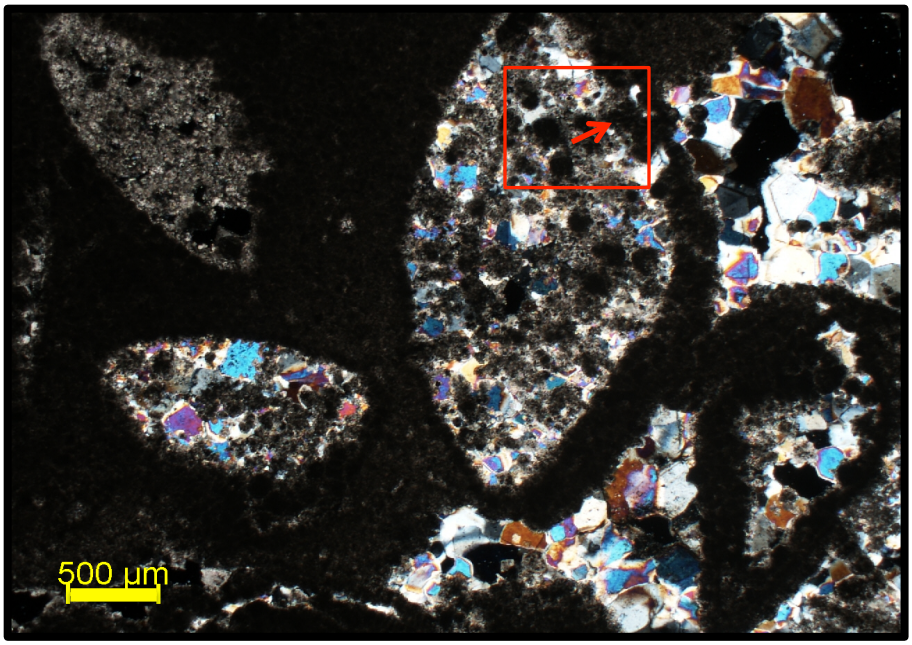


**Figure 34** Photomicrograph of authigenic quartz that precipitated in vugy and moldic pores in the rock. The outer wall of the dissolved allochems is preserved by coarse cloudy dolomite (red arrow). The red square is a close-up shot shown in Fig. 35 (cross nicols).

Authigenic quartz precipitated during and after dolomitization. Figure 35 shows cloudy and coarse dolomite rhombs that preserved the outer wall of the dissolved skeletal grains and experienced dissolution around their rhombic fringes. A different generation of dolomite, with cloudy cores, precipitated in between quartz crystals. Calcite spar cement is also associated with quartz in the voids in the dolomite (Fig. 36). Remnants of anhydrite encased in quartz imply that the quartz crystals most probably had replaced anhydrite.

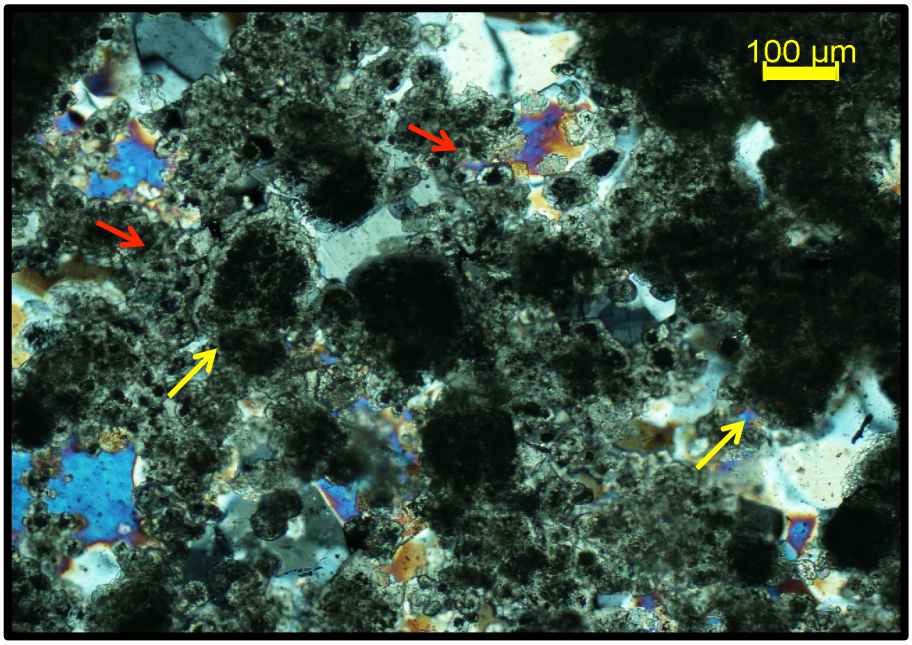


**Figure 35** A close-up view of a void filled with authigenic quartz. Note the presence of coarse cloudy dolomite rhombs (yellow arrow) and another generation of finer-grain dolomites (red arrow) (cross nicols).

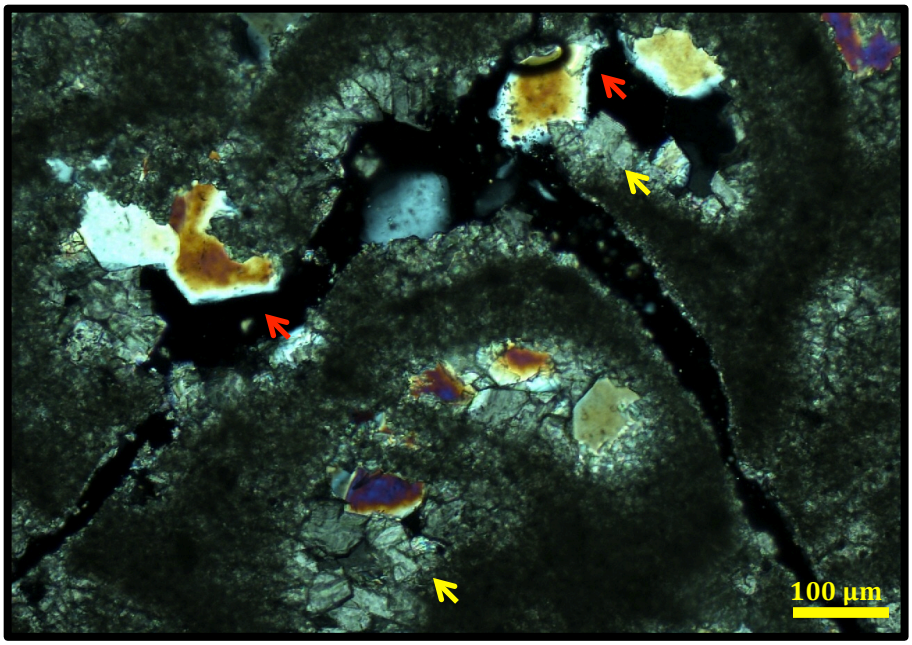


**Figure 36** Authigenic quartz (red arrows) and spar cement (yellow arrows) within dolomite pores (cross nicols).

Petrographic examination does not tell whether the pore filling calcite and dolomite, associated with quartz, were precipitated before or after quartz precipitation. But the coexistence of the different minerals is probably the result of changes in the diagenetic fluid's composition with respect to the precipitants.

The petrographic attributes of authigenic quartz highly resemble authigenic quartz for Pleistocene dolomites from Abu Dhabi described by Chafetz and Zhang (1998). The authigenic quartz in Abu Dhabi is associated with dolomites formed in a sabkha complex depositional environment and the quartz crystals grew in voids of leached dolomite and evaporites under the influence of meteoric water a few tens of meters below the surface.

### 3.1.2 Dolomitization

Petrographically distinctive groups of dolomite crystals repeatedly appear within the Paleocene-Eocene carbonates. The dolomites are classified based on texture and fabric as follow: (1) non-planar (5-20 μm) dolomite, (2) non-planar (20-50 μm) dolomite, (3) planar-s (20-50 μm) dolomite, (4) planar-s to non-planar (50-100 μm) dolomite, (5) dolomicrite. Figures 37, 38, 39, 40, and 41 represent each group of dolomite, respectively. The dolomite colors for the first three groups above are grayish-white, reddish-white, and brownish-white. The last group, the coarsest one, is brownish-white and cloudy charcoal colors.

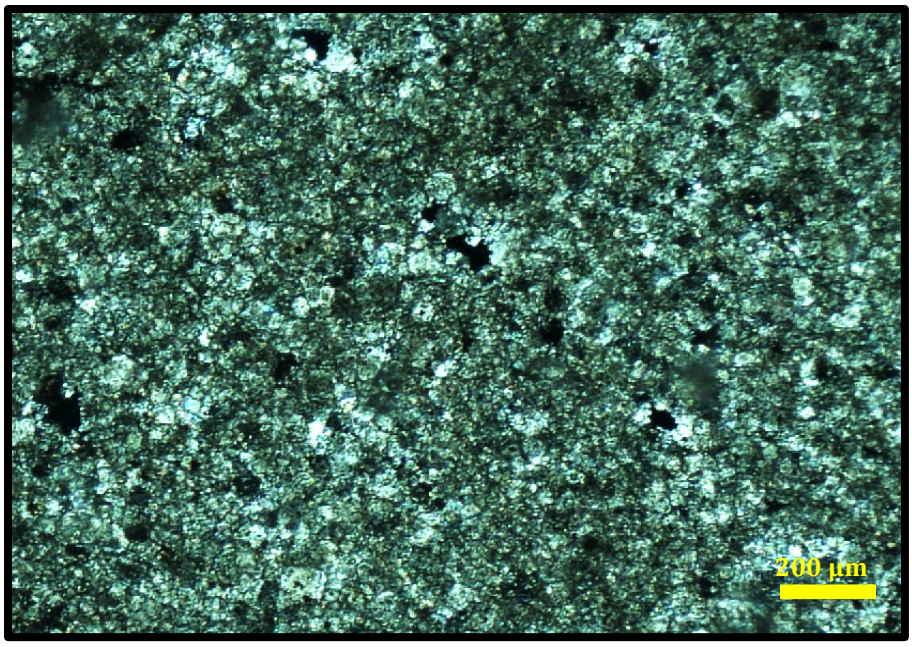


**Figure 37** Non-planar very finely to finely crystalline (5-20 μm) dolomite (cross nicols).

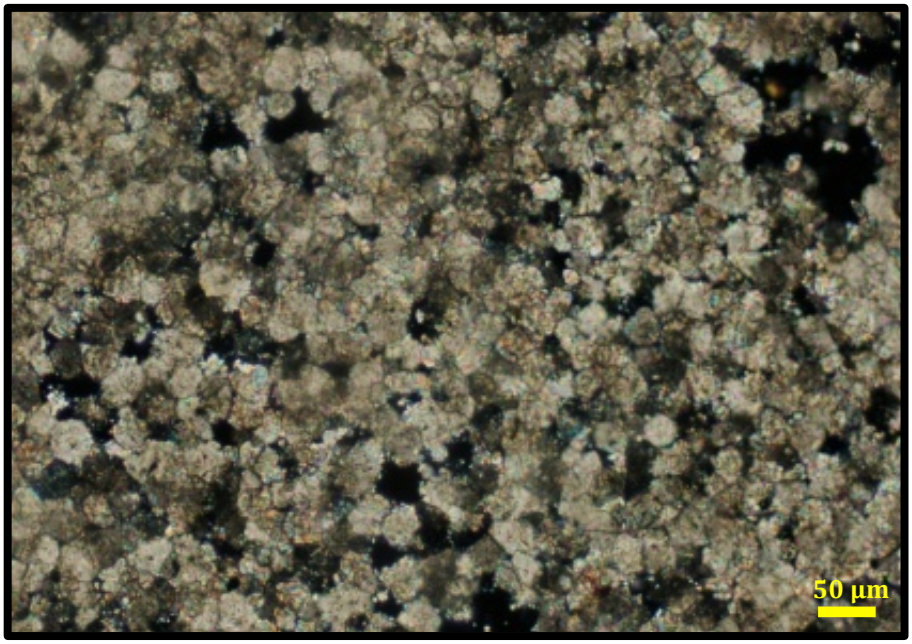


**Figure 38** Planar-s finely crystalline (20-50 µm) dolomite (cross nicols).

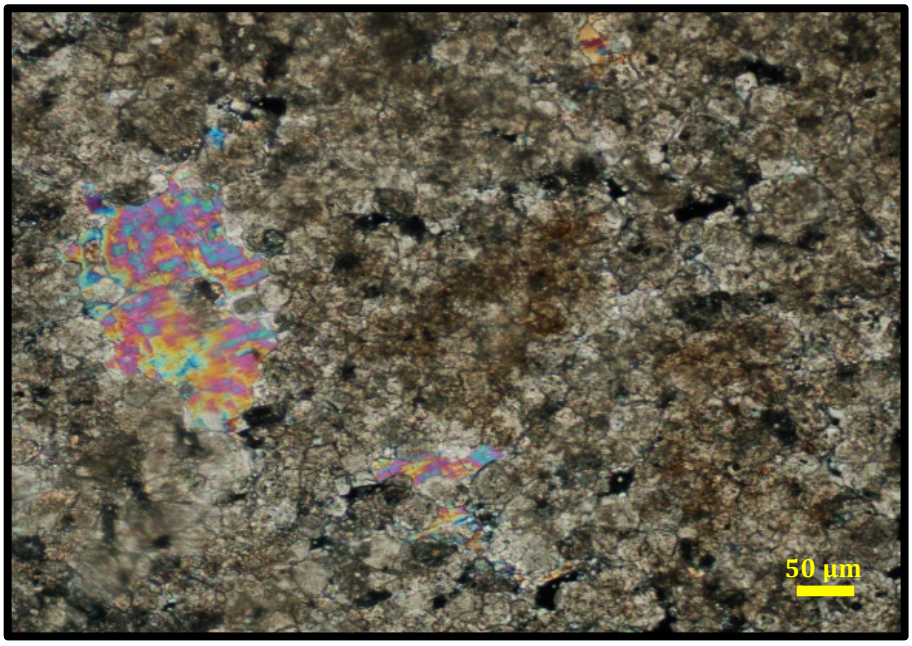


**Figure 39** Non-planar finely crystalline (20-50 µm) dolomite with anhydrite filling vugy porosity (cross nicols).

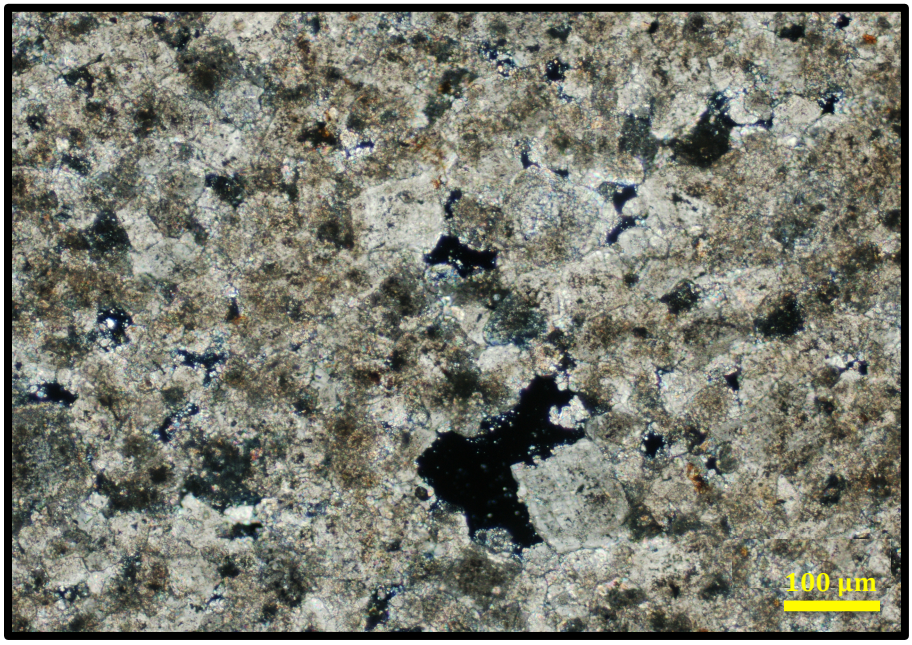


**Figure 40** Non-planar finely to medium crystalline (50-100 µm) dolomite. Some of the coarse dolomite rhombs have planar faces that resulted from growth into void space (cross nicols).

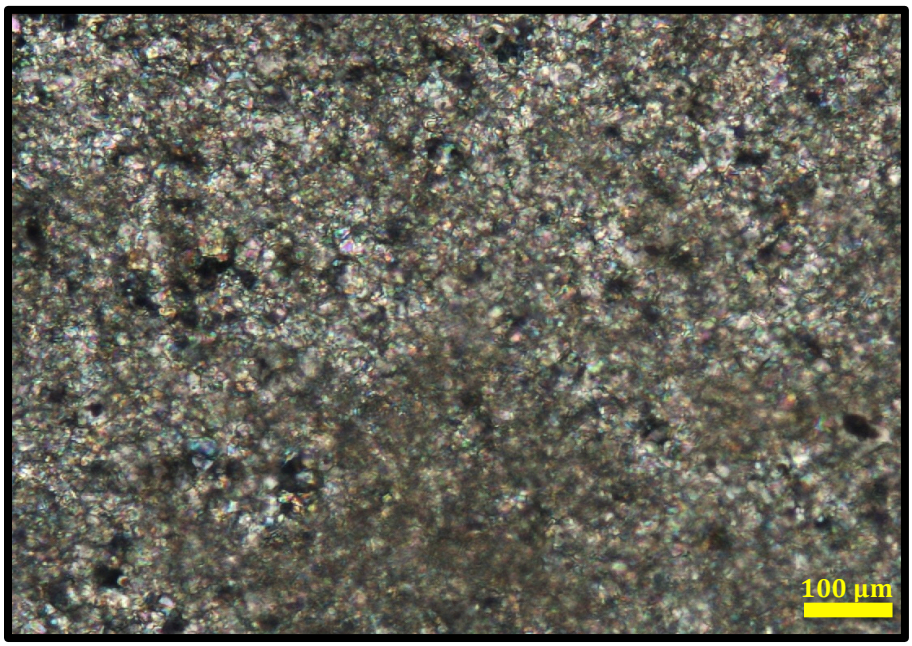


**Figure 41** Photomicrograph of dolomicrite (cross nicols).

Dolomitization is mainly pervasive and fabric destructive, however, where allochems have been preserved, they are included in the dolomite microfacies name (e.g., non-planar (20-50 μm) bioclast-rich dolomite). In addition, dolomites with micritic grain size were identified based on geochemical analysis. This microfacies was called dolomicrite.

Pore-filling evaporites and evaporite nodules were frequently observed within all of the dolomite groups. The evaporites commonly dominate the upper part of the dolomitized horizons. Pore-filling authigenic quartz is generally associated with relatively coarse and porous dolomites. In addition, pore-filling and -lining calcite spars were observed within all of the dolomite groups. The presence of spar cement is not common, and there is no regular relationship for its existence or non-existence, but in general, the bigger the pores, the coarser the spar crystals (Figs. 29 and 30). Moreover, it can be assumed that the distribution of the spar cement is highly controlled by the circulation efficiency and availability of diagenetic fluids since it fills and lines pores in the same rock (Fig. 42). In some thin sections, authigenic quartz and calcite spar crystal mutually fill the pores in dolomite. Authigenic quartz and dolomite rhombs, that differ from the main dolomite type in the rock, fill pores. Both pore-filling spar and dolomite were precipitated before or after quartz precipitation because they are intergrown (Fig 36 and 37).

Dolomites in both Umm Er Radhuma and Dammam Formations generally share the same features. Two differences were observed relative to the locations of Nahr Umr

No.1 and Zubair No.1 wells. First, gypsum and anhydrite associated with dolomitic facies are more abundant in the proximal Zubair No.1 well compared to the distal Nahr Umr

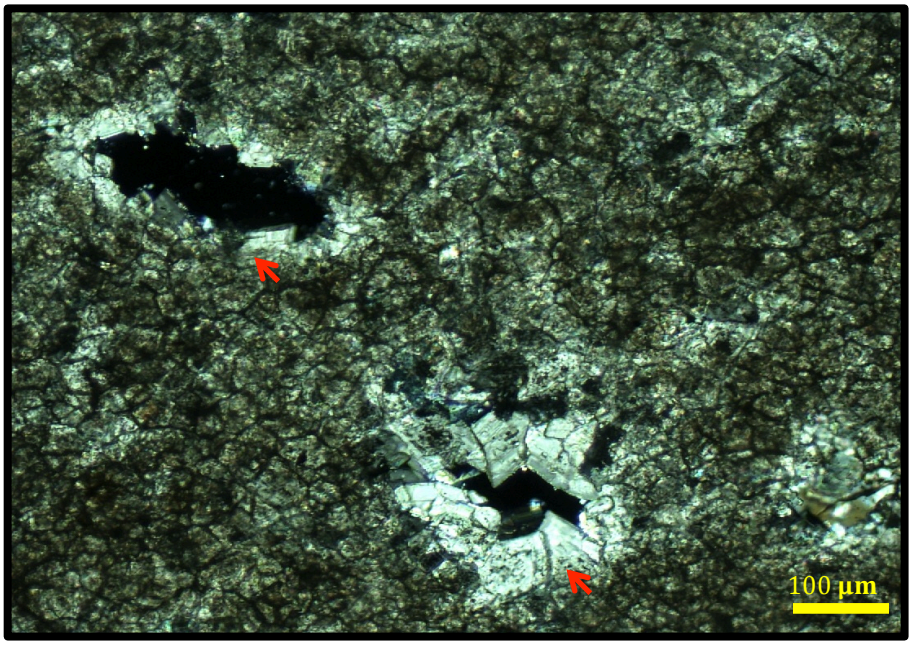


**Figure 42** Pore-filling and -lining spar cement (red arrows) that becomes coarser toward the pore center (cross nicols).

No.1 well. Second, syntaxial dolomite cements are around dolomite rhombs more common in the Nahr Umr No.1 compared to Zubair No.1.

The dolomite groups repeatedly appear in different intervals in the two wells with no regular pattern relative to their vertical succession. This implies that the dolomites were formed in different settings during multiple episodes of dolomitization (Mackenzie, 1981; Chafetz et al., 1999; Jones, 2005; Choquette and Hiatt, 2008).

### 3.1.2.1 Dolomite Fabric

Sucrosic dolomite fabric is the dominant type of fabric in both Umm Er Radhuma and Dammam Formations. Dolomite rhombs are planar-s to non-planar. Non-planar very finely to finely crystalline dolomite replacing micrite was observed in many thin sections (Fig. 43). There is a sharp contact between dolomite and micritic matrix. In some thin sections, some well-developed dolomite rhombs are identifiable away from the contact (Fig. 44).

The crystal–crystal interfaces in the dolomites from the Umm Er Radhuma and Dammam Formations range from planar to non-planar according to Sibley and Gregg's (1987) terminology. The planar fabric is sparse, and it is mainly identified as pore lining- and -filling crystals with dark cores (Fig. 45).

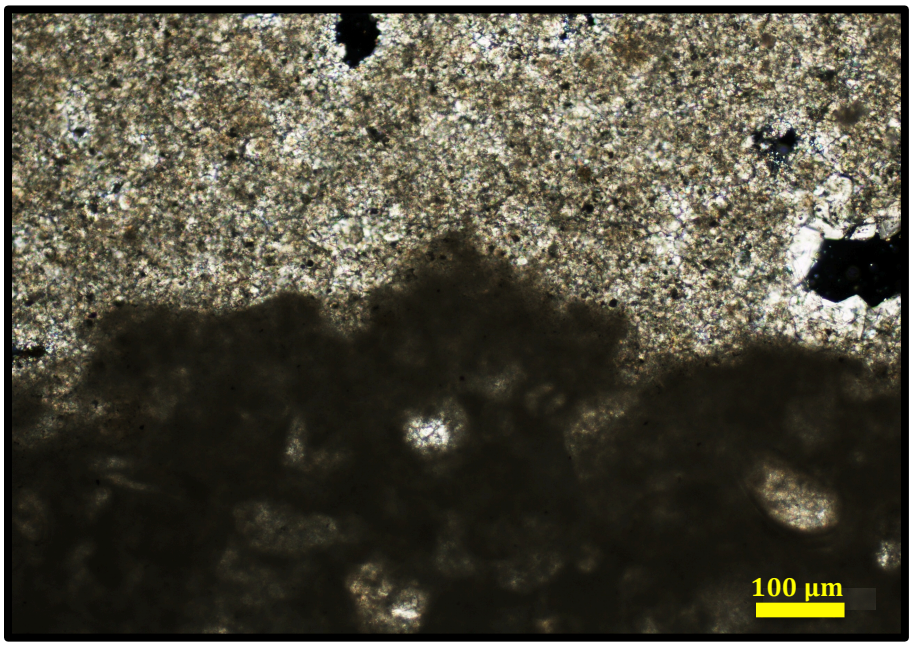


**Figure 43** Non-planar very finely to finely crystalline (5-20 µm) dolomite replacing micrite. Note the sharp contact between dolomite and micrite and coarser dolomite rhombs in pore space (cross nicols).

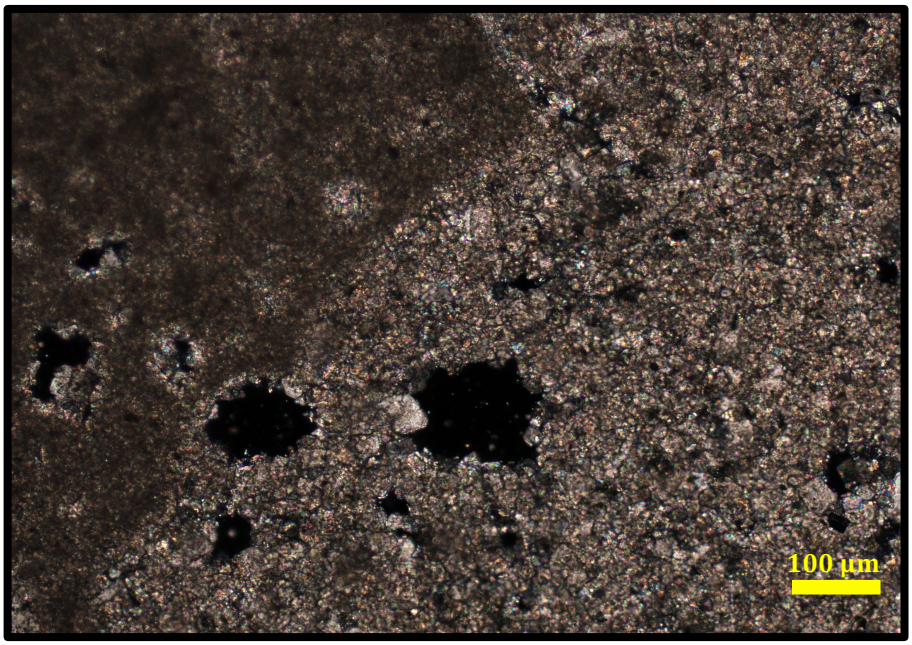


**Figure 44** A photomicrograph of identifiable dolomite rhombs away from the contact in between finely crystalline non-planar dolomite and micritic matrix (cross nicols).

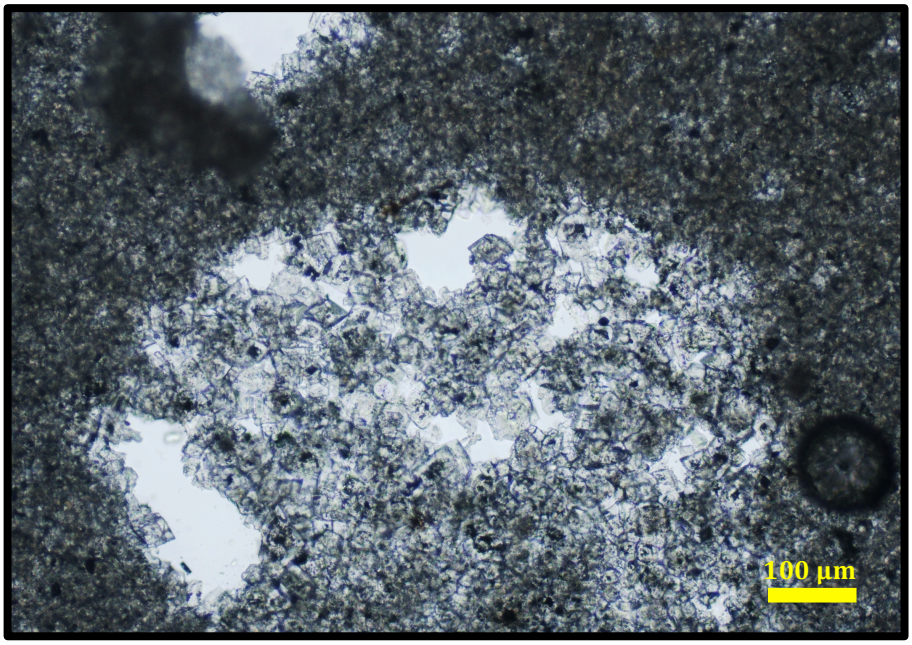


**Figure 45** A photomicrograph for planar (euhedral) dolomite crystals formed in the pore of finely crystalline non-planar dolomite (plain nicols).

In some thin sections, crystals with planar-e boundaries occur as aggregates of coarse crystals within dolomites dominated by planar-s and non-planar crystal boundaries. Most of the planar-s to non-planar dolomite crystals have irregular intercrystalline boundaries. This can be the result of competition for growth space with neighboring crystals. A single crystal with both planar and non-planar faces indicates available growth space in front of the crystal face (Fig. 40).

The dolomite fabrics in this study highly resemble the type of fabrics described by Randazzo and Zachós (1984) for dolomites formed by the replacement of micrite supported sediments during early diagenesis. Sutured mosaic and sieve mosaic are the most popular fabric types although micro-textured sutured and sieve mosaic exist. Randazzo and Zachós's (1984) fabric classification is descriptively mentioned regardless of the homogeneity versus the heterogeneity of the dolomitization processes responsible for each type of the fabrics as suggested by those authors. Modern studies that have dealt with crystal-scale compositional analyses of dolomites have revealed that the genesis of dolomitization is difficult to interpret solely based on petrographic observations (Jones, 2005; Choquette and Hiatt, 2008). All of the studies, however, agree on the micrite supported origin for dolomites with fabrics similar to the types mentioned above.

### 3.1.2.2 Dolomite Crystal Size

The crystal size for different dolomites varies greatly. The sizes of the crystals range from 5 to 100 μm in length. The finely crystalline non-planar dolomite crystals are the most common size of crystal throughout the dolomitized interval. The sizes of dolomite crystals were measured according to their longest axis because most of the dolomites are composed of subhedral to anhedral crystals. Dolomitization is generally pervasive and non-mimetic.

The pore type within dolomitic matrices is mostly moldic and probably formed from leaching of calcareous organisms based on their morphology. Moldic pores are better preserved in very finely and finely crystalline dolomites. Vugy porosity is mostly associated with dolomites that have relatively coarse crystal dolomites. The vugs are most probably remnants of moldic pores obliterated by further dolomitization and crystal growth.

Coarse dolomite crystals are usually the successors of coarse-grained sediments because permeability can be maintained for a longer time to allow efficient fluid circulation (Gao and Land, 1991; Budd, 1997). However, nucleation rate and growth kinetics also control the crystal size distribution. Micritic limestone provides abundant active nucleation sites, yielding a higher nucleation rate, because of the high surface area to volume ratio (Sibley and Gregg, 1987), and thus produces smaller dolomite crystals. On the other hand, growth kinetics depends on temperature and saturation with respect to $Mg^{+2}$, and the relationship between growth kinetics and temperature for naturally occurring dolomites is poorly understood (Sibley and Gregg, 1987; Kaczmarek and

Sibley, 2007). Yet, it is widely accepted that super-saturation, and dense nucleation sites are favored conditions for producing finely crystalline dolomites.

If the Paleocene-Eocene dolomites are syndepositional dolomites formed within a sabkha dolomitization setting, their texture and fabric is being greatly modified by later diagenetic and/or dolomitization processes that resulted in the variety of textures and fabrics. The only modern sabkha dolomite forms in evaporitic tidal flats along the western and southern margins of the Arabian Gulf (McKenzie, 1981; Wenk et al., 1993; Chafetz and Rush, 1994).

Holocene dolomite crystals of the Abu Dhabi sabkha are euhedral 0.1- 2 μm in size for intertidal dolomites and up to 5 μm in size for subtidal dolomites (Wenk et al., 1993). Crystal size and shape of the Pleistocene Arabian Gulf sabkha dolomites show modifications caused by diagenesis within the meteoric zone (Chafetz et al., 1999). The Pleistocene sabkha dolomite crystals are subhedral to anhedral with size range from 2 to 15 μm (Chafetz and Rush, 1994). The crystal size and geometry of ancient sabkha dolomites experienced many changes with time because of the multiple diagenetic phases they went through (Mackenzie, 1981). The general trend for the evolution of shallow dolomites, formed by replacing carbonate mud-rich rocks and/or sediments, show coarsening of the dolomite crystals with increasing dolomitization phases (Fig. 46) (Sibley and Greigg, 1987; Choquette and Hiatt, 2008).

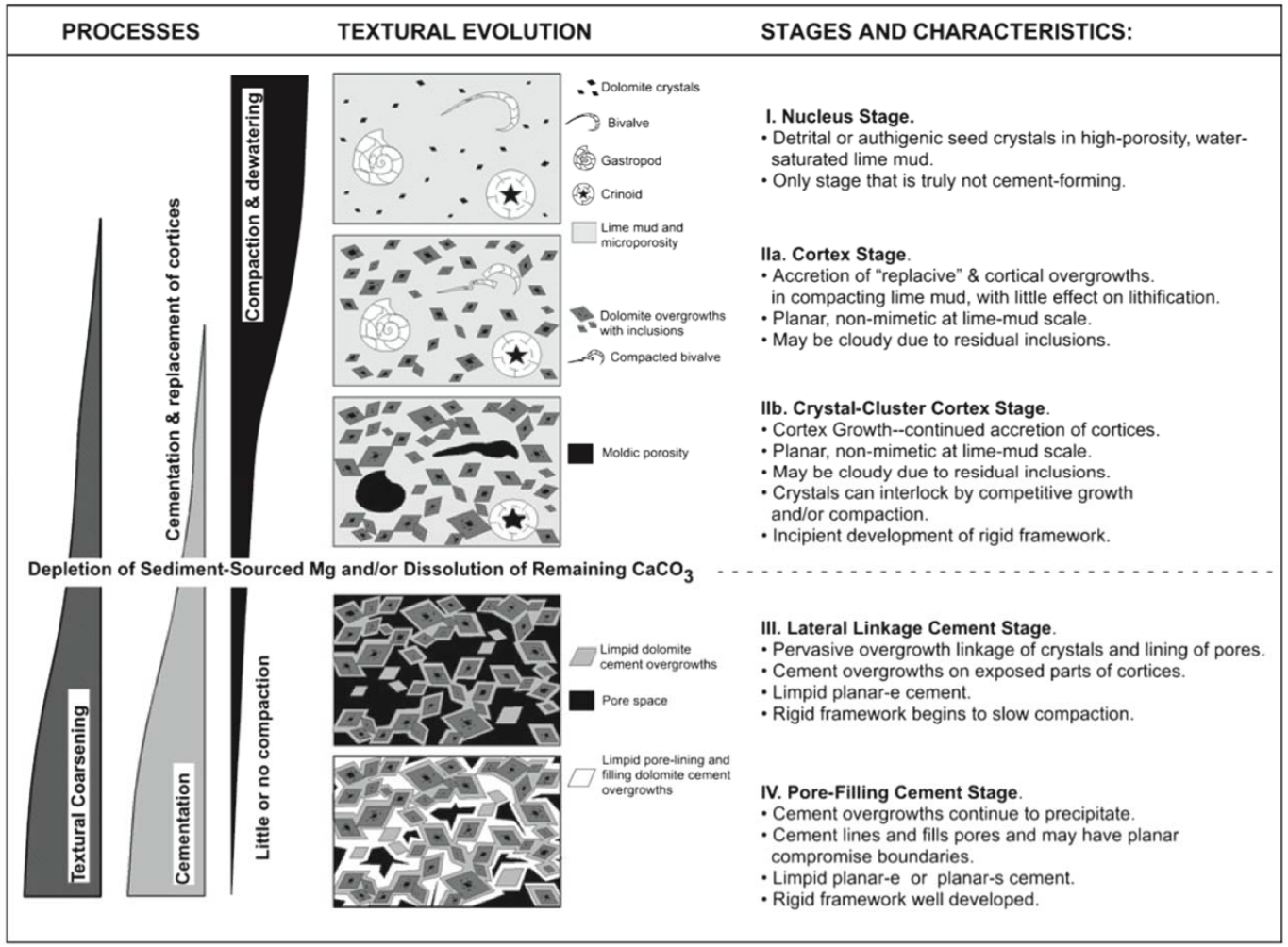


**Figure 46** A general trend for dolomite crystal size development formed through the replacement of micrite supported limestone within a shallow burial environment (from Choquette and Hiatt, 2008).

### 3.1.2.3 Dolomite Cement

Two distinctive classes of dolomite cement were observed; one formed in voids and the other around dolomite crystals. Dolomite crystals filling and lining moldic and vugy pores are common within the entire Paleocene-Eocene interval. The crystals for this type of dolomite cement are generally euhedral crystals with dark cores (Fig. 47).

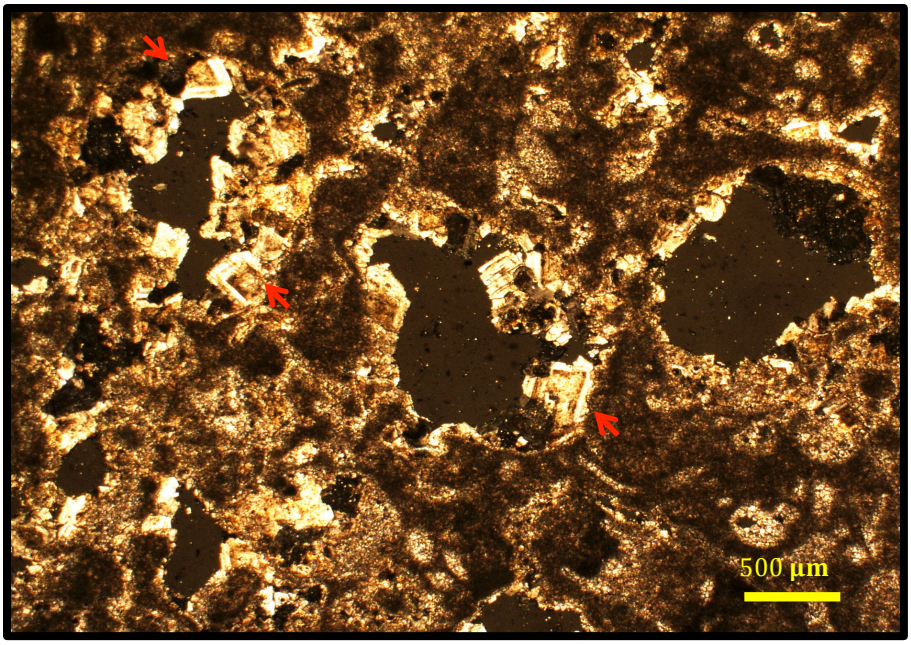


**Figure 47** Coarse euhedral pore-lining dolomite (red arrows) rhombs with cloudy core (cross nicols).

A second and prevailing type of dolomite cement is the syntaxial overgrowth cement around dolomite rhombs. The presence of the latter type of cement is not restricted to a specific dolomite fabric since it engulfs matrix-forming dolomite rhombs and pore filling rhombs. However, it is better developed around dolomites with relatively coarse crystal sizes and better vugy porosity but also exists in dolomites with no pore space (Fig. 48). Conditions such as effective circulation of dolomitizing fluids and free

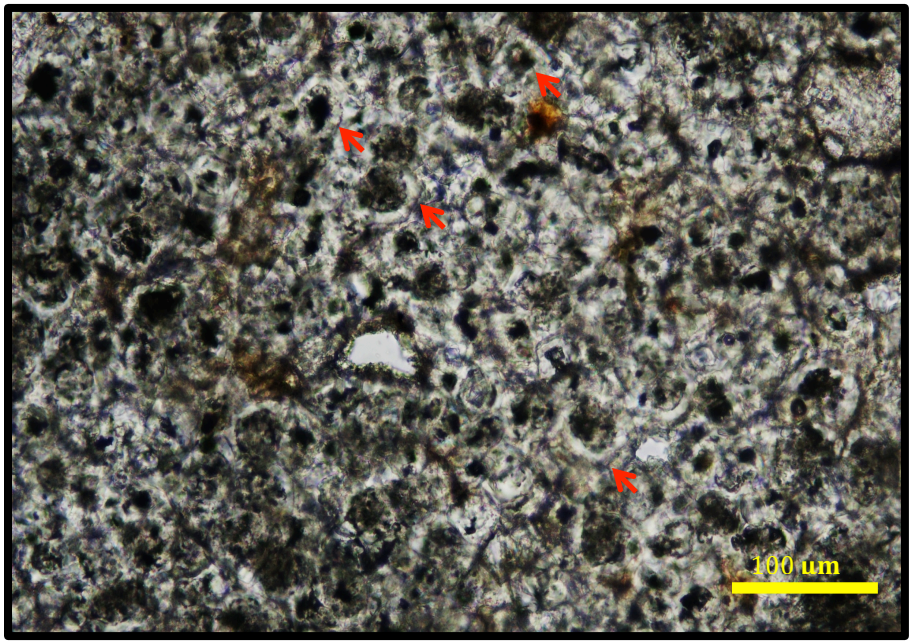


**Figure 48** Syntaxial dolomite cement rim (red arrows) around dolomite rhombs with cloudy core. Dolomite crystal geometry is highly altered by growth competition and compaction (plain light).

space for dolomite crystal to grow are favored for the formation of this type of cement (Budd, 1997; Wheeler, 1999; Choquette and Hiatt, 2008). Based on petrographic observations, most of the allochems had been leached prior to or during dolomitization since only micritized relics of skeletal grains were found in the dolomites. The originally grain-rich micritic limestone would have better porosity and permeability compared to grain-sparse micritic limestone, and both grain dissolution and dolomitization could lead to an increase in porosity and permeability (Choquette and Pray, 1970; Moore, 2001). Thus, this type of cement may predominate in the originally porous facies.

The syntaxial overgrowth cement is a few microns thick and exclusively appears as a clear rim. The euhedral to subhedral shape of the dolomite crystals is observable, but

the type of the contact between dolomite crystals and cements show different patterns. Irregular contact between a crystal and its rim characterizes cloudy euhedral crystals (Fig. 49). A second and less common type of contact is represented by a sharp and straight boundary with dolomite crystals retaining their plane faces (Fig. 50).

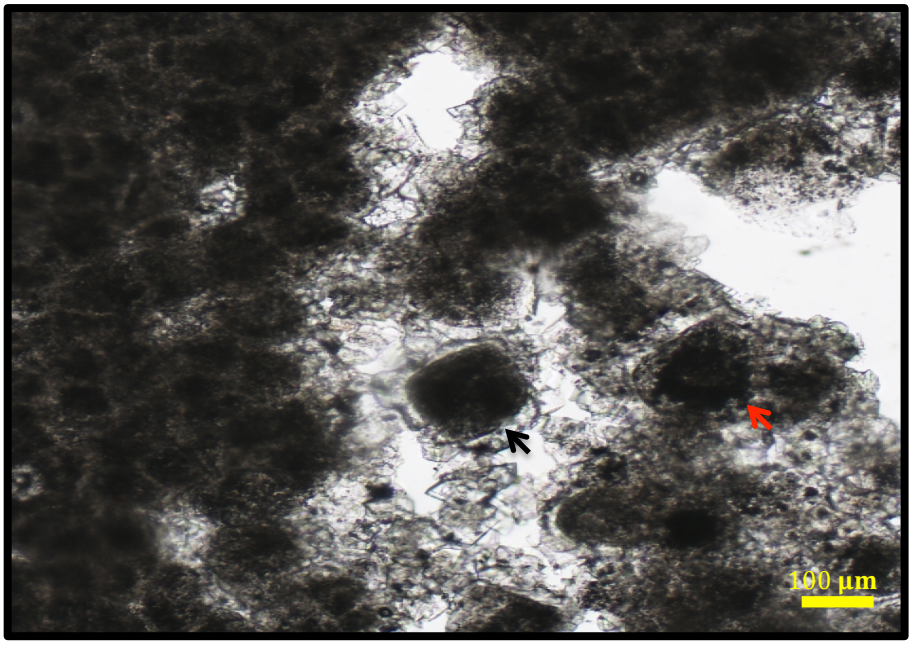


**Figure 49** Dolomite cement rim with irregular contact (blk arrow) between the cloudy rhombs and their cement. Note that some rhombs (red arrow) show rounded geometry (plain light).

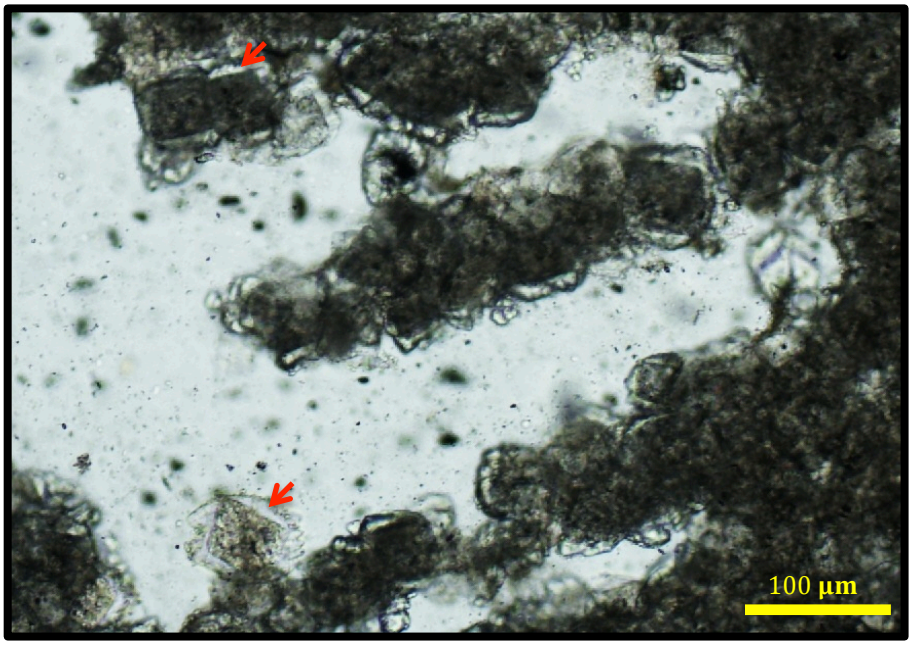


**Figure 50** Dolomite rhombs showing sharp contact (red arrow) between the cloudy dolomite rhombs and dolomite cement rim (plain light).

## 3.2 Stratigraphy

### 3.2.1 Microfacies Analyses

The petrographic study allows for the identification of tidal flats and lagoon carbonates and evaporites accreted in supratidal, intertidal, and subtidal zones. Petrographic evidence supporting these depositional environments comes from the depositional texture identified from the thin sections. The dominance of the micrite and micritic matrix (sparse to packed biomicrite, peloidal biomicrite) and the scarcity of sparry marine cementation (e.g. biosparite, pelsparite, etc.) strongly support a shallow marginal marine depositional setting for theses rocks with minimum wave influence. According to Hardie and Shinn (1986), wave energy is diminished on tidal flats and shallow lagoons where wide shelf lagoons are protected by barrier islands (e.g., Abu Dhabi, Arabian Gulf).

Another indication for marginal and shallow marine depositional setting is the interbedding of allochem-rich sections with unfossiliferous evaporitic dolomicrite and evaporitic dolomite. The evaporite minerals within a carbonate matrix are mainly gypsum and anhydrite. Fenestral pores filled with evaporites are commonly observed in the thin section (Fig. 51). These petrographic characteristics of evaporite-bearing Paleocene-Eocene carbonates in southern Iraq resembles the Holocene evaporites of Abu Dhabi (Warren and Kendall, 1985) and the Pleistocene evaporites of Al Jubyl (Chafetz and Rush, 1994) that were deposited in coastal sabkha and shallow lagoonal settings.

The dominance of the micrite and micritic matrix suggests low energy depositional setting. Many authors have interpreted the Paleocene-Eocene rocks in

southern Iraq had been deposited within evaporitic tidal flats and shallow restricted lagoons on a shallow carbonate platform (Alsharhan and Nairn, 1995; Ziegler, 2001; Jassim and Goff, 2006).

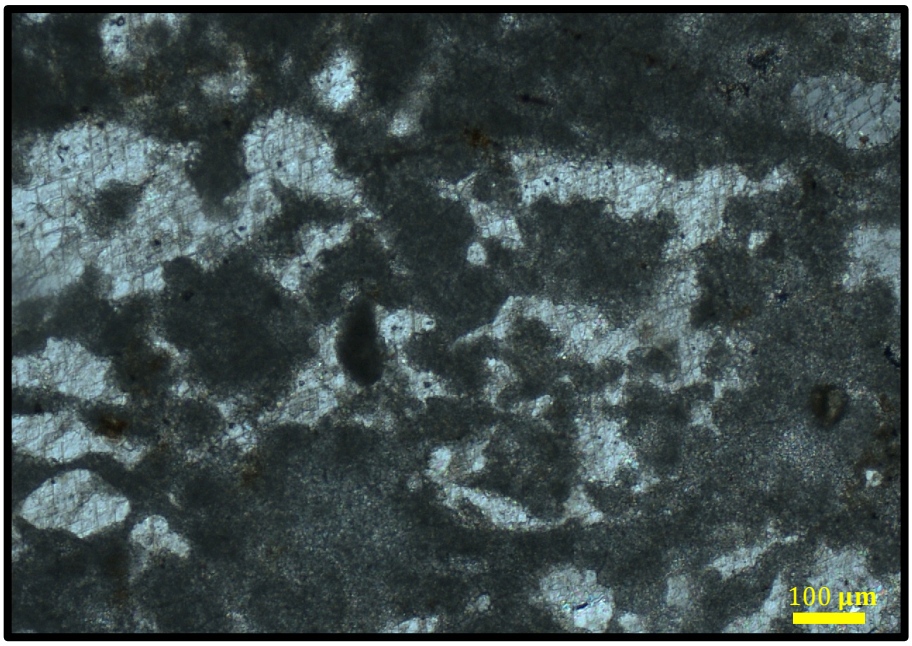


**Figure 51** Fenestral pores (bird's eye) filled with gypsum and nodular gypsum; a common exposure surface feature in arid carbonate-evaporite platforms (cross nicols).

### 3.2.2 Method for Identifying the Cyclicity of the Paleocene-Eocene Deposits

The poor well log pattern and layer cake-like seismic reflection makes the available successive thin sections the only method to determine whatever cyclic patterns (or depositional sequences) exist in the Paleocene-Eocene section in southern Iraq. The equivalent section in Al-Wafra Field, located in the Kuwait and Saudi Arabia Partitioned Zone, includes stacked shallowing-upward cycles of peritidal carbonates and evaporites

deposited on a gently sloping ramp (Dull, 2004; Bachtel et al., 2011; Toomey et al., 2011).

Shallowing-upward cycles are common in ancient (Wilson, 1975; James, 1984; Hardie, 1986; Pratt et al., 1992) and modern Abu Dhabi (Alsharhan and Kendall, 2003; Kirkham, 1998) peritidal carbonates settings. Cores were not available in this study to identify sedimentary structure associated with supratidal, intertidal, and subtidal zones. In addition, the complex diagenetic textures represented by grain dissolution, dolomitization, and pore-filling cementation are sporadic, and are not related to depositional settings or cycles.

Therefore, cycle stacking patterns were identified based on the composition of the microfacies as following: (1) allochem-free evaporitic dolomicrite and evaporitic dolomite were interpreted as supratidal microfacies, (2) sparse biodolomicrite, peldolomicrite and peldolosparite, and sparse peloidal biodolomicrite and peloidal biodolosparite were interpreted as intertidal microfacies, (3) peloidal biodolomicrite and biodolomicrite were interpreted as subtidal microfacies. A single cycle generally is composed of a vertical microfacies succession represented by subtidal microfacies at base, intertidal microfacies in the middle, and supratidal microfacies at top. Yet, fining-upward versus coarsening-upward successions were also considered, and a few cycles in Nahr Umr No.1 well were observed based on that.

The extensive fabric destructive dolomitization makes the identification of the original microfacies impossible in some intervals, and seldom are relics and micritized grains identified. In some intervals, the dolomites are capped by unfossiliferous micrite

that includes evaporite minerals in the form of nodules and pore-fillings. Where this kind of vertical succession exists, it can be assumed that the dolomites formed in sabkha or seepage-reflux settings, and were overlaid by unfossiliferous and evaporite-rich tidal flat micrites during progradational phases. Yet, this vertical succession is inconsistent because rises and falls of the relative sea level would cause vertical and lateral shifts and generated different stacking patterns throughout the Paleocene-Eocene interval.

The evaporite-bearing carbonates are exclusively interpreted here to represent exposure surfaces at the top of each cycle. Evaporitic exposure surfaces can result from: (1) filling of the accommodation space on a prograding coastal sabkha during highstands (Tucker, 1991), (2) drop in the relative sea level that expose a platform top, and (3) during early transgression times when coastal sabkha environment is reestablished in distal parts of the platform (Warren and Kendall, 1985).

The differentiation between the processes that result in exposure surfaces is important in studying the stratigraphic and sedimentological evolution of the Paleogene interval, however, the absence of sedimentary structures and distinctive surfaces make this irresolvable. Other shortcomings associated with using this method are: (1) missing subtidal and intertidal cycles because of the subtle gradational contact between these cycles (Spence and Tucker, 1999), and (2) missing supratidal deposits because of evaporites dissolution during transgression, or deflation during regression. However, the same exposure surface approach was followed to identify cycles in Al-Wafra Field where diagenesis did not allow the identification of the original rock (Bachtel et al., 2011; Toomey et al., 2011).

### 3.2.3 The Cyclicity of the Paleocene-Eocene Deposits

Based on the method mentioned above, Figure 52 represents the cycles identified in Nahr Umr No.1 and Zubair No.1 wells. Fifteen cycles were identified in Nahr Umr No.1 versus 14 cycles in Zubair No.1. Although the number of cycles in the two wells are close, it does not suggest correlation because the 120 m thick Rus Formation in Zubair No.1 does not exist in Nahr Umr No.1. In addition, there are missing intervals and a wider sampling range in Zubair No.1.

In term of cycle thickness, Nahr Umr No.1 includes cycles with an average thickness around 30 m whereas the average cycle thickness in Zubair No.1 is around 20 m. This is most probably the result of the difference in the depositional setting because the distal Nahr Umr No.1 experienced greater deposition and less erosion compared to Zubair No.1. In addition, microfacies in Zubair No.1 are highly altered by recrystallization and dolomitization, and relics of skeletal grains, i.e., moldic pores and micritized grains, are sparse. This is probably a result of the landward location of the well where dissolution of allochems and recrystallization of the matrix by freshwater commonly occurred. The extensive appearance of evaporites in the Zubair No.1 well also makes it difficult to determine the exposure surface based cycle boundaries. In some intervals (e.g., 1000-1160 m) the cycle boundaries were based on subtle changes in the evaporite abundance and availability of allochems.

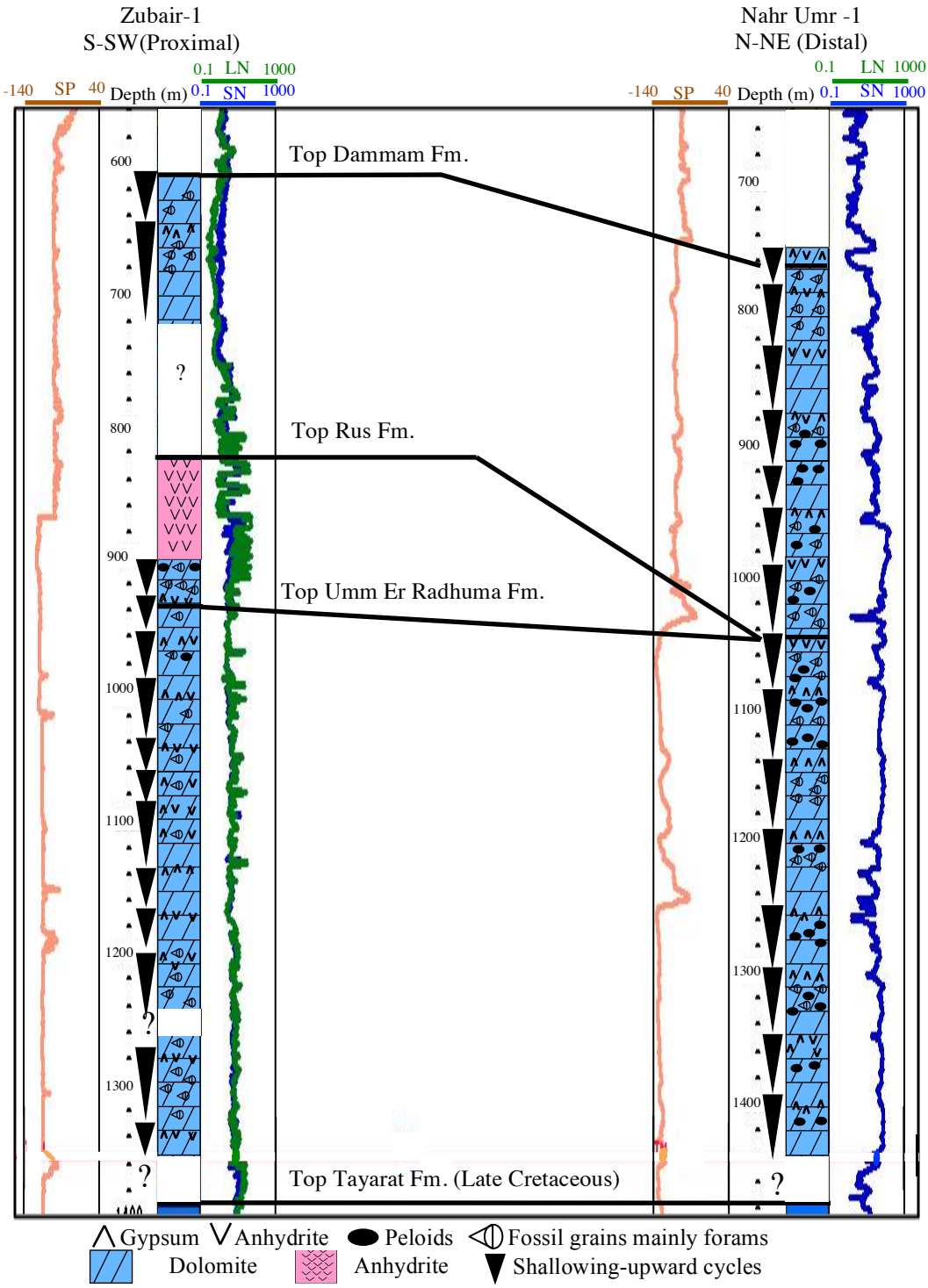


**Figure 52** A figure depicts the shallowing-upward cycles identified in Zubair No.1 (14 cycles) and Nahr Umr No.1 (15 cycles) wells. Spontaneous potential (SP) and shallow (SN) and deep (LN) resistivity logs are also plotted. SP logs do not show any particular pattern in both wells. Resistivity log in Zubair No.1 show irregular reflection against the evaporitic Rus Formation. Kicks in resistivity log against evaporitic facies can be noticed in Nahr Umr No.1 well, but it is not uniform and distinctive for the evaporitic facies only.

The identification of cycles capped by gypsum and anhydrite in the proximal Nahr Umr No.1 indicate that it was exposed during falls in the relative sea level. This is reasonable because it is on a low gradient (generally <1°) homoclinal ramp. A strip of 20-50 km wide would be exposed as a result of a 10 m drop in the relative sea level (Burchette and Tucker, 1992).

The water depth on the Paleogene ramp in southern Iraq never exceeded 50 m and was only 20 m during most of the time during the Paleocene-Eocene Periods (Jassim and Budday, 2006). Therefore, $4^{th}$ and $5^{th}$ order fluctuations in the relative sea level could expose and submerge tidal flats and lagoons. This lateral transition of adjacent facies belts during falls and rises in the relative sea-level produced the vertical succession composed of stacks of shallow ramp carbonate and evaporite deposits.

The Arabian Plate Cycle Chart was constructed by Haq and Al-Qahtani (2005) to represent changes in relative sea-level governed by tectonics and eustacy. Eleven cycles were identified through the Paleocene-Eocene interval, close to the number of the cycles identified in this study. The cycles of Haq and Al-Qahtani (2005) are based on sonic and gamma ray logs from a single well in Oman (Fig. 53), and most of the cycles were developed during the deposition of the Rus Formation. Based on composite geological logs of the wells within the study area, the Rus Formation includes thin carbonate layers, however, the carbonate layers do not show correlation between the wells, and were not counted in this study.

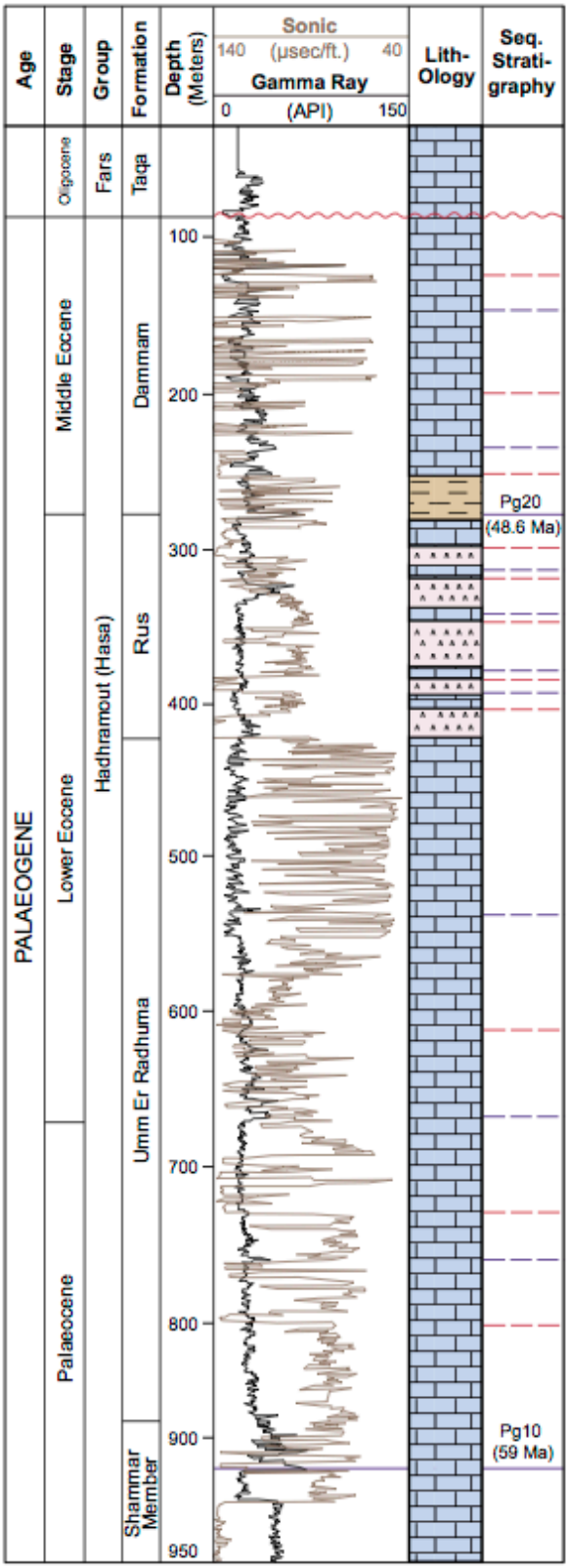


**Figure 53** A lithostratigraphic section based on the well Baladi-1 in Oman. Eleven cycles are represented by sequence boundaries (dashed red lines) and maximum flooding surfaces (dashed purple lines). Notice that 5 cycles are from Rus Formation. Pg 10 and Pg 20 are plate wide maximum flooding surfaces adopted from Sharland et al., 2001(from Haq and Al-Qahtani (2005) after Hughes Clarke, 1988, and Sharland et al., 2001).

The cyclicity of the Paleocene/Eocene interval has been thoroughly studied in the Al-Wafra Field that is relatively close to this study. Four cycles for the Second Eocene reservoir (Dull, 2004) and 11 cycles for the First Eocene reservoir (Toomey et al., 2011) are reported based on closely cored and logged wells. The cycles in Al-Wafra Field are mainly shallowing-upward cycles with their petrographic composition similar to what is observed in this study.

The numbers of cycles in this study, Al-Wafra Field, and Haq and Al-Qahtani (2005) are similar, and discrepancy is expected based on the type of data manipulated in each study, and the superimposition of regional tectonics in each area on the plate wide margin tectonics.

### 3.2.4 Tectonic Implications on Cyclicity

The study area is underlain by infra-Cambrian salt and basement faults (see section 1.1). Based on the Quaternary sequence in western and central Abu Dhabi, the infra-Cambrian salt movement along with the Zagros Orogeny has influenced the stratigraphic development of the shallow subtidal and widespread coastal sabkha deposits through creating localized and differential fluctuations of the relative sea-level on the order of a few meters (Kirkham, 1998).

Basement faults were also reactivated during the Tertiary (Jassim and Budday, 2006). The presence of basement faults would generally result in continuously or episodically slow subsidence rates that favored the deposition of the carbonates on the slightly dipping and relatively shallow carbonate ramp (Burchette and Tucker, 1992). However, basement faults can highly alter the geometry of a peripheral foreland basin that would result in differential sedimentation across tectonic highs and lows (Catuneanu, 2004). The flexural profile was already altered in the western hinterland part of the study area where basement faults accommodated compression and did not allow the development of a prominent peripheral bulge (Grabowski, 2012; personal communication). This influenced the sedimentological composition because limited siliciclastic sediments were transported to the carbonate basin.

Sharland et al. (2001) established the sequence stratigraphic framework of Arabian Plate based on major tectonically driven plate-wide unconformities. Accordingly, the Paleocene-Eocene section was represented as a single tectonostratigraphic megasequence (AP10) bounded by two unconformities in the Early

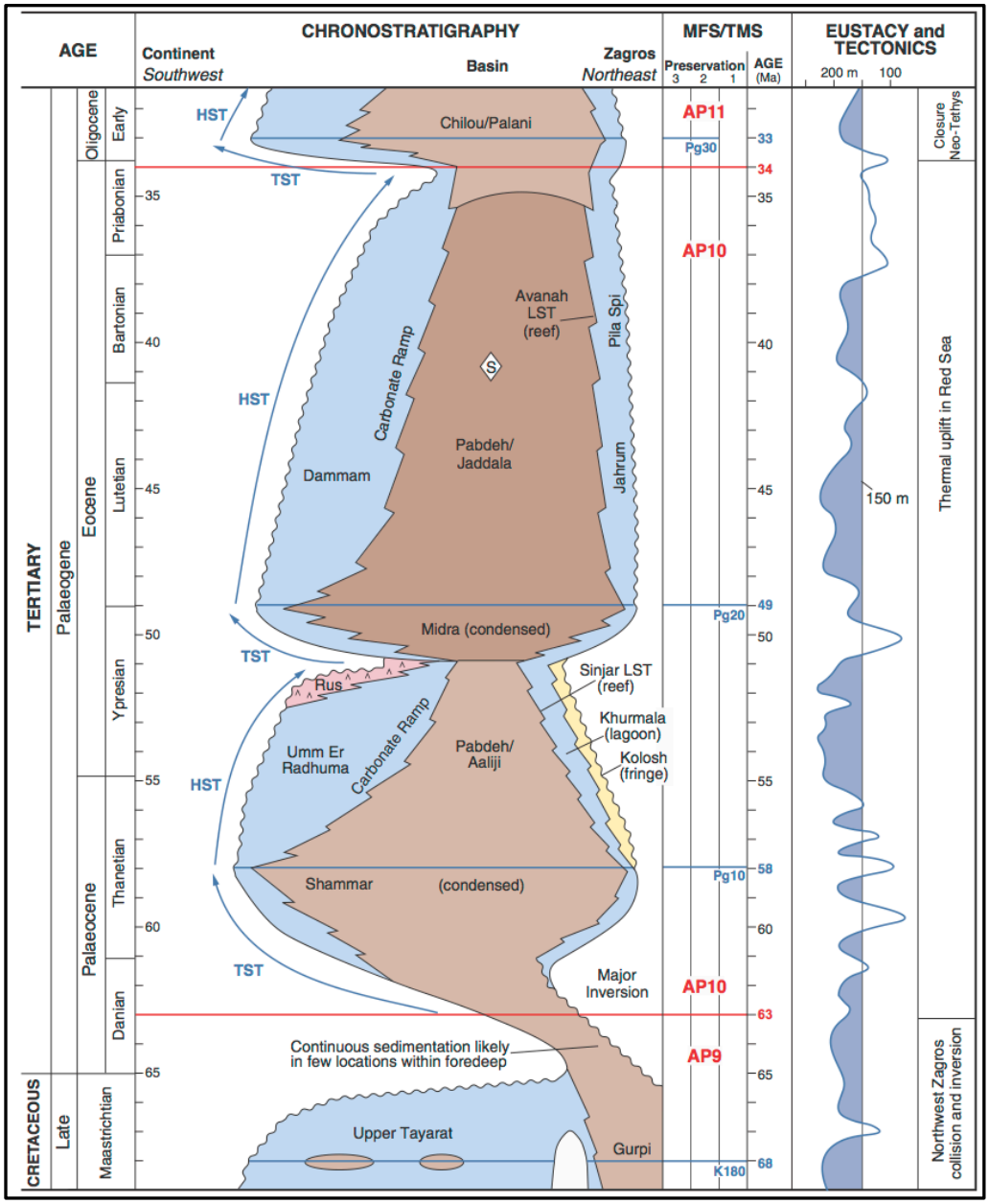


**Figure 54** Tectonostratigraphic megasequence (AP10) representing the Paleocene-Eocene section bounded by two unconformities in the Early Paleocene and Late Eocene. The southwest side of the schematic section represents the sequence stratigraphic development of the study area. All of the Umm Er Radhuma, Rus, and Dammam formations were deposited during long-lasting highstands preceded by plate wide transgressions shown as Pg10 and Pg20 (from Sharland et al., 2001).

Paleocene and Late Eocene (Fig. 54). Both of Umm Er Radhuma and Dammam Formations were deposited during long-lasting highstands preceded by short transgressions. This resulted in thick aggrading carbonate deposits that experienced limited progradation during early highstands (Sharland et al., 2001; Ziegler, 2001).

The aggradational stacking pattern for Umm Er Radhuma and Dammam Formations is interpreted by Jassim and Budday (2006) to be the result of carbonate sediments unable to build into the deep basin. However, the progradational, aggradational, and retrogrational stacking patterns of a carbonate ramp sitting on peripheral bulges (Fig. 55) is controlled by the flexural nature of the foreland basin (Yang and Dorobek, 1995). Therefore, the crustal geodynamics that is highly influenced by basement faults has direct implications on the stratigraphic development.

Following the discussion above, the impact of tectonics on the general stratigraphic development of the Paleocene-Eocene interval is inevitable. Unfortunately the data set in this study is not enough to scrutinize the structural development, however, modern studies suggest that fault movements beneath a carbonate platform directly influence the cyclic pattern of peritidal carbonates (e.g., De Benedictis et al., 2007; Bosence et al., 2009). This can be another reason behind inconsistency between the number and thickness of the cycles within the study area compared to cycles in Al-Wafra Field and Haq and Al-Qahtani (2005).

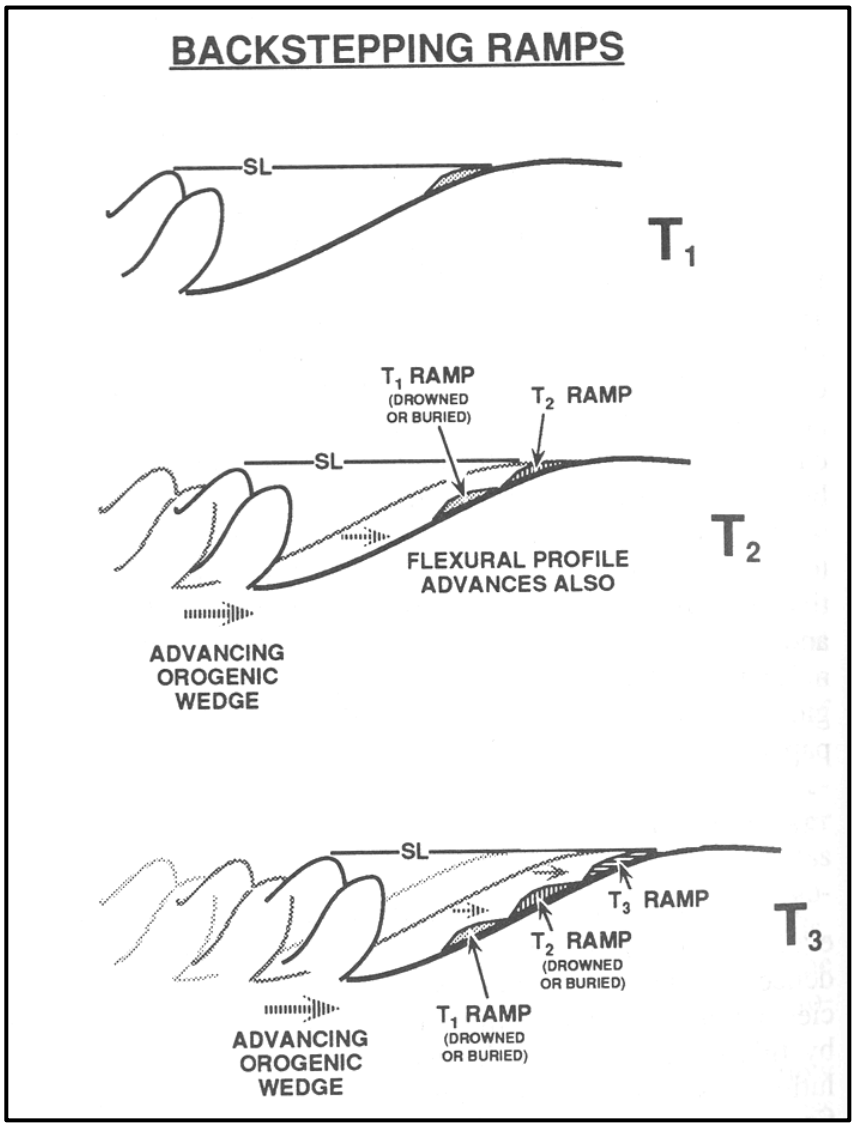


**Figure 55** A diagram illustrating a backstepping carbonate ramp sitting on a peripheral bulge of a foreland basin (from Yang and Dorobek, 1995).

### 3.2.5 Implications of the Rus Formation on the Regional Stratigraphy

The extensive and thick presence of the Rus Formation within the study area (Figs. 56 and 57) highly controls the diagenetic and stratigraphic evolution from Paleocene to Middle Eocene strata. Samples that belong to the Rus Formation were not included in this study except for 30 m representing the basal carbonate horizon in Zubair No.1 well.

The deposition of the Rus Formation took place in salina/sabkha settings (Alsharhan and Narin, 1995; Ziegler, 2001; Jassim and Budday, 2006). The incremental increase of temperature by 4 to 5 °C in the tropics during the Early Cenozoic would have been a major factor that enhanced evaporite deposition (Zachos et al., 2005). For thick evaporites to be deposited, a barrier is required for lagoons and extensive shallow platforms to become restricted and hypersaline. It is theoretically possible for evaporite ramps to form around evaporite basins, but the absence of a definite modern example makes the presence of evaporites ramps restricted to rimmed ramps (James and Kendall, 1992).

Neither shelf-break nor rimmed ramp geometries were identified from seismic sections (unpublished ExxonMobil data) that show stacked sheet-like reflections for the entire Paleocene-Eocene carbonates and evaporites section. The Rus Formation is identified by its strong reflection that dies out toward the distal Nahr Umr No.1 well.

Jassim and Budday (2006) proposed nummulite shoals that belong to the Dammam Formation in front of the Rus evaporites (Fig. 58). This could provide the barrier required for restriction, but it also implies that the Dammam Formation is

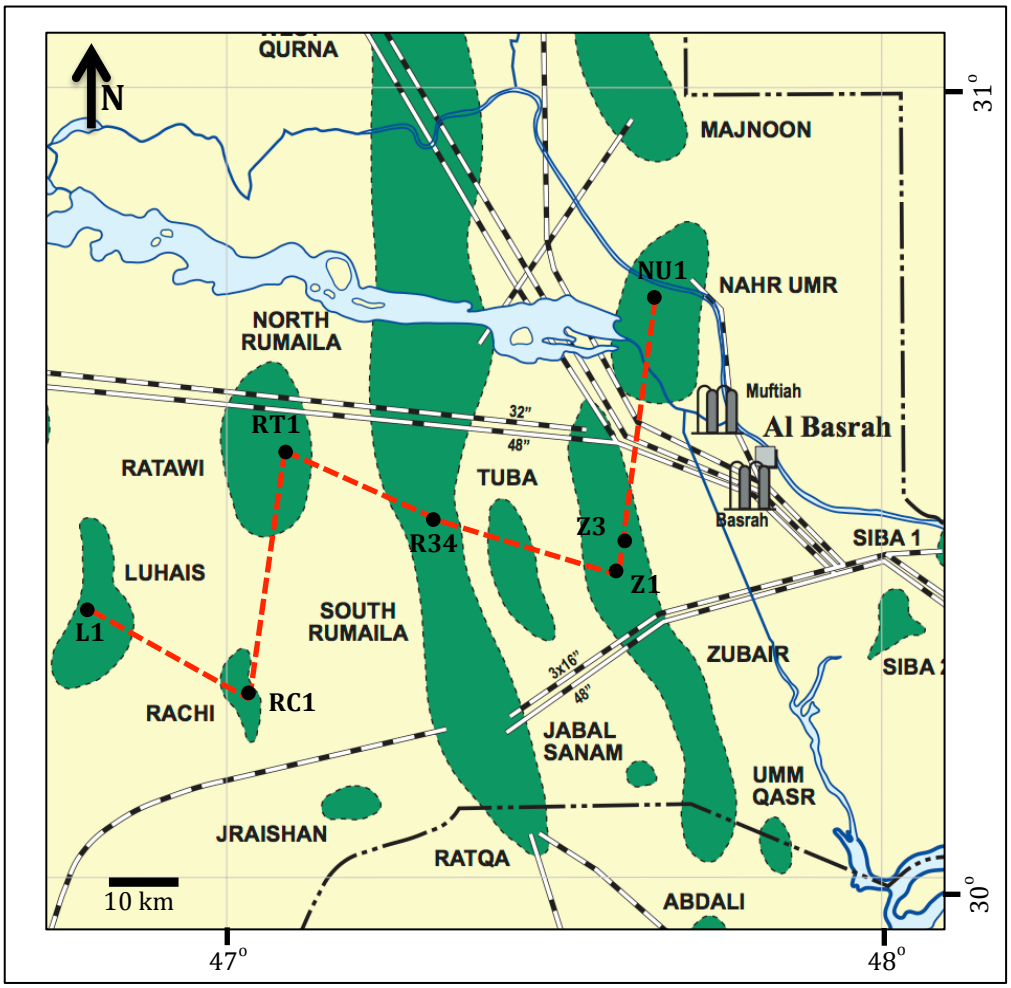


**Figure 56** A map showing the cross-section line (dashed red line) used for the lithostratigraphic correlation of figure 57 from the wells Luhais-01 (L1), Rachi-01 (RC1), Ratawi-01 (RT1), Rumaila-34 (R34), Zubair-1and-3 (Z1 and Z3), and Nahr Umr-1 (Nu1)(modified from Iraq Field Atlas, 2003).

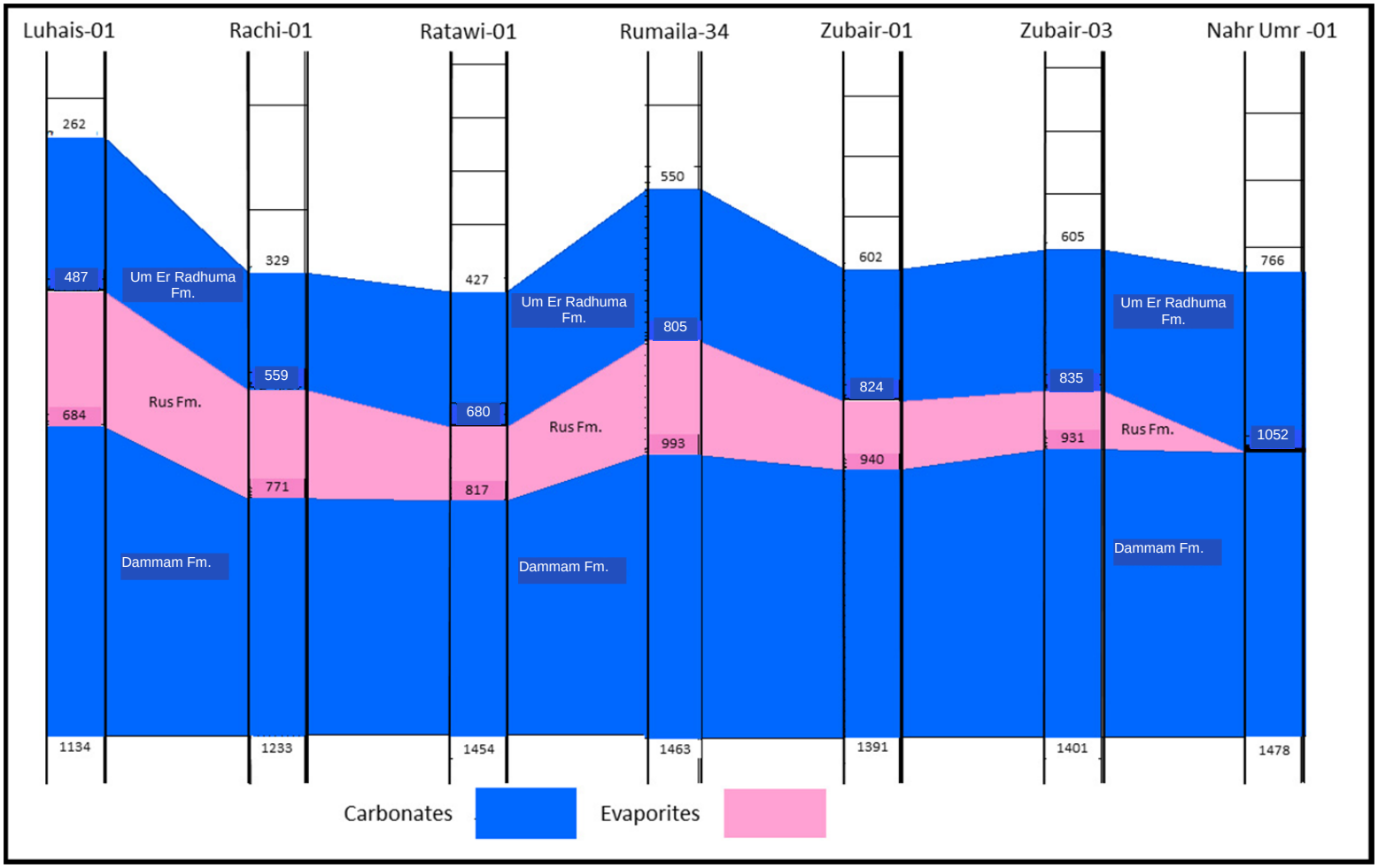


**Figure 57** A lithostratigraphic cross-section representing the regional relationship of the Um Er Radhuma, Rus, and Dammam formations based on the wells in Figure 56.

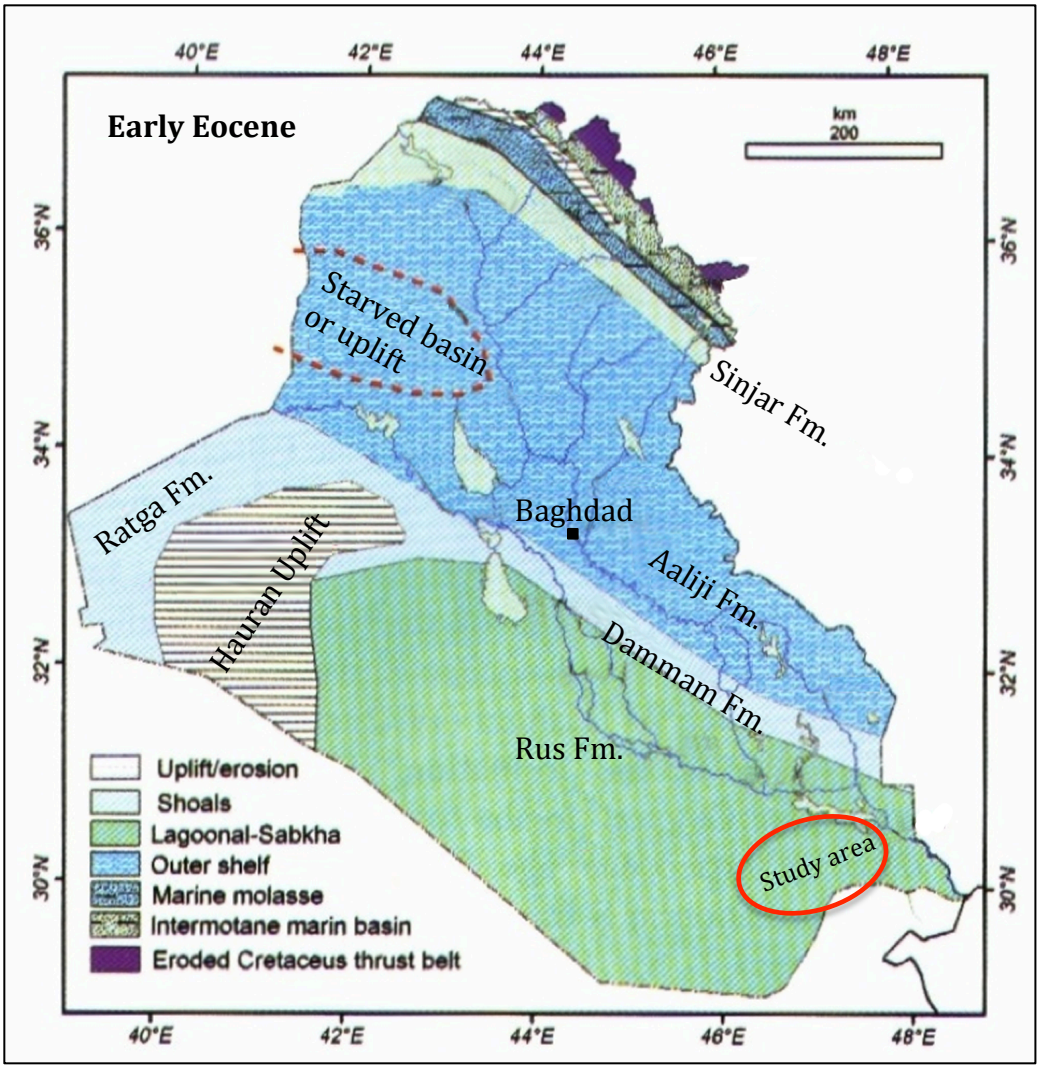


**Figure 58** Early Eocene paleofacies map showing shoals of the Dammam Formation in front of the Rus evaporites (modified from Jassim and Budday, 2006).

chronostratigraphically equivalent to the Rus Formation. So, a different interpretation is that the shoals represent a member of the Rus Formation formed in association with better seawater circulation.

On the other hand, it is possible that the shoals were nummulite buildups. Nummulites were major component of carbonate ramp buildups along with other benthic

foraminifera in the Peri-Tethyan Ocean throughout the Cretaceous and Early Tertiary (Burchette and Tucker, 1992; Philips, 2003). The nummulites buildups would have formed during the late highstand of the underlying Umm Er Radhuma Formation when the rise of relative sea level slowed. This would have resulted in growth and expansion of buildups, and formed a low relief sill encompassing the hypersaline lagoon. This assumption may be valid based on the laterally gradational contact in between the Rus and Umm Er Radhuma formations on the distal part of the platform.

The presence of the Rus Formation has direct implication on dolomitization processes. Dolomite distribution in the modern Abu Dhabi ramp is strongly controlled by the distribution of salina and sabkha settings through controlling the hydrology of ground water and brines (Warren, 2000). Thus, based on the juxtaposition of the Rus Formation, it is reasonable to assume that sabkha and seepage-reflux dolomitization processes led to the dolomitization of the underlying Umm Er Radhuma Formation, but these processes would not last if an early basal seal was formed. However, large evaporitic basins would have porous pathways for brine reflux or for upward discharge of groundwater to the basin (Kendall, 1992).

The hydrogeology of modern dolomitization settings strongly controls the spatial and temporal distribution of dolomites. The data set in this study is not enough to examine the influence of the Rus Formation on the regional hydrogeology, thus dolomitization, although it is reasonably significant.

# CHAPTER 4 ELEMENTAL COMPOSITION

## 4.1 X-ray Analysis Results

A total of twenty-six rock chip samples were selected, representative of 3 m sampling intervals, in Nahr Umr No.1 well (Table 1). The samples were chosen based on their petrographic features. Because no previous studies concerning the mineralogy of Paleocene-Eocene carbonates in southern Iraq had been conducted, all of the samples were first analyzed for their mineralogical composition based on X-ray diffraction analyses.

The X-ray diffraction results indicated that dolomite is the main mineral based on the strong d104 dolomite peak (Fig. 59). Minerals detected with dolomite are exclusively calcite and quartz (Fig. 60). Pore-filling calcite cement and authigenic quartz were observed in thin sections of the analyzed samples, and X-ray results confirmed their presence. A weak quartz peak appears in some dolomite samples in which no quartz was observed in thin sections (Fig. 61). This may be due to the absence of quartz in the thin sections whereas quartz existed in the analyzed powder of the 3 m sample interval. A subtle calcite peak, associated with the strong dolomite peak, was observed in a few samples from the relatively coarse dolomite group, i.e., 20-50 μm dolomite crystals. A few of the samples show prominent calcite peaks (Figs. 60 and 62), nonetheless, dolomite is pervasive in those rocks, and the calcite peaks represent pore-filling calcite cement. This was confirmed based on petrographic examination of thin sections representing the sample intervals. Thus, calcite is mainly from the pore-filling cement rather than coexisting calcite and dolomite in the rock matrix. X-ray results were useful

to appreciate $Ca^{2+}$ enrichment by pore-filling calcite cement since ICP-AES provides the bulk content of $Ca^{2+}$ and $Mg^{2+}$.

| Sample No. | Sample intervals (depth ft.) | Sample intervals (depth m) |
|---|---|---|
| 1 | 2760-2770 | 841-844 |
| 2 | 2810-2820 | 856-859 |
| 3 | 2840-2850 | 866-869 |
| 4 | 2920-2930 | 890-893 |
| 5 | 2940-2950 | 896-899 |
| 6 | 3020-3030 | 920-923 |
| 7 | 3140-3150 | 957-960 |
| 8 | 3200-3210 | 975-978 |
| 9 | 3280-3290 | 1000-1003 |
| 10 | 3310-3320 | 1009-1012 |
| 11 | 3370-3380 | 1027-1030 |
| 12 | 3450-3460 | 1052-1055 |
| 13 | 3520-3530 | 1073-1076 |
| 14 | 3570-3580 | 1088-1091 |
| 15 | 3610-3620 | 1100-1103 |
| 16 | 3650-3660 | 1112-1116 |
| 17 | 3750-3760 | 1143-1146 |
| 18 | 3870-3880 | 1180-1183 |
| 19 | 3980-3990 | 1213-1216 |
| 20 | 4040-4050 | 1231-1234 |
| 21 | 4100-4110 | 1250-1253 |
| 22 | 4290-4300 | 1308-1311 |
| 23 | 4310-4320 | 1314-1317 |
| 24 | 4640-4650 | 1414-1417 |
| 25 | 4710-4720 | 1436-1439 |
| 26 | 4720-4730 | 1439-1442 |

**Table 1** The selected samples for geochemical analyses with their corresponding intervals in Nahr Umr No.1 well.

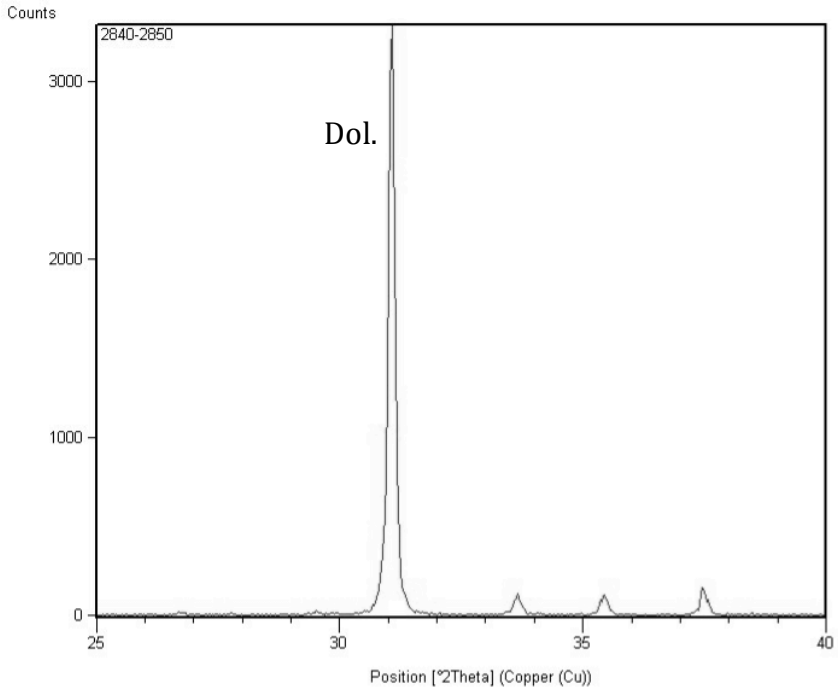


**Figure 59** The dolomite d104 peak is the exclusive peak in most of the samples. Other dolomite peaks are 006, 015, and 110 from left to right, respectively.

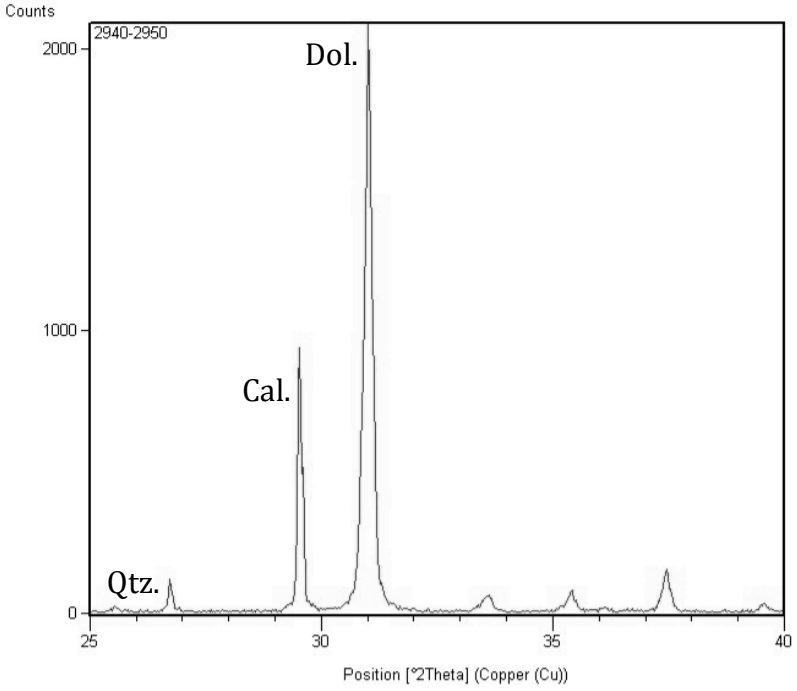


**Figure 60** X-ray diffraction result matches a sample that included dolomite, quartz, and calcite.

Non-planar 5-20 μm dolomite samples are the most abundant constituent throughout the Paleocene-Eocene section. Non-planar and planar-s 20-50 μm dolomites and dolomicrite were chosen to be geochemically analyzed. Table 2 represents the crystal size determined petrographically and mineralogical content of the samples from X-ray results.

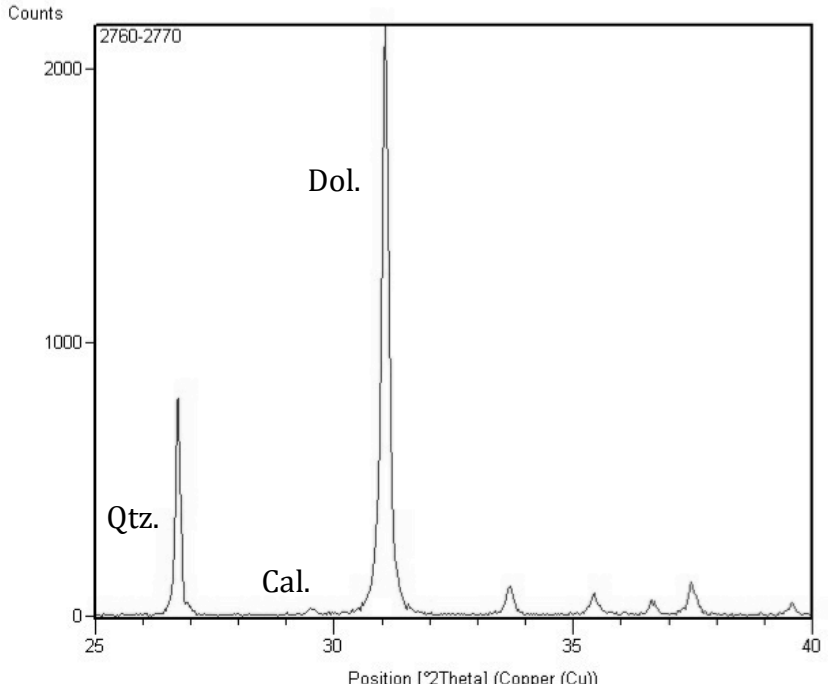


**Figure 61** X-ray diffraction result showing dolomite and quartz as the main minerals with a very weak calcite peak.

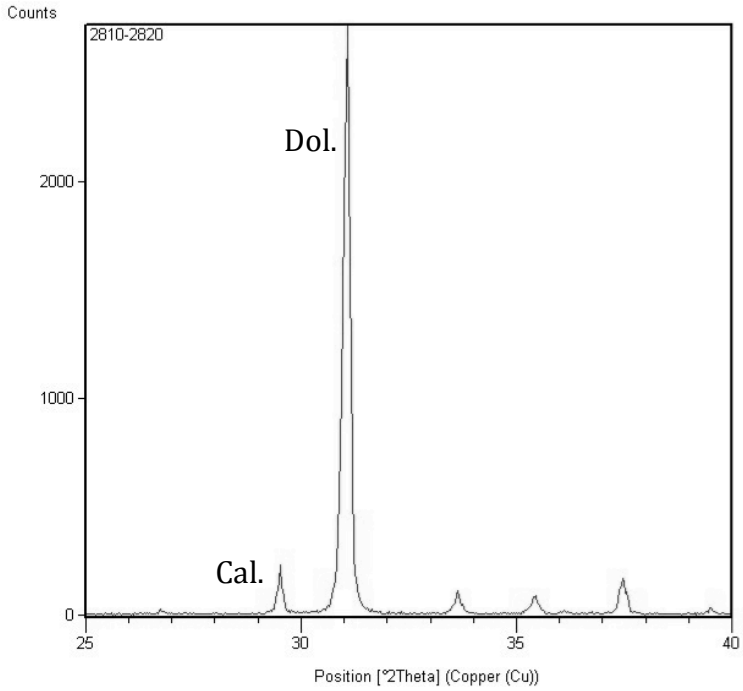


**Figure 62** X-ray diffraction showing the strong dolomite peak and weaker calcite peak. Pore-filling calcite cement was observed in thin section of the corresponding sample interval.

The degree of order for the dolomites was determined from the ratio of 015 peak to 110 peak intensities. The average order of the dolomites is 0.64 with a range from 0.46 to 0.88 (n = 26; std. = 0.11). No explicit relationship was found between the degrees of order and both crystal size and stratigraphic position although there is a very weak trend toward relatively better ordered dolomites lower in the section (Fig. 63).

The non-planar to planar-s dolomite crystal habit in all of the samples is the main reason behind implicit relationship between crystal size and degree of order. Dolomite crystals have sutured and intergrown crystal boundaries that suggest irregular crystal faces. In addition, most of the dolomites have probably replaced micrite, and represented by equant crystals rather than pronounced rhombohedral crystal shape.

| Sample No. | Description | Calcite peak | Quartz peak |
|---|---|---|---|
| 1 | Non-planar (20-50 μm) dolomite | N/A | Medium |
| 2 | Non-planar (20-50 μm) dolomite | Very small | N/A |
| 3 | Non-planar (20-50 μm) dolomite | N/A | N/A |
| 4 | Non-planar (5-20 μm) dolomite | Small | N/A |
| 5 | Non-planar (5-20 μm) dolomite | Medium | Medium |
| 6 | Non-planar (5-20 μm) dolomite | Small | Small |
| 7 | Non-planar (5-20 μm) dolomite | Medium | Medium |
| 8 | Non-planar (5-20 μm) dolomite | Very small | N/A |
| 9 | Non-planar (20-50 μm) dolomite | N/A | N/A |
| 10 | Non-planar (5-20 μm) dolomite | Very small | N/A |
| 11 | Non-planar (5-20 μm) dolomite | Very small | N/A |
| 12 | Non-planar (5-20 μm) dolomite | Very small | N/A |
| 13 | Dolomicrite | Small | N/A |
| 14 | Non-planar (5-20 μm) dolomite | N/A | N/A |
| 15 | Non-planar (20-50 μm) dolomite | Medium | N/A |
| 16 | Planar-s (20-50 μm) dolomite | N/A | N/A |
| 17 | Dolomicrite | N/A | Small |
| 18 | Non-planar (20-50 μm) dolomite | N/A | N/A |
| 19 | Non-planar (5-20 μm) dolomite | N/A | Small |
| 20 | Non-planar (20-50 μm) dolomite | N/A | N/A |
| 21 | Non-planar (5-20 μm) dolomite | N/A | N/A |
| 22 | Non-planar (20-50 μm) dolomite | N/A | N/A |
| 23 | Non-planar (20-50 μm) dolomite | Very small | Small |
| 24 | Non-planar (5-20 μm) dolomite | Very small | N/A |
| 25 | Planar-s (20-50 μm) dolomite | Very small | N/A |
| 26 | Planar-s (20-50 μm) dolomite | N/A | N/A |

**Table 2** The selected samples for geochemical analyses with their crystal size from petrography and mineralogical content of the samples from X-ray results. The very small, small, and medium calcite peak descriptions correspond to calcite peaks in Figs. 61, 62, and 60, respectively. The small and medium quartz peak descriptions correspond to quartz peaks in Figs. 60 and 61, respectively.

Other common factors causing weak degree of order in dolomites, although not examined here, are: (1) stress generated from growth competition and compaction result in microstructure defects in crystal planes (Wenk et al., 1983), (2) stress produced by pore filling water, i.e., hydrostatic pressure, would result in defects on the crystal face during crystal growth (Choquette and Hiatt, 2008), (3) corrosion of crystal faces in contact with compositionally different fluids, and (5) continual growth of dolomite crystals with compositionally different zones (Jones, 2005).

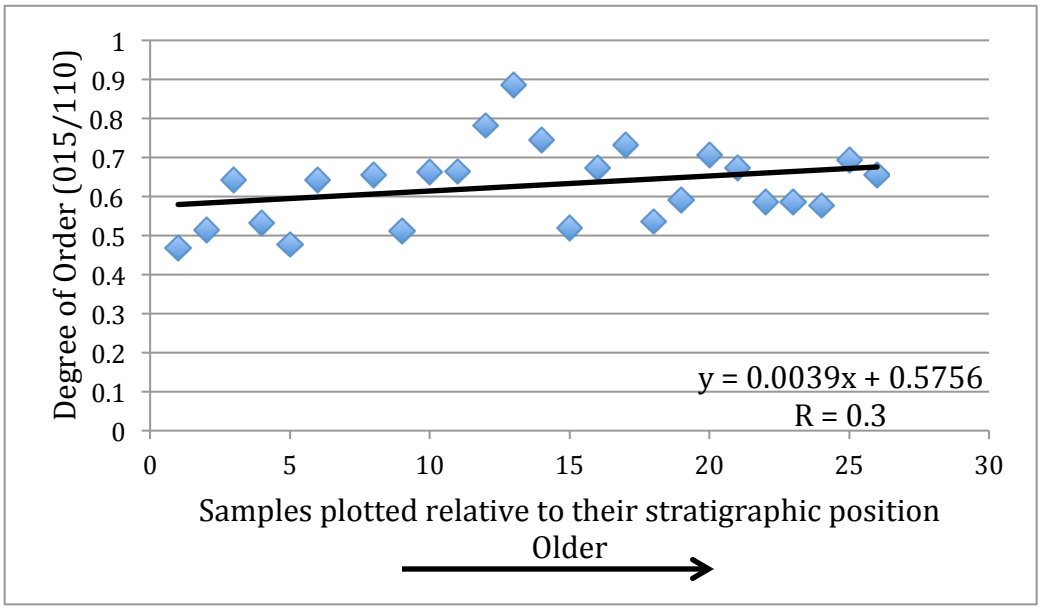


**Figure 63** A plot showing the relationship between dolomite and degree of order with a slight trend of better order for older dolomites from left to right.

The difference in major and trace element content in dolomite also affects the degrees of order. Cation atoms with different ionic radii produces different lattice plane spacing relative to their abundance (Goldsmith and Graf, 1958).

Therefore, it is reasonable to assume that compositionally different diagenetic

fluids with different water-rock interaction, growth, and compaction rates formed the replacement dolomites throughout the Paleocene-Eocene with different degrees of order.

## 4.2 Major Elements ($Ca^{2+}$ and $Mg^{2+}$) of the Paleocene-Eocene Dolomites

The twenty-six samples in Table 1 were analyzed by ICP-AES to determine their major elemental content. The mineral dolomite is dominant in all of the samples. $Ca^{2+}$ and $Mg^{2+}$ are the main cations in dolomite. Stoichiometric dolomite has 50:50 $Ca^{2+}$ to $Mg^{2+}$ ratio. Well ordered dolomite has $Mg^{2+}$ and $Ca^{2+}$ in alternate cation layers separated by $CO_3$. The stoichiometry of dolomite is measured through the molar % $CaCO_3$ calculated from the molar ratio [Ca / (Ca+Mg)]*100.

Table 3 includes stoichiometry calculations for the sampled Paleocene-Eocene dolomites. The molar % $CaCO_3$ range from 48.8% to 54.1% with average of 50.8% (n = 23; std. = 1.08). The highest mole % $CaCO_3$ modal class is between 50% and 51%. Samples 5, 7, and 15 were not included in stoichiometry calculation because they were contaminated by calcite cement filling the pores. This does not imply that the other samples are pore-filling calcite free, but the abundance of calcite cement in the three samples above was confirmed based on petrography and X-ray results.

### 4.2.1 Major Elements ($Ca^{2+}$ and $Mg^{2+}$) Discussion

Holocene sabkha dolomites from Abu Dhabi are poorly ordered and very finely crystalline with molar % $CaCO_3$ range between 52% and 54.6% (MacKenzie, 1981). Holocene tidal flat dolomites from the Little Bahamas Bank are poorly ordered with molar % $CaCO_3$ range between 51% and 61%, and poorly ordered lacustrine dolomites that were observed around and beneath the Bahamian lakes have molar % $CaCO_3$ that range between 59% and 61% (Mitchell and Horton, 1995b).

| Sample No. | Description | molar % $CaCO_3$ | $Ca^{2+}$ (ppm) | $Mg^{2+}$ (ppm) |
|---|---|---|---|---|
| 1 | Non-planar (20-50 μm) dolomite | 48.8 | 176,870 | 113,400 |
| 2 | Non-planar (20-50 μm) dolomite | 51.6 | 222,100 | 132,100 |
| 3 | Non-planar (20-50 μm) dolomite | 50.0 | 208,560 | 131,700 |
| 4 | Non-planar (5-20 μm) dolomite | 52.2 | 220,150 | 127,500 |
| 5* | Non-planar (5-20 μm) dolomite | 54.9* | 221,420 | 115,400 |
| 6 | Non-planar (5-20 μm) dolomite | 51.4 | 205,370 | 124,800 |
| 7* | Non-planar (5-20 μm) dolomite | 60.0* | 228,107 | 98,785 |
| 8 | Non-planar (5-20 μm) dolomite | 50.4 | 210,015 | 132,300 |
| 9 | Non-planar (20-50 μm) dolomite | 49.9 | 207,552 | 132,950 |
| 10 | Non-planar (5-20 μm) dolomite | 49.5 | 208,132 | 135,525 |
| 11 | Non-planar (5-20 μm) dolomite | 50.4 | 213,165 | 133,750 |
| 12 | Non-planar (5-20 μm) dolomite | 50.4 | 209,967 | 132,025 |
| 13 | Dolomicrite | 50.9 | 206,200 | 127,500 |
| 14 | Non-planar (5-20 μm) dolomite | 50.9 | 191,340 | 118,700 |
| 15* | Non-planar (20-50 μm) dolomite | 56.7* | 220,690 | 108,600 |
| 16 | Planar-s (20-50 μm) dolomite | 52.2 | 210,567 | 124,075 |
| 17 | Dolomicrite | 51.5 | 203,295 | 124,050 |
| 18 | Non-planar (20-50 μm) dolomite | 50.5 | 205,572 | 130,425 |
| 19 | Non-planar (5-20 μm) dolomite | 49.9 | 200,825 | 131,225 |
| 20 | Non-planar (20-50 μm) dolomite | 49.8 | 198,100 | 129,650 |
| 21 | Non-planar (5-20 μm) dolomite | 50.4 | 199,055 | 127,175 |
| 22 | Non-planar (20-50 μm) dolomite | 51.7 | 206,910 | 125,150 |
| 23 | Non-planar (20-50 μm) dolomite | 54.1 | 219,030 | 120,900 |
| 24 | Non-planar (5-20 μm) dolomite | 50.2 | 208,570 | 134,050 |
| 25 | Planar-s (20-50 μm) dolomite | 51.0 | 210,520 | 130,500 |
| 26 | Planar-s (20-50 μm) dolomite | 50.7 | 208,230 | 130,700 |

**Table 3** Stoichiometry (molar % $CaCO_3$) for the 26 samples. Samples with * sign were excluded from average stoichiometry calculations because pore-filling calcite cement is predominant in these sample. Note that sample 23 has a high calcite content, but no calcite peak from XRD, or calcite cement from petrography was observed, thus it is included for average stoichiometry calculation.

Subtidal Holocene dolomite from the Little Bahamas Bank are markedly enriched in $Ca^{2+}$, 60% $CaCO_3$, and poorly ordered (Mitchell and Horton, 1995a). The subtidal Holocene dolomites in Abu Dhabi are both ordered and disordered, and have excess $Ca^{2+}$ with molar % $CaCO_3$ of 54% (Frisia, 1994). Nearly ordered dolomites with excess in

$Ca^{2+}$ were observed from Abu Dhabi dolomites that directly precipitated within pores of tidal flat and lagoonal sediments (Wenk et al., 1993; Frisia, 1994). These dolomite precipitates coexist with dolomite rhombs that formed through the replacement of aragonite needles in dissolution-precipitation process, and both replacement and precipitation processes occur simultaneously during early diagenesis.

The general trend of dolomite "aging" is toward increase of crystal size and degree of order, and stabilization with respect to Ca:Mg, i.e., more stoichiometric. The Paleocene-Eocene dolomites with their average molar % $CaCO_3$ of 50.8% are near stoichiometric, and very close to the Phanerozoic nearly ordered dolomites of 51 % $CaCO_3$ (Sperber et al., 1984). Only one study was found concerning the stoichiometry of Paleocene-Eocene dolomites within the eastern Arabian Plate. Holail et al. (2005) reported the stoichiometry of the Dammam Formation in Qatar with two types of dolomites that consisted 51% $CaCO_3$ and 54% $CaCO_3$. The total subsurface thickness of Dammam Formation in Qatar is around 35 m with the dolomitized section being around 23 m.

The relationship between dolomite crystal size, stoichiometry, and degree of order is random in this study (Fig. 64). Studies of Late Cenozoic dolomites provide insights into dolomite texture, stoichiometry, and degree of order. The Miocene dolomite of the Little Bahamas Bank is coarser relative to the younger overlying Pliocene dolomite. However, the former is Ca-rich ($Ca_{.60}Mg_{.40}CO_3$); whereas the latter is near stoichiometric ($Ca_{.51}Mg_{.49}CO_3$) (Vahrenkamp and Swart, 1994). Nevertheless, the Ca/Mg ratio varies considerably within the 80 m thick Miocene-Pliocene dolomite section of the Little Bahamas Bank (Fig. 65).

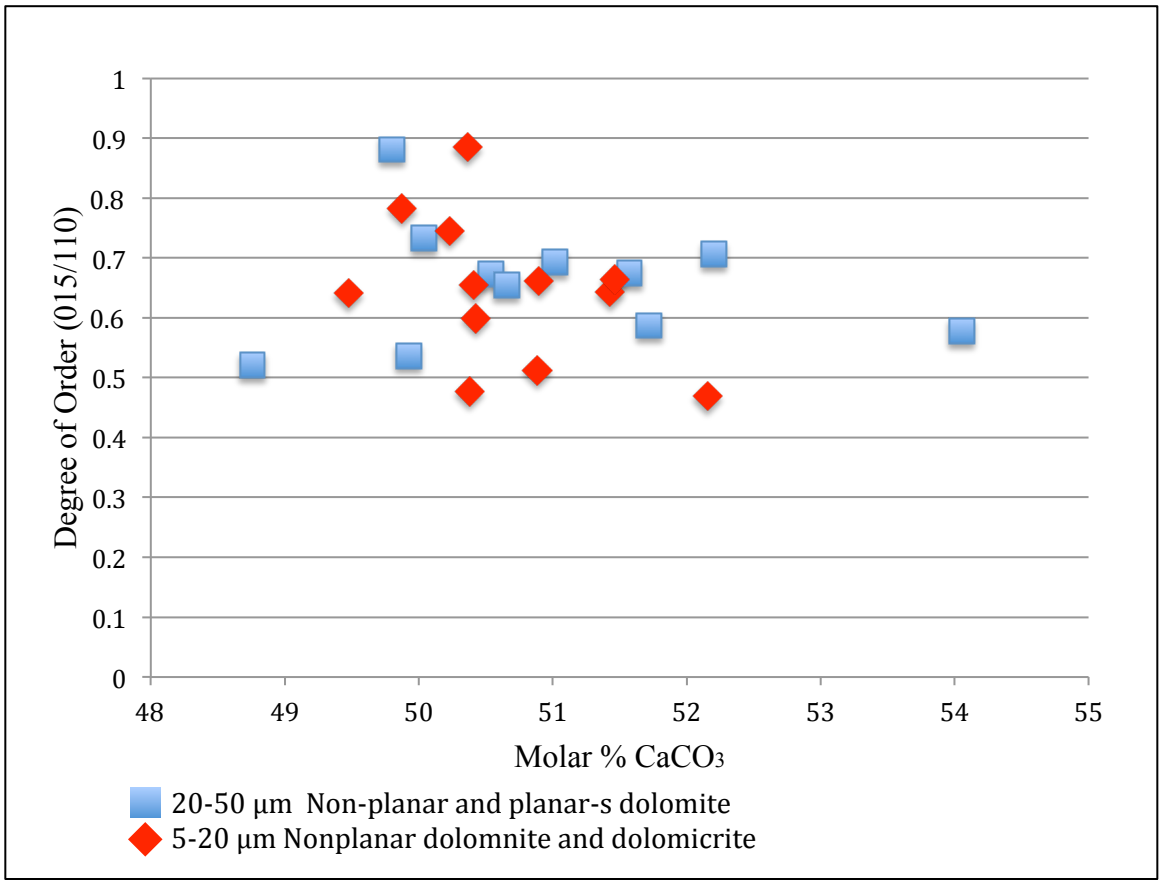


**Figure 64** A scatter bivariate plot displays the lack of relationship between molar % $CaCO_3$, degree of order, dolomite crystal sizes. Samples 5, 7, and 15 are not plotted.

The Pleistocene dolomites of the Arabian Gulf are better ordered, coarser, and nearly stoichiometric relative to their analogous Holocene dolomites from Abu Dhabi, but no changes regarding stoichiometry, crystal size, and degree of order were observed within the (> 56 m) thick dolomite section (Chafetz and Rush, 1994).

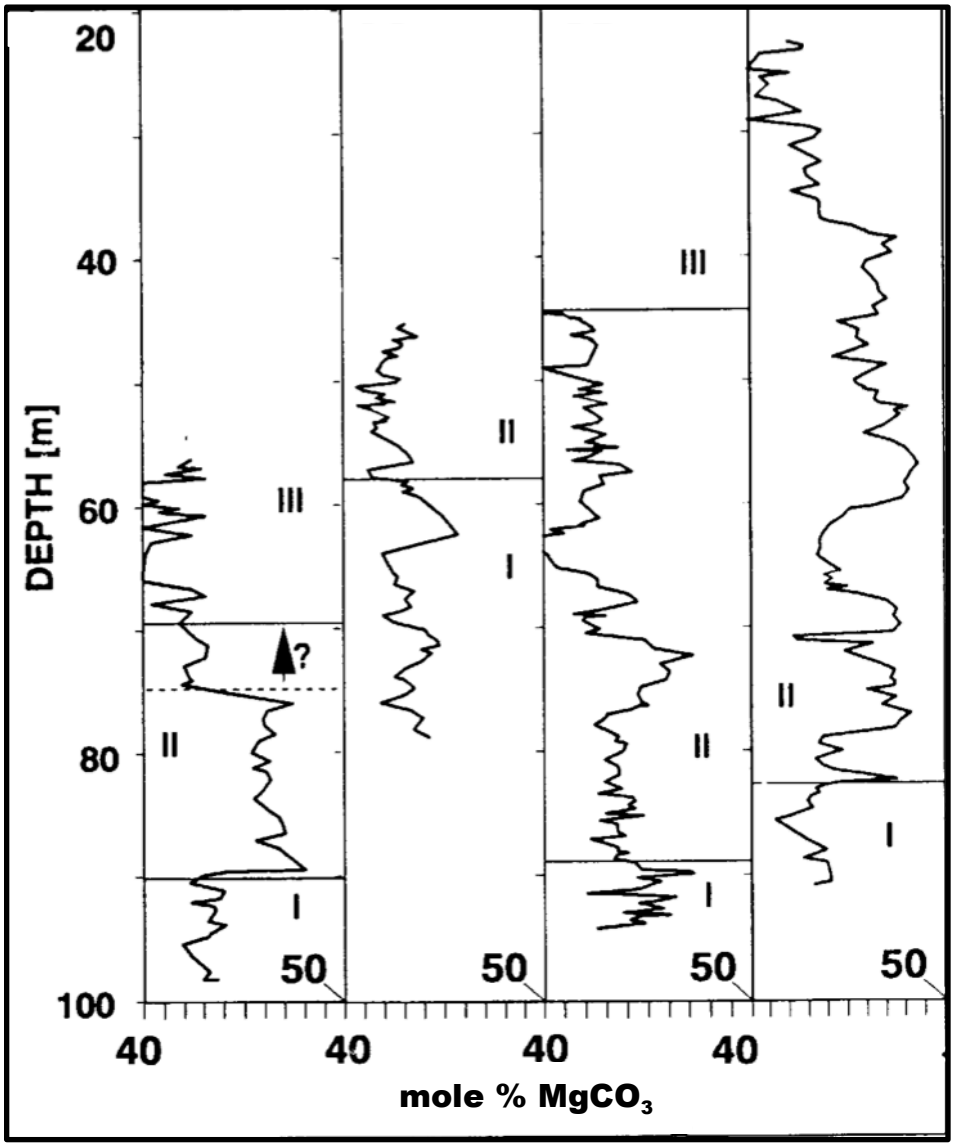


**Figure 65** Mole % $MgCO_3$ composition of the Little Bahamas Bank dolomites from four cores. Note the fluctuations in mole % $MgCO_3$ with depth. I, II, III are age boundaries based on Sr isotopes. See Vahrenkamp and Swart, 1994 for further details.

The studies of the Bahamas and Arabian Gulf Late Cenozoic dolomites have revealed that dolomites were formed through multiple episodes of dolomitization during syn-deposition and later diagenesis. The textural and geochemical properties of dolomite precipitates are modified in multiple diagenetic episodes from surface to burial with a trend toward more geochemically stabilized and texturally mature dolomites (MacKenzie, 1981). The early properties are partially or completely obliterated by the last diagenetic event (Land, 1985).

The Paleocene-Eocene dolomites in this study were selected from widely spaced intervals within the stratigraphic section. The average stoichiometry of the dolomites is similar to most of the nearly stoichiometric Phanerozoic dolomites. This means that the dolomites are nearly stabilized in term of Ca/Mg ratio, but the lack of apparent relationship between stoichiometry, crystal size, and degree of order suggests that the dolomites went through different textural stabilization phases during their 31 my history. The mechanisms by which modern tidal flat dolomites form are highly controlled by Mg/Ca ratio in sediments and pore waters, and pore water salinity, alkalinity, temperature, and sulfate content (Folk and Land, 1975; MacKenzie, 1981, Land, 1985, Mitchell and Horton, 1995b). Perhaps the diagenetic fluid was not constant. The permeability and porosity would also have played a major role in controlling rock-water interaction ratios, thus dolomitization processes.

## 4.3 Trace Elements ($Sr^{2+}$, $Na^{2+}$, $Fe^{2+}$, and $Mn^{2+}$) of the Paleocene-Eocene Dolomites

### 4.3.1 Trace Elements in Dolomite

Trace elements are used in combination with petrography and isotopic composition in order to determine dolomitization settings and dolomite paragenesis (Land, 1985; Gao et al, 1992; Warren, 2000). Table 4 shows the concentrations of $Sr^{2+}$, $Na^{2+}$, $Fe^{2+}$, and $Mn^{2+}$ elements in dolomites of this study.

Carbonate precipitants incorporate trace elements in their crystal structure. As they become older, however, the initial content of these elements can undergo changes during multiple dissolution-precipitation diagenetic episodes, and the solid phase elemental content under equilibrium precipitation is determined by:

$$({}^{m}Me/{}^{m}Ca)_s = D({}^{m}Me/{}^{m}Ca)_w$$

where m = molar concentration, Me = trace element, Ca = Carbonate, s = solid, w = liquid, and D = distribution coefficient (Veizer, 1983a). According to the equation above, a trace element is enriched in the solid phase relative to the liquid phase when D value is greater than one, and depleted in the solid phase when the D value is less than one. Solid and liquid phases will have the same relative amount of the trace element compared to the relative abundance when the D value is one (Veizer, 1983a).

The incorporation of trace and minor elements in a growing carbonate crystal in solution can take place by: (1) minor and trace element substitution for $Ca^{+2}$ in the carbonate crystal lattice, (2) interstitial placement between lattice planes, (3) occupation of free lattice positions that resulted from defects in the structure, (4) absorption in the

lattice by remnant ionic charges, and (5) inclusion of impurities (McIntire, 1963, and Zemann, 1969, cited in Veizer, 1983a).

| Samples | $Sr^{+2}$ (ppm) | $Na^{+2}$ (ppm) | $Fe^{+2}$ (ppm) | $Mn^{+2}$ (ppm) |
|---|---|---|---|---|
| 1 | 60 | 682 | 125 | 20 |
| 2 | 86 | 649 | 66 | 35 |
| 3 | 72 | 623 | 62 | 49 |
| 4 | 163 | 762 | 135 | 50 |
| 5 | 153 | 716 | 127 | 74 |
| 6 | 100 | 607 | 115 | 22 |
| 7 | 51 | 1014 | 421 | 168 |
| 8 | 197 | 649 | 111 | 36 |
| 9 | 104 | 515 | 119 | 27 |
| 10 | 102 | 602 | 83 | 26 |
| 11 | 96 | 530 | 179 | 31 |
| 12 | 148 | 626 | 252 | 46 |
| 13 | 112 | 617 | 280 | 27 |
| 14 | 94 | 493 | 228 | 22 |
| 15 | 146 | 594 | 168 | 28 |
| 16 | 87 | 650 | 146 | 16 |
| 17 | 107 | 524 | 290 | 41 |
| 18 | 118 | 489 | 104 | 29 |
| 19 | 100 | 570 | 161 | 29 |
| 20 | 90 | 745 | 213 | 31 |
| 21 | 82 | 557 | 86 | 33 |
| 22 | 85 | 400 | 38 | 26 |
| 23 | 86 | 570 | 53 | 25 |
| 24 | 71 | 583 | 44 | 29 |
| 25 | 72 | 572 | 119 | 31 |
| 26 | 70 | 670 | 83 | 33 |

**Table 4** Measured trace element abundance for the 26 dolomite samples.

Because trace elements larger than $Ca^{+2}$ are limited to $Ca^{+2}$ sites, and the mineral dolomite has two major cations, $Ca^{+2}$ and $Mg^{+2}$, the abundance of trace elements with large radii is controlled by $Ca^{+2}$ content in the dolomite lattice. The remaining four ways of element incorporation in dolomite are random and difficult to be recognized (Veizer, 1983a).

The crystal structure also controls the incorporation of trace elements in carbonates. The $Ca^{+2}$ site in orthorhombic aragonite is larger than the $Ca^{+2}$ site in the rhombohedral calcite and dolomite, therefore, cations with large radii like $Sr^{+2}$ are more enriched in aragonite than calcite and dolomite. Consequently, dolomite has the lowest $Sr^{+2}$ because of the rhombohedral crystal structure and enrichment of $Mg^{+2}$ at the expense of $Ca^{+2}$ (Banner, 1995).

A major shortcoming associated with studying trace element in dolomites is the weakly known distribution coefficients of trace elements in dolomite. This is mainly the outcome of the inability to synthesize dolomite in the laboratory under normal temperature and with natural water. Thus, a wide range of distribution coefficient values is assumed for different elements in dolomite (Veizer, 1983a; Budd, 1997). The inadequately known distribution coefficient (D) value for dolomite has resulted in computing different "D" values in studying ancient dolomites, and if the "D" is normalized in all of the studies, the ranges of $Sr^{2+}$ content overlaps significantly (Budd, 1997). Vahrenkamp and Swart (1990) proposed a "D" value of 0.0118 for stoichiometric dolomite and added 0.0039 for every additional mole % $CaCO_3$. Yet, variations in kinetic effects, parent fluid chemistry, and inclusion amount of Sr-rich solids results in different incorporation level of $Sr^{2+}$ in dolomites (Budd, 1997).

The ionic strength of the diagenetic fluid in the dolomitization process is also important. For example, because of the high ionic strength of seawater relative to meteoric water, a mixture of meteoric and seawater will have Sr/Ca molar ratios akin to that of seawater if the mixture composes more than 5% seawater (Warren, 2000). And a dolomite with marine $Sr^{2+}$ content may precipitate from a meteoric and seawater mixture with more than 20% seawater.

Moreover, the ionic charge of a trace element controls the levels of its incorporation into dolomite lattice. For example, the ionic charge, i.e., the redox potential, for $Mn^{+2}$ and $Fe^{+2}$ makes their incorporation in dolomite to be limited to anoxic environments because it requires a divalent state (Budd, 1997).

The abundance of diagenetic fluid is correspondingly a significant factor in trace element incorporation into dolomite. The elemental content of the replaced carbonate dominates the trace element content in dolomite if dolomitization takes place in a relatively closed system (Warren, 2000). Thus, at the lowest rock-water interaction, dolomite with $Sr^{2+}$ contents of 500–600 ppm will form from the replacement of marine aragonite, with its high $Sr^{2+}$ content of 8000 to 10,000 ppm. Dolomites with 200–300 ppm $Sr^{2+}$ content should form from marine high- and low- Mg calcite precursors, with $Sr^{2+}$ content of 1000 – 2000 ppm, but Sr-depleted dolomites should form from diagenetic low-Mg calcite precursor, with its much lower $Sr^{2+}$ content (Warren, 2000).

### 4.3.2 Strontium ($Sr^{2+}$) Content of the Paleocene-Eocene Dolomites

Strontium values were measured by ICP-AES for the twenty-six samples. $Sr^{2+}$ content in dolomite is commonly used to identify dolomitization settings and dolomite

paragenesis within a single stratigraphic succession that includes different dolomites (e.g. Veizer et al., 1978; Gao et al., 1992; Vahrenkamp and Swart, 1994; Mresah, 1998; Kyser et al., 2002).

The $Sr^{2+}$ values for the Paleocene-Eocene dolomites range from 60 to 197ppm with an average of 102 ppm (Fig. 66). The $Sr^{2+}$ values of the dolomites do not show a distinctive distribution (Fig. 67), and no regular relationship was found between $Sr^{2+}$ content and molar % $CaCO_3$, crystal size (Fig. 68), and stratigraphic position.

The $Sr^{2+}$ concentrations are independent of the types of dolomite microfacies, i.e., evaporitic vs. evaporite-free dolomites. Ancient arid supratidal (evaporitic) dolomites are commonly more enriched in $Sr^{2+}$ because of the imprint of hypersaline seawater whereas subtidal dolomites tend to have $Sr^{2+}$ contents closer to seawater (Ye and Mazzullo, 1993).

#### 4.3.2.1 Strontium ($Sr^{2+}$) Discussion

The $Sr^{2+}$ values of the Paleocene-Eocene dolomites in this study are lower than the modern dolomites forming in contact with hypersaline and normal seawater. Modern sabkha dolomites from the Arabian Gulf are formed by direct precipitation and replacement in contact with hypersaline fluid, and have average $Sr^{2+}$ content around 600 ppm (Land and Hoops, 1973). Modern supratidal dolomites from Florida Keys and the Little Bahamas Bank have average $Sr^{2+}$ content of 620 ppm and 640 ppm, respectively (Land and Hoops, 1973). When these dolomites undergo further diagenesis with incorporation of meteoric water, their $Sr^{2+}$ composition falls dramatically.

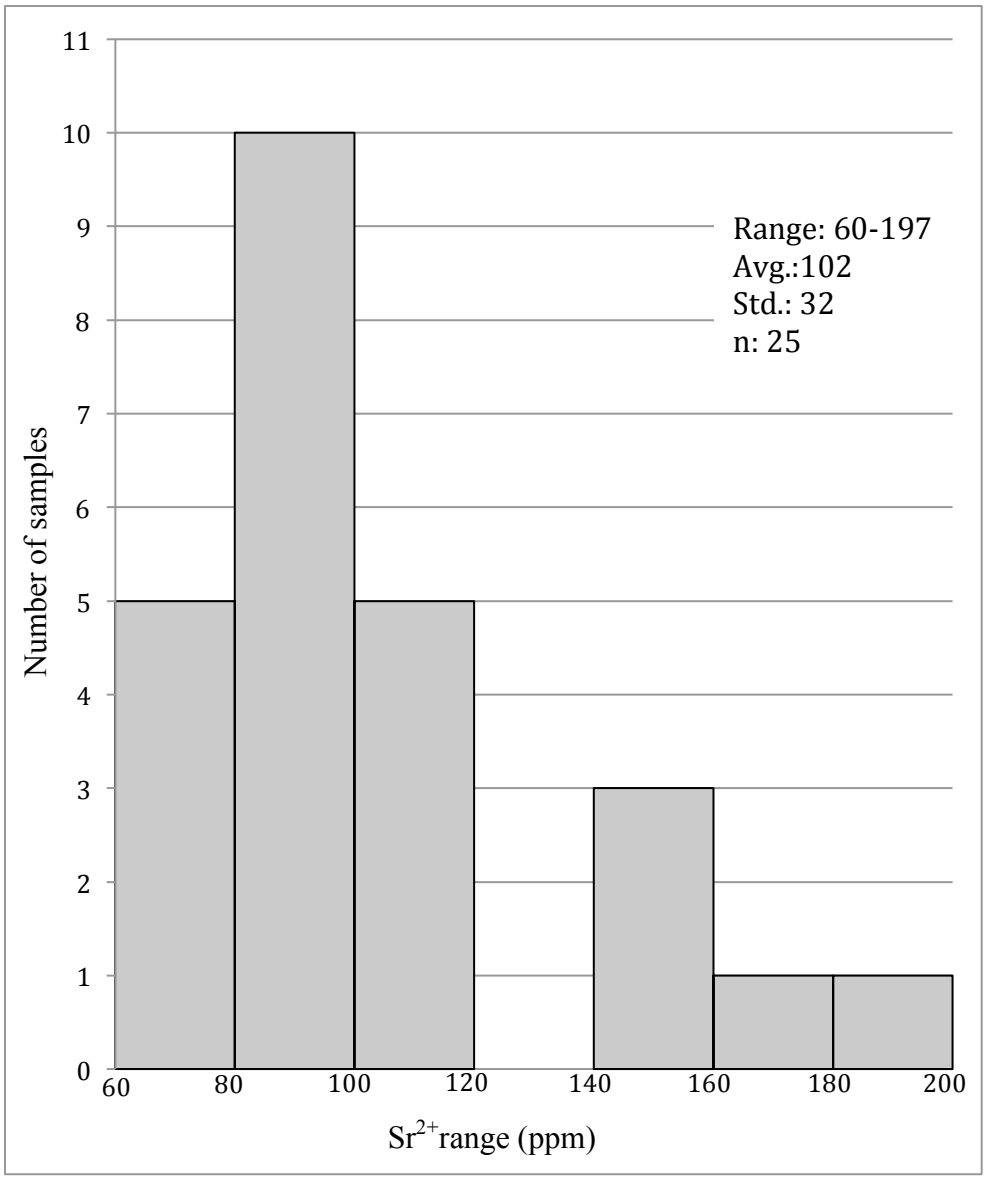


**Figure 66** Distribution of $Sr^{2+}$ abundances in the dolomite samples.

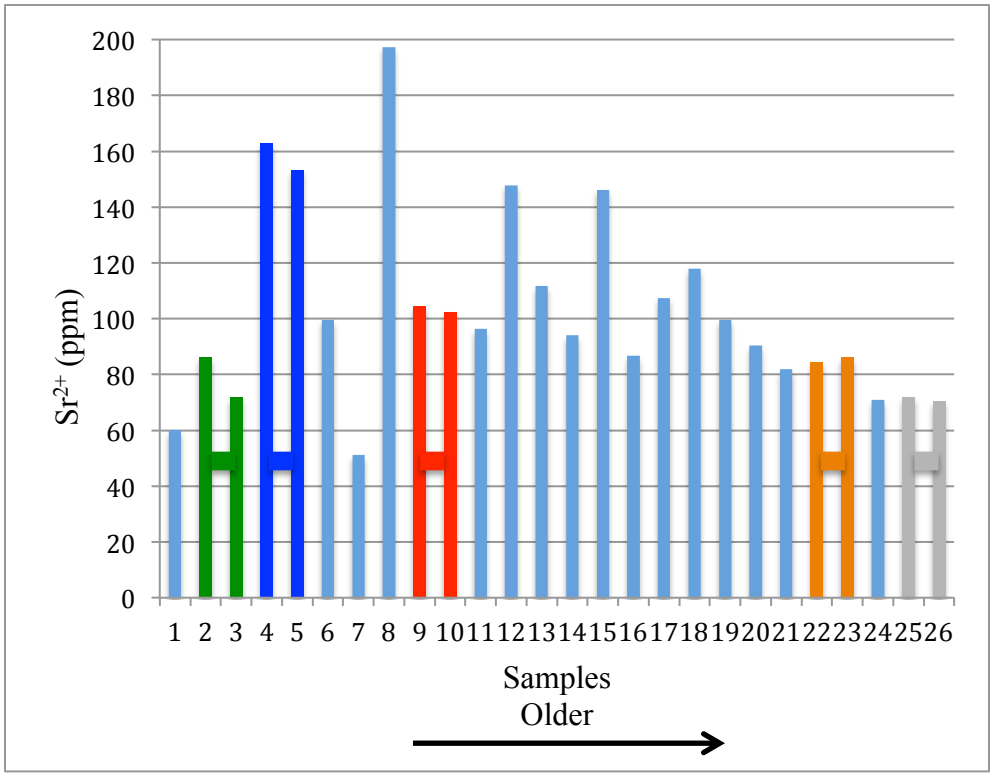


**Figure 67** $Sr^{2+}$ values for the 26-dolomite samples. The linked bars with matching color represent samples within the same dolomite interval.

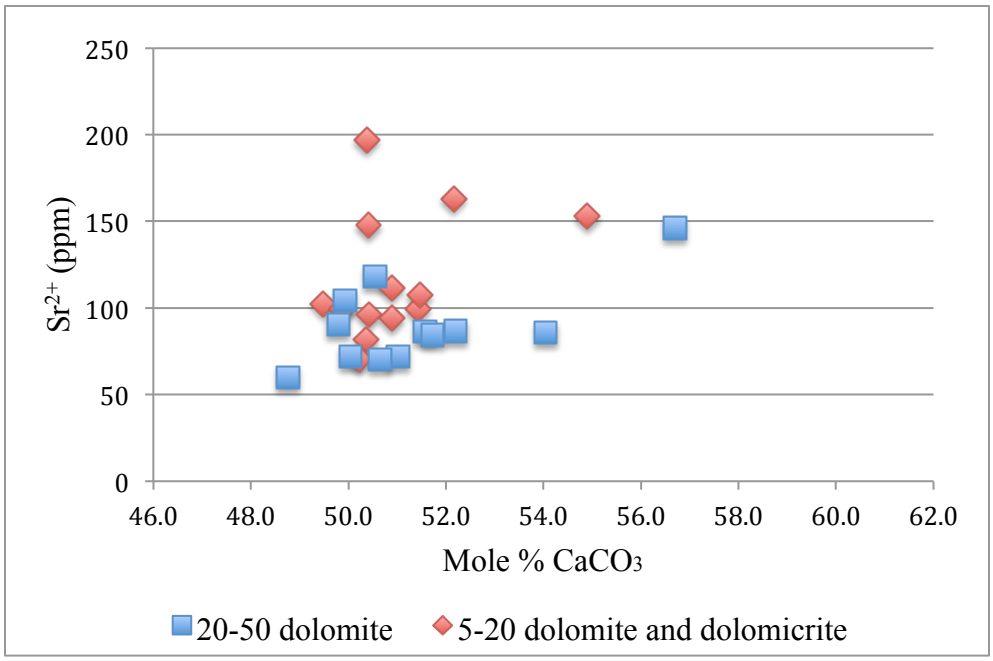


**Figure 68** A plot showing the absence of relationship between $Sr^{2+}$ content, mole % $CaCO_3$, and dolomite crystal size.

A Paleocene example in which $Sr^{2+}$ content was used to distinguish between different dolomitization settings, thus fluids, is discussed here because of its similar age to this study. Mresah (1998) utilized $Sr^{2+}$ concentration along with petrographic and isotopic attributes to distinguish different dolomites within the Paleocene Northeast Sirte Basin, Libya. Basinal dolomite, pervasive platform interior and platform margin dolomite, and evaporitic platform dolomicrite have $Sr^{2+}$ averages as follows: 89, 72, and 639 ppm, respectively. The highest difference in $Sr^{2+}$ content is between evaporitic dolomicrite and pervasive dolomite with the former being dolomitized by hypersaline seawater dolomitizing fluid. In contrast, the latter is dolomitized by mixed meteoric and marine water in an open system (Mresah, 1998).

The $Sr^{2+}$ content range for different dolomites in the previous example and examples mentioned above commonly overlap. Budd (1997) estimated a range of 150-300 ppm to represent dolomites formed from normal seawater based on an extensive data base representing the Late Cenozoic post-depositional carbonate island dolomites. A higher $Sr^{2+}$ content resulted from dolomitization of aragonitic carbonates in a closed system, or dolomitization with hypersaline water, whereas a lower content is due to dilution of seawater by meteoric water.

A general trend toward more $Sr^{2+}$ depleted and more stoichiometric dolomite with "ageing" is widely accepted (Land, 1985; Warren, 2000). The Miocene-Pliocene Little Bahamas Bank dolomite have $Sr^{2+}$ range of 70-300 ppm and are formed from normal seawater, yet a range of 30-100 ppm is estimated with further diagenesis and stabilization in the future (Vahrenkamp and Swart, 1994). Ancient tidal flat evaporitic dolomites are usually depleted in $Sr^{2+}$. For example, the Lower Permian Wichita Formation dolomite of

the Midland Basin, Texas, has $Sr^{2+}$ range of 25-125 ppm (Ye and Mazzullo, 1993). The Lower Ordovician upper Arbuckle Group in southwestern Oklahoma has a $Sr^{2+}$ range of 34-89 ppm (Gao et al., 1992). The low Sr content in the last two examples is attributed to modifications of early dolomite with meteoric water.

The Paleocene-Eocene dolomites in this study formed on extensive tidal flats, and if the early dolomitizing fluids were hypersaline, or marine water, the dolomites have gone through later dolomitization phases in contact with meteoric or mixed meteoric and marine water based on their $Sr^{2+}$ content. The irreconcilable relation between $Sr^{2+}$ values and microfacies indicate that dolomitization took place at different water-rock interaction with variable dolomitizing fluid chemistry.

### 4.3.3 Sodium Content of the Paleocene-Eocene Dolomites

Sodium is commonly used along with strontium to infer the salinity of dolomitizing fluids. The $Na^{2+}$ values for dolomite in this study range from 400 to 762 ppm with an average of 600 ppm (Fig. 69). Sample No. 7 was reasonably excluded from average and standard deviation calculations, and from plots showing elemental relationships. The sample has distinguishably high $Na^{2+}$, $Fe^{2+}$, and $Mn^{2+}$ concentrations relative to the other samples, and the lowest $Sr^{2+}$. A duplicate of the sample gave the same result that insured the reliability of the measurements. This sample also has the highest $Ca^{2+}$ concentration and a predominant XRD calcite peak. The sample is enriched in calcite through pore-filling calcite cement that probably formed in deep burial depth based on high $Fe^{2+}$ and $Mn^{2+}$ content, and with basinal saline waters based on the high $Na^{2+}$ content. Additional line of evidence supporting the deep cementation setting is the

lowest $\delta^{18}O$ value of the sample.

Most of the $Na^{2+}$values are between 550 and 650 ppm, thus different dolomites based on their $Na^{2+}$ are not recorded (Fig. 70). In addition, $Na^{2+}$ and $Sr^{2+}$ show a scattered relationship (Fig. 71).

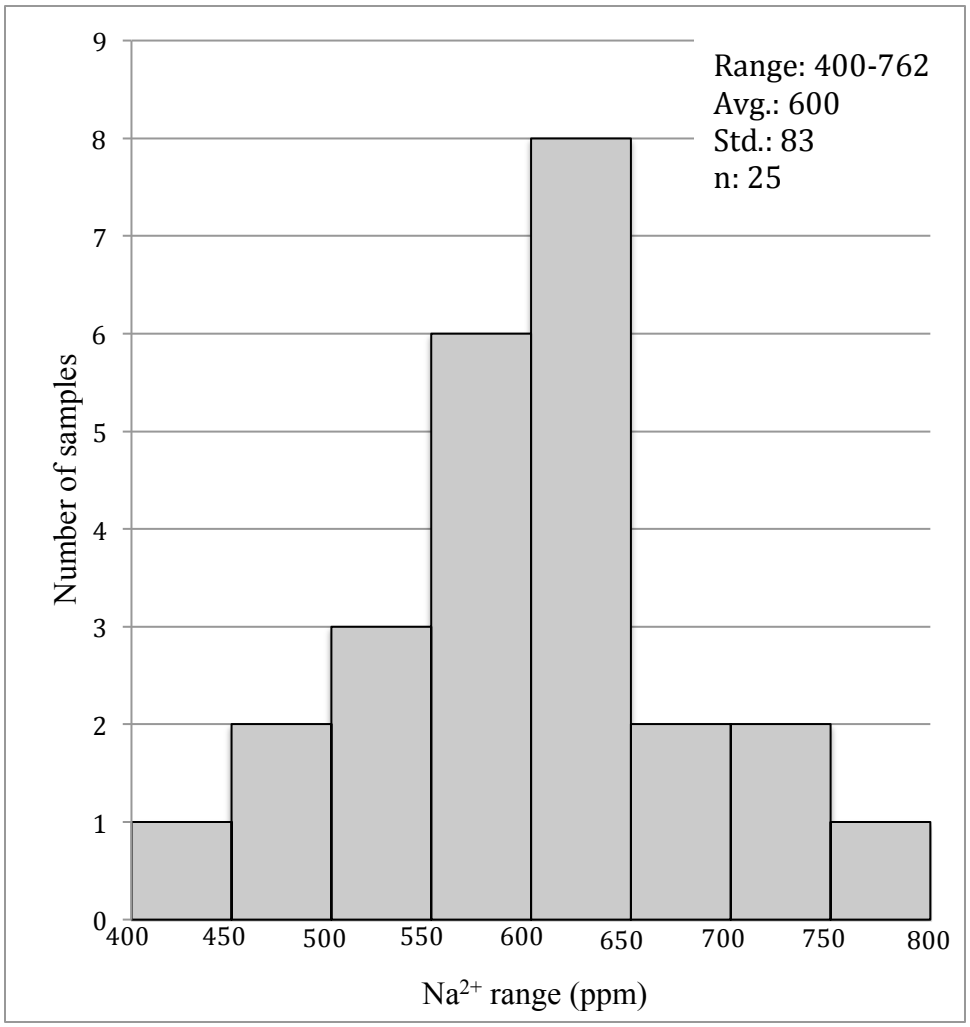


**Figure 69** Distribution of $Na^{2+}$ abundance in the dolomite samples.

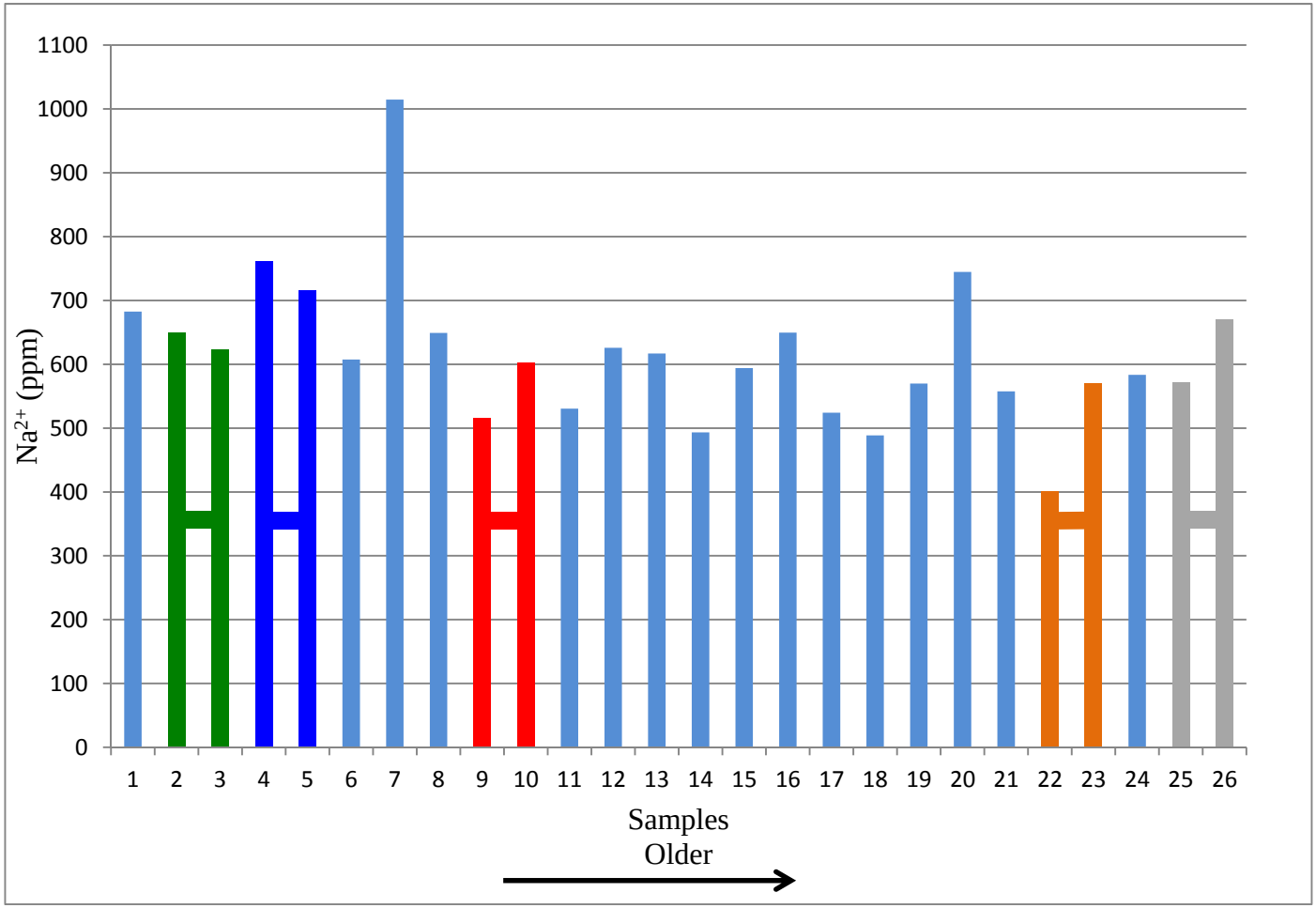


**Figure 70** Samples plotted in ascending order of $Na^{2+}$ values. Note that the incremental pattern is generally gradational. The linked bars with matching color represent samples within the same dolomite interval.

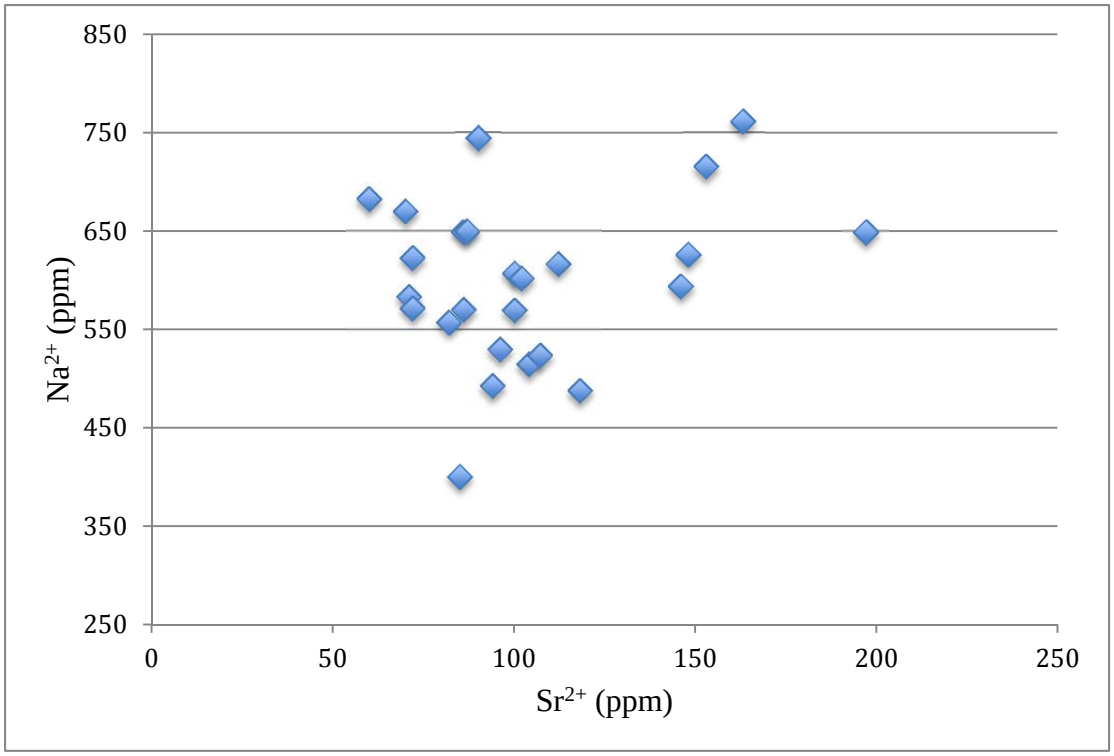


**Figure 71** A scatter plot for $Na^{2+}$ and $Sr^{2+}$values.

#### 4.3.3.1 Sodium ($Na^{2+}$) Discussion

Modern marine dolomites in the Arabian Gulf have a $Na^{2+}$ average of 2350 ± 40 ppm, and supratidal dolomite from Sugarloaf Key, Florida, and Little Bahamas Bank have $Na^{2+}$ averages of 1780 and 3050 ± 40 ppm, respectively (Land and Hoops, 1973). Late Cenozoic dolomites on carbonate islands have $Na^{2+}$ averages that range from 280 to 710 ppm. Ranges for dolomites interpreted as having formed in normal seawater and hypersaline water versus dolomites interpreted as mixed meteoric and marine water in origin distinctly overlap (Budd, 1997).

The $Na^{2+}$ content in anhydrite- and gypsum-bearing Neogene, the Bira and Gesher formations, dolomites shows a very wide range from 400 to 2700 ppm (Sass and Bein, 1988). The wide range is the result of multiple changes in the Ca/Mg and Na/Ca ratios in evaporitic seawater. The modifications of these ratios was controlled by precipitation of evaporites and dolomites and changes in surface and pore fluids chemistry (Sass and Bein, 1988).

Very little is known about the distribution coefficient value for $Na^{2+}$ in dolomite. $Na^{2+}$ values for ancient dolomites are widely reported as high or low relative to other dolomites in the same section or in other studies (Tucker and Wright, 1990; Budd, 1997). Moreover, it is unclear if $Na^{2+}$ incorporates in dolomite as a cation substitute, fluid inclusion (Tucker and Wright, 1990), or occupies defected lattice sites (Budd, 1997).

Sodium abundance in this study essentially does not show a relationship with the degree of order (Fig. 72) and its range overlaps with marine and mixed marine and meteoric dolomites.

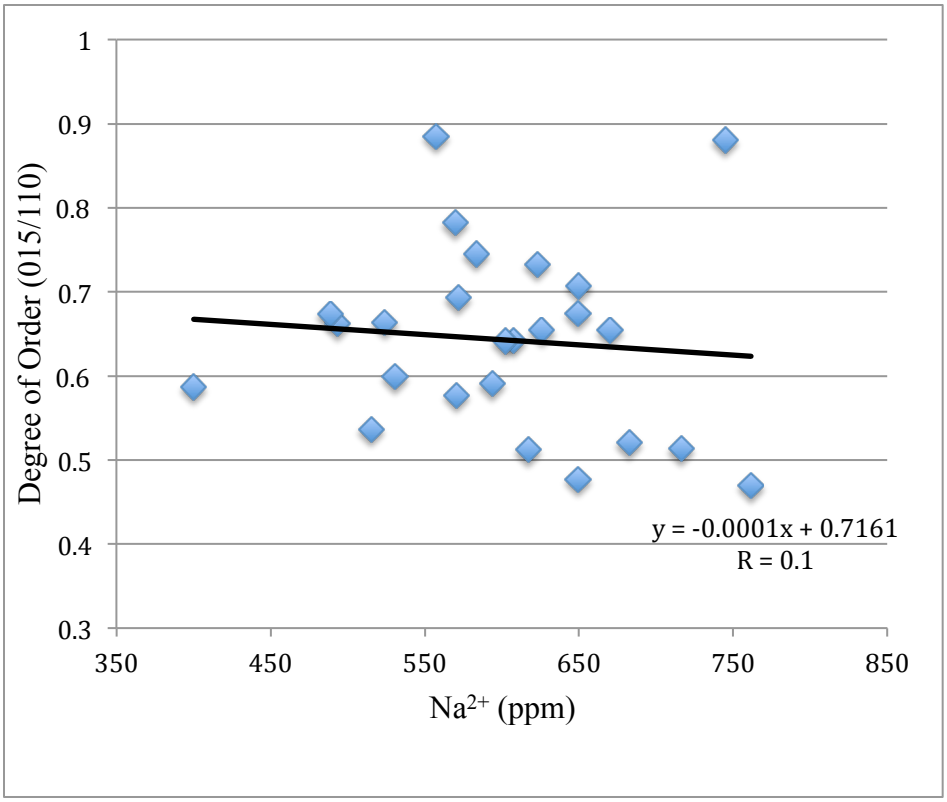


**Figure 72** A plot showing the relationship between $Na^{2+}$ values and degree of order for the dolomite samples.

### 4.3.4 Iron and Manganese ($Fe^{2+}$and $Mn^{2+}$) Content of the Paleocene-Eocene Dolomites

The iron concentrations in the dolomites show a very wide range from 38 to 290 ppm with an average of 135 ppm (Fig. 73). Manganese, in contrast, has a lower range from 16 to 74 ppm with an average of 33 pm (Fig. 74). The relationship between $Fe^{2+}$and $Mn^{2+}$ is random. This is mainly due to the low $Mn^{2+}$ content with modal range of 25-35 ppm. The overall low $Mn^{2+}$ abundance and its modal distribution did not allow its correlation with other geochemical attributes, therefore, its significance is marginalized.

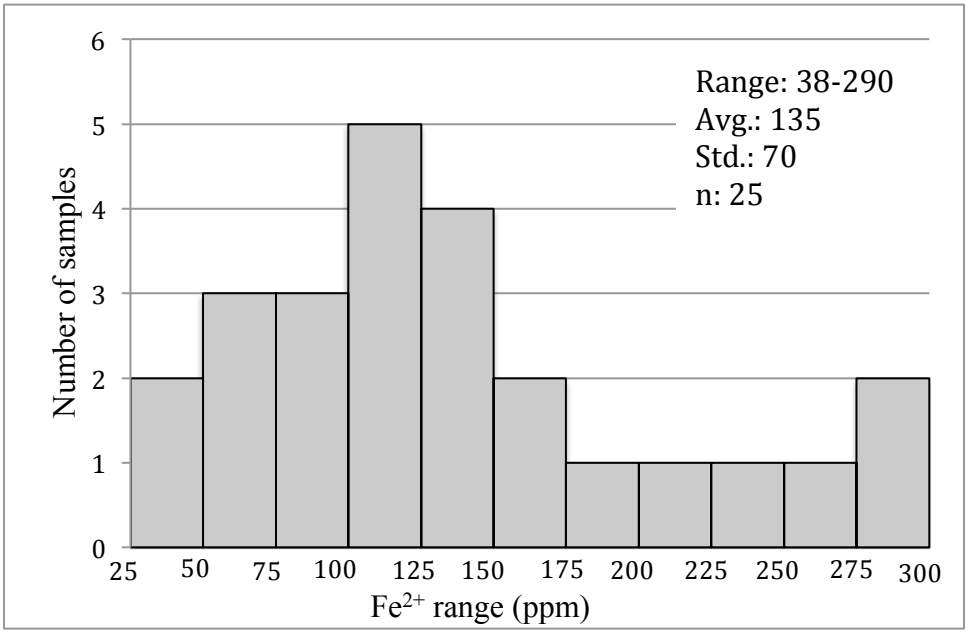


**Figure 73** Distribution of $Fe^{2+}$ abundances in the dolomite samples.

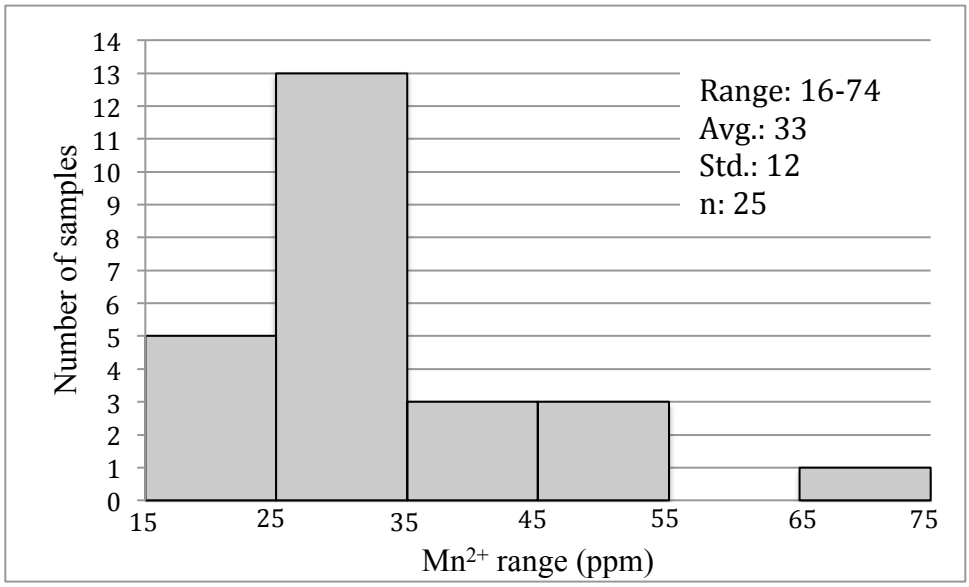


**Figure 74** Distribution of $Mn^{2+}$ abundances in the dolomite samples.

The relationships between $Fe^{2+}$ and crystal size, degree of order, molar % $CaCO_3$, and $\delta^{13}C$ are negligible, as shown by regression lines with very low R values.

#### 4.3.4.1 Iron ($Fe^{2+}$) and Manganese ($Mn^{2+}$) Discussion

$Fe^{2+}$ and $Mn^{2+}$ are extremely depleted in seawater with the average for each of them being 0.002 ppm, but they are preferentially incorporated into dolomite because of the larger than unity distribution factor for both elements (Veizer, 1983a). However, the incorporation level for $Fe^{2+}$ and $Mn^{2+}$ is limited to their availability in pore fluid and the necessary reducing condition during dolomitization (Veizer, 1983a, Budd, 1997).

Modern dolomites vary highly in their $Fe^{2+}$ and $Mn^{2+}$ content, with an $Fe^{2+}$ range of tens to several thousands, and an $Mn^{2+}$ range of 3 to 100 ppm (Vahrenkamp and Swart, 1994). Modern dolomites beneath Andros Island have formed in contact with saline groundwater, which is modified from normal seawater, and have $Fe^{2+}$ range from100 to 200 ppm; $Mn^{2+}$ is generally lower than 20 ppm (Whitaker et al., 1994). Sparse $Fe^{2+}$ and $Mn^{2+}$ sources, limited to hydroxides in precursor carbonates, and slightly reducing conditions are the factors behind the relatively low $Fe^{2+}$ and $Mn^{2+}$ contents in the Andros Island dolomites. $Fe^{2+}$ and $Mn^{2+}$ contents in Late Cenozoic marine dolomites of the Little Bahamas Bank are exclusively controlled by the precursor carbonates. The $Fe^{2+}$ and $Mn^{2+}$ ranges are 10-300 and 5-100 ppm, respectively, and the original compositions are about 15 and 5 ppm, respectively (Vahrenkamp and Swart, 1994).

$Fe^{2+}$ and $Mn^{2+}$ are more enriched in meteoric water than seawater (Brand and Veizer, 1981; Veizer, 1983a). Thus dolomites formed in contact with meteoric water would be depleted in $Sr^{2+}$ and $Na^{2+}$ and enriched in $Fe^{2+}$ and $Mn^{2+}$. The Paleocene-Eocene

dolomites in this study show an inverse relationship between $Sr^{2+}$ and $Fe^{2+}$ values (Fig. 75). This may suggest that when more meteoric water was involved in the dolomite formation, it produced the more $Sr^{2+}$-depleted and more $Fe^{2+}$-enriched dolomites.

Dolomites with low $Fe^{2+}$ (average >300 ppm) and low $Mn^{2+}$ (average >50 ppm) are formed either in contact with oxidizing pore water, or because of the $Fe^{2+}$ and $Mn^{2+}$ scarcity in the reducing pore water (Budd, 1997). The Paleocene-Eocene dolomites in this study were probably formed in a reducing environment based on the dominantly negative $\delta^{13}C$ values (next chapter), therefore, the low $Fe^{2+}$ and $Mn^{2+}$ probably reflects their limited content in the pore water.

Two assumptions can be made in order to explain the relatively low content of $Fe^{2+}$: (1) limited $Fe^{2+}$ source, and (2) consumption of $Fe^{2+}$ by sulfides. $Fe^{2+}$ is sourced to the pore fluids in carbonate platforms from precursor carbonates (Vahrenkamp and Swart, 1994), nearby paleosols (Humphry, 1988), or detrital siliciclastics (Budd, 1997).

The types of precursor carbonates in this study are difficult to infer from petrography due to pervasive dolomitization. Paleosols are absent within the Paleocene-Eocene carbonate section and this is supported by the arid to semi-arid climate of the area during the Paleogene (Dull, 2004; Golonka, et al 1994). It is likely that the prolonged arid climate was interrupted by a cooler and wetter climate throughout the Paleogene that corresponded with soil development. However, no paleosol horizons are reported from the outcrops in the western side (landward) of the study area in Iraq (Jassim and Budday, 2006), nor were paleosol horizon observed from cores in Al-Wafra field between Kuwait and Saudi Arabia (Dull, 2004; Bachtel et al., 2011; Toomey et al., 2011). Thus, either

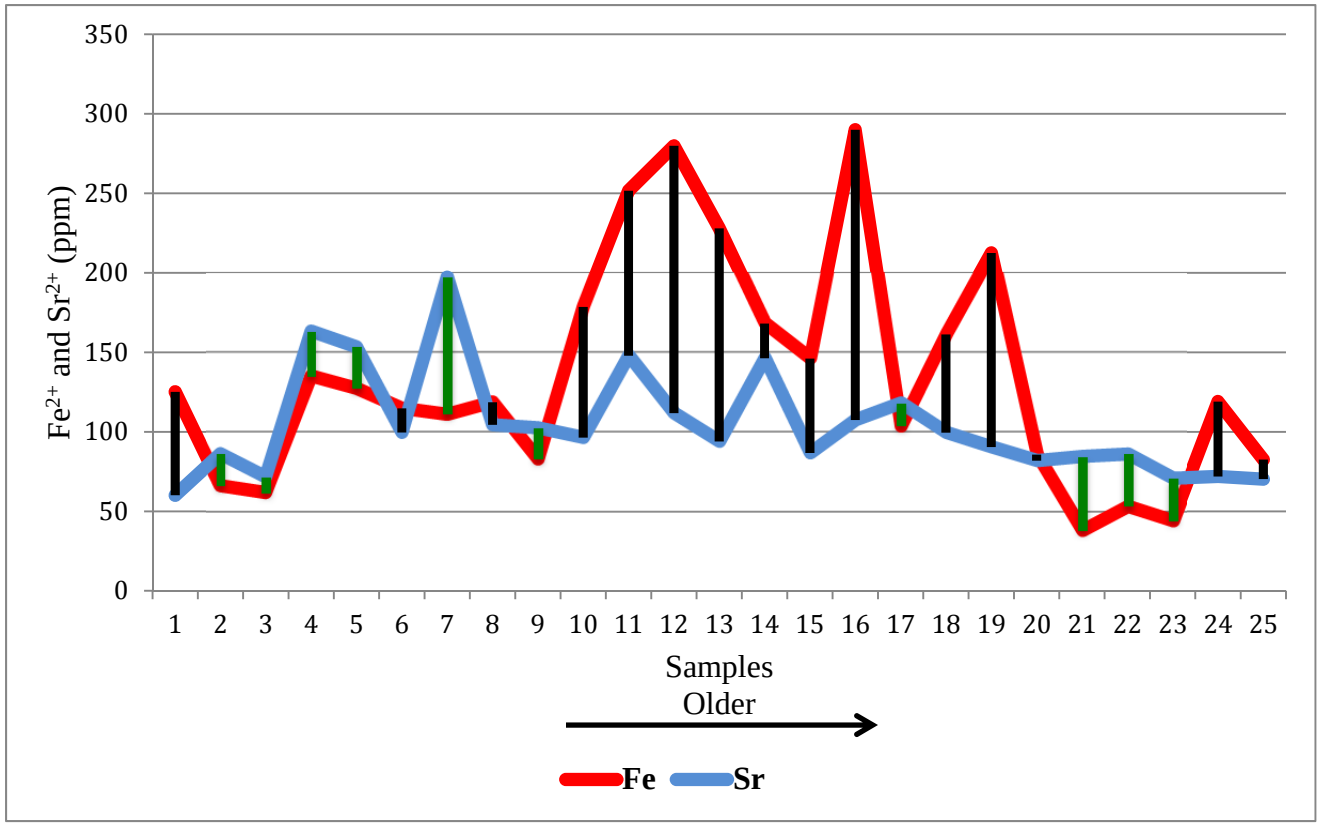


**Figure 75** A plot of $Fe^{2+}$ and $Sr^{2+}$ values. Black bars show samples depleted in $Sr^{2+}$ and enriched in $Fe^{2+}$, whereas the green bars show samples depleted in $Fe^{2+}$ and enriched in $Sr^{2+}$.

soil had not been formed or it was eroded. The last mentioned source of $Fe^{2+}$ and $Mn^{2+}$ would be detrital siliciclastics, which were not observed in thin section, and their transportation to the carbonate basin was impeded because of the minor uplift in the hinterland (Grabowski, 2012; personal communication).

Consumption of $Fe^{2+}$ by sulfides (Burns et al., 1988), on the other, is a plausible reason for the $Fe^{2+}$ paucity. The negative $\delta^{13}C$ values (next chapter) are probably the result of dolomitization within the sulfate reduction zone. However, no iron sulfide minerals were observed during petrographic examination, and iron sulfide peaks (e.g., pyrite) were not observed from XRD. Therefore, the abundance of $Fe^{2+}$ and $Mn^{2+}$ in the pore fluids, thus dolomites, was mainly controlled by their availability and the reducing conditions.

# CHAPTER 5 ISOTOPIC COMPOSITION

## 5.1 $\delta^{13}C$ Composition

The $\delta^{13}C$ values range from -8.73 to -0.40‰ PDB with an average of -5.25‰ PDB. The $\delta^{13}C$ values show a negatively skewed distribution (Fig. 76), with the highest modal class between -6‰ and -7‰. Table 5 includes $\delta^{13}C$ and $\delta^{18}O$ values for the 26 dolomite samples.

Pairs of samples from the same dolomite horizon have a maximum difference of 1.7 ‰ between their $\delta^{13}C$ values, and a minimum difference of 0.4‰. There is no strong relationship between $\delta^{13}C$ values and the types of the microfacies or with the other geochemical attributes.

Low $\delta^{13}C$ values for the Paleocene-Eocene dolomites in southern Iraq were expected because stratigraphically correlative dolomites along the eastern margin of the Arabian Plate have low $\delta^{13}C$ values for their dolomites. The Dammam Formation dolomites in Qatar (Middle Eocene age) have a $\delta^{13}C$ range of -0.9 to -8.9‰ PDB (Holail et al. 2005). Dolomites of the First Eocene reservoir (Paleocene-Eocene age) in Al-Wafra field, between Kuwait and Saudi Arabia, have a $\delta^{13}C$ range of –2.5 to 2.5‰ PDB (Saller et al., 2011). In addition, it is worth mentioning that the last stage pore-filling calcite in the dolomites for the two examples above have low to very low $\delta^{13}C$ values, that is -2.6 to -7.8‰ in Qatar (Holail, 2005) and -17.1 to -34.9‰ in Kuwai-Saudi Arabia (Saller et al., 2011). The $\delta^{13}C$ values for the dolomites in this study may be the result of calcite cement mixed with the dolomites, i.e., whole-rock samples were analyzed.

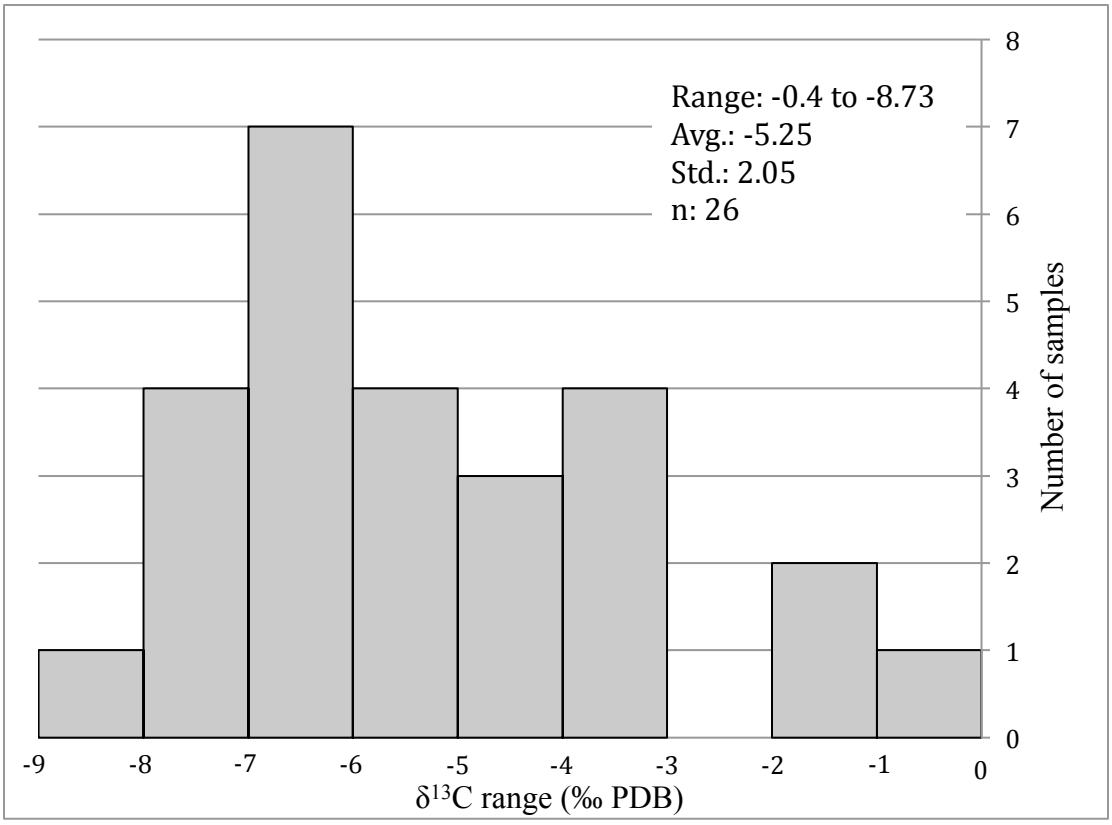


**Figure 76** Distribution of $\delta^{13}C$ values for the dolomite samples.

| No. | $\delta^{13}C$ (‰ PDB) | $\delta^{18}O$ (‰ PDB) | No. | $\delta^{13}C$ (‰ PDB) | $\delta^{18}O$ (‰ PDB) |
|---|---|---|---|---|---|
| 1 | -0.40 | 1.08 | 14 | -5.29 | 2.40 |
| 2 | -1.68 | 0.73 | 15 | -7.43 | 0.14 |
| 3 | -3.09 | 0.35 | 16 | -4.69 | 2.03 |
| 4 | -6.82 | 0.41 | 17 | -3.15 | 1.76 |
| 5 | -6.45 | -0.53 | 18 | -6.73 | 1.12 |
| 6 | -6.11 | -0.08 | 19 | -7.68 | 1.49 |
| 7 | -5.38 | -1.46 | 20 | -7.03 | 2.21 |
| 8 | -8.73 | 0.66 | 21 | -5.51 | 1.61 |
| 9 | -6.39 | 1.25 | 22 | -5.22 | 1.11 |
| 10 | -6.21 | 0.51 | 23 | -4.91 | 0.93 |
| 11 | -6.33 | 0.80 | 24 | -3.72 | 0.72 |
| 12 | -4.77 | 1.29 | 25 | -1.52 | -0.40 |
| 13 | -7.59 | 1.98 | 26 | -3.72 | -0.48 |

**Table 5** Measured $\delta^{13}C$ and $\delta^{18}O$ values for the 26 dolomite samples.

### 5.1.1 $\delta^{13}C$ Discussion

The dominantly negative $\delta^{13}C$ values for the Paleocene-Eocene dolomites in this study are generally the result of the globally negative excursions of $\delta^{13}C$ values in the world oceans during the Paleocene-Eocene (Zachos et al., 2001; Higgins and Schrag, 2006). The marine, atmospheric, and terrestrial carbon reservoirs experienced around 3‰ negative excursion in $\delta^{13}C$ values during the Late Paleocene Thermal Maximum (Zachos et al., 2001). Higgins and Schrag (2006) reported a 2.5‰ drop in the global inorganic carbon pool during the Paleocene-Eocene Thermal Maximum (PETM) that was followed by a gradual return to the pre-excursion values around 1‰ PDB.

Bacterial sulfate reduction, anaerobic methane oxidation, organic carbon mineralization were active processes during the hyperthermal intervals because of the abundant methane supply from different sources (see Higgins and Schrag [2006]). The processes mentioned above increased dissolved inorganic carbon and alkalinity in pore fluids, yet shallow depth pore fluids were typified by low values (-5 to -25‰ PDB) because of methane oxidation and sulfate reduction. In contrast, the values were enriched (0 to 15‰ PDB) below the sulfate-methane transition because isotopically heavy $CO_2$ was produced through methanogenesis (Higgins and Schrag, 2006).

The isotopic composition of replacement dolomite depends highly on the isotopic composition of the precursor carbonates at a low rock-water interaction ratio, whereas directly precipitated dolomite, e.g., subtidal dolomite, would have $\delta^{13}C$ values close to those of seawater. Whether the Paleocene-Eocene dolomites are replacement or direct precipitates, the isotopic imprint of the negative $\delta^{13}C$ value excursions associated with the hyperthermal events are probably preserved in the dolomites. Articles regarding the influence of the globally $^{13}C$-depleted carbonates on dolomitization were not found. The reason behind this is probably the limitation of Sr isotope dating (a commonly used method in dating different dolomite generations [e.g. Ye and Mazzullo, 1993; Swart and Vahrenkamp, 1994; Gao et al. 1995]) of the Paleocene and Eocene epochs. Thus, it is difficult to correlate the $\delta^{13}C$ values of the dolomites with negative excursion events.

The Paleocene and Eocene marine carbon pool went through major fluctuations with values ranging from 1 to 3‰ before PETM, -1.5‰ during PETM, and 1‰ from Middle Eocene to Oligocene (Fig. 77). The Paleocene-Eocene interval dolomites in this

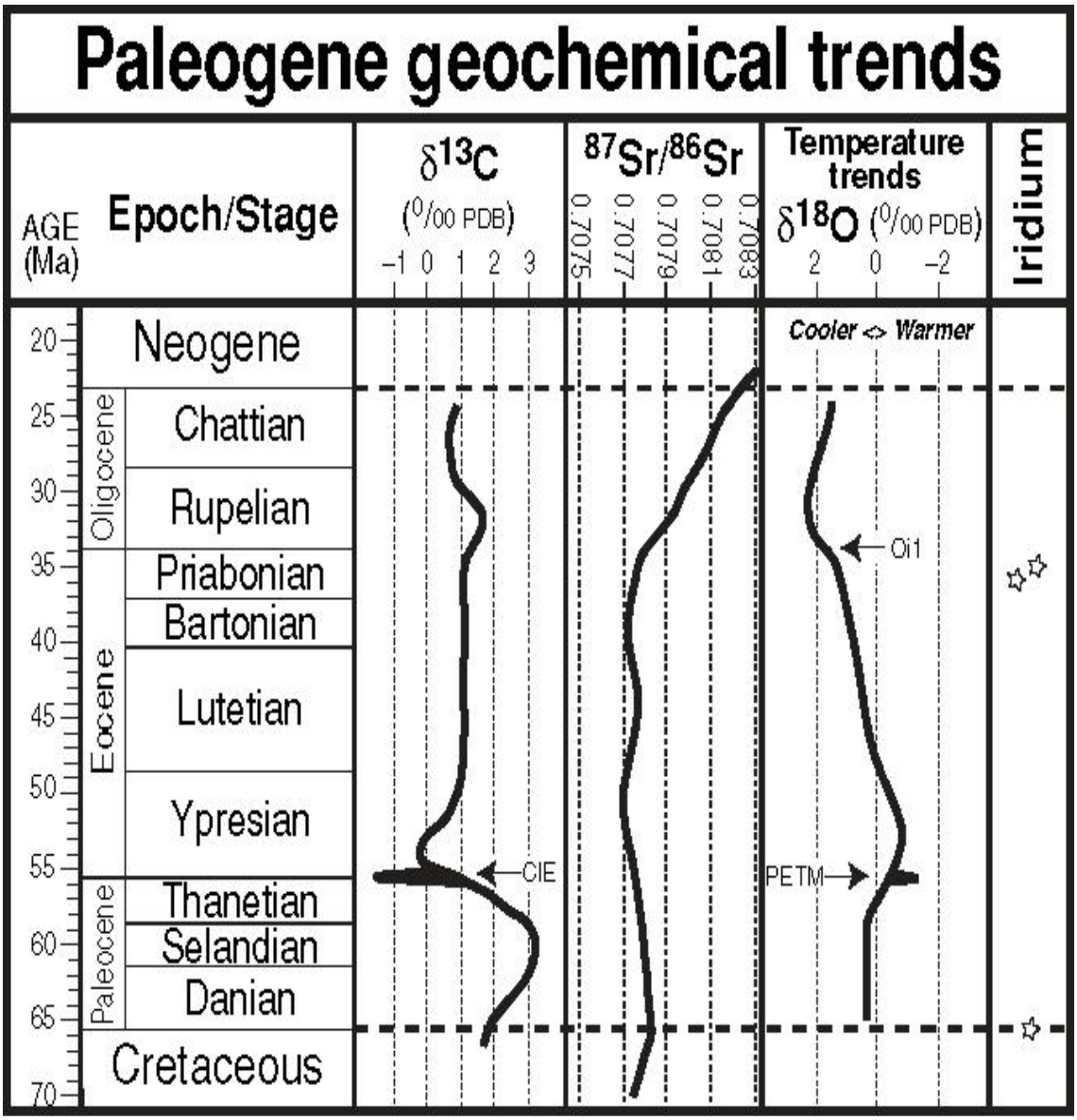


**Figure 77** The world ocean $\delta^{13}C$ and $\delta^{18}O$ curves based on calcareous benthic foraminifera during the Paleogene (from Gradstein et al., 2004).

study display their highest modal class between -6 and -7‰ and this suggests that there was another mechanism by which more organic carbon was added to the dolomites.

Dolomitization in contact with mixed meteoric and marine water will produce $^{13}C$-depleted dolomite if the meteoric water percolates from a soil horizon that is generally enriched in $^{12}C$ (Allan and Mathews, 1982). Higgins and Schrag (2006) calculated a higher negative excursion by 5 to 6‰ in PTEM paleosols and skeletal enamel because of the preferential $^{13}C$-discrimination. Therefore, the most $^{13}C$-depleted dolomites would probably be associated with the Paleocene-Eocene boundary, that is the contact between Umm Er Radhuma and Dammam Formations. However, although the average$^{13}C$ of seven samples around the contact is – 6 ‰, the most negative values are not at the Paleocene-Eocene boundary (Fig. 78).

Moreover, paleosol horizons are not reported in studies of the Paleocene-Eocene carbonates on the eastern Arabian Plate (see the previous chapter). Assuming that the soil horizons were stripped away by erosion, and the negative $\delta^{13}C$ values are the preserved imprints, then the most negative $\delta^{13}C$ values should accompany the most $Fe^{2+}$- and $Mn^{2+}$ -enriched dolomites. But, such a relationship does not exist.

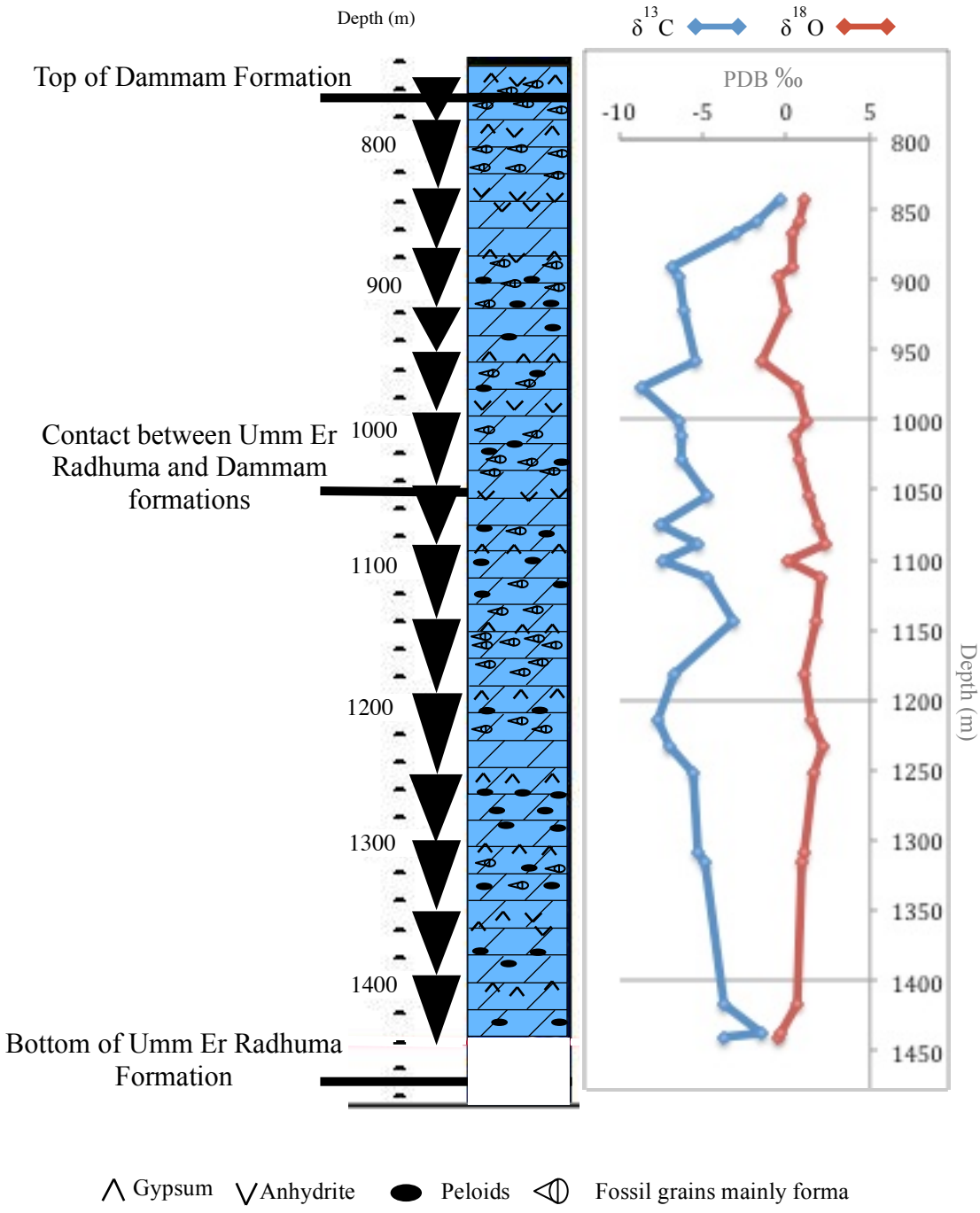


**Figure 78** $\delta^{13}C$ and $\delta^{18}O$ values for the 26 samples from Nahr Umr -1 plotted next to the dolomite microfacies

Another possible reason why the predominantly negative $\delta^{13}C$ values occur in the dolomites is that the process took place within the sulfate reduction zone. Available organic matter, i.e., microbial mats (Andrews, 1991) and dissolved sulfates, i.e., gypsum and anhydrite, could provide enough sulfates to support a thriving population of sulfate-reducing bacteria (Machel et al., 1995). The byproducts of sulfate-reducing bacteria consumption of organic matter are $H_2S$ and $HCO_3^-$.

Andrews (1991) found that decayed microbial mat horizons are $H_2S$-rich and composed of dolomite within the Holocene sediments on the Crane Key, Florida. The Crane Key dolomites appear in two horizons with distinctive spherular and rhombic textures and are poorly ordered and non-stoichiometric. Rhombic dolomite occurs at relatively deeper horizon and has $\delta^{13}C$ values of -3 to -2‰ PDB (Andrew, 1991).

Negative $\delta^{13}C$ values for dolomites beneath or within microbial mats are reported in other modern dolomites (e.g., Mitchell and Horton, 1995b) and in ancient dolomites (e.g., Chafetz et al., 1999). Yet, a recent study shows that modern microbially mediated dolomites within the Abu Dhabi microbial mats have values ranging from 1.77‰ to 0.10‰ PDB (Bontognali et al., 2010). In contrast, modern dolomites from the Brejo do Espinho Lagoon (Brazil) microbial mats have dominant negative values ranging from -1.99‰ to -9.10‰ PDB (Sánchez-Román et al., 2009a). The Brejo do Espinho Lagoon microbial mats consist of stratified mat-forming microbial communities that include aerobic bacteria in the uppermost part below the sediment-water interface and anaerobic bacteria in deeper part of the mat. The much more negative values are associated within the anoxic lower part of the microbial mat due to the dominance of anaerobic sulfate-reducing bacteria (Sánchez-Román et al., 2009a).

The presence of microbially mediated dolomites with $^{13}C$-depleted values is not restricted to microbial mats. Sulfate-reducing bacteria are active within organic-rich carbonate sediments under reducing conditions. Modern dolomite precipitants are documented in ephemeral hypersaline lakes and lagoons that are composed of an organic-rich layer at the sediment-water interface. (e.g., Lagoa Vermelha, Brazil [Vasconcelos and MacKenzie, 1997]; Coorong Region, South Australia [Wright and Wacey, 2005]). Ancient dolomites that are $^{13}C$-depleted are also postulated to be the result of sulfate-reducing bacteria in organic-rich sediments (e.g., Burns et al., 1988; Nielsen et al., 1997).

Concerning the dominantly negative $\delta^{13}C$ values for the Paleocene-Eocene dolomites in this study, the dolomite is interpreted to be microbially mediated dolomite, this is based on four lines of reasoning: (1) the dominance of micrite (based on petrography) implies restricted lagoon environments that may have had a layer of organic matter at the sediment-water interface, (2) microbial mats were probably abundant on the Arabian Plate Paleocene-Eocene tidal flats because successive shallowing upward cycles are commonly capped by algal boundstone (Dull, 2004; Toomey et al., 2001), (3) the sulphur fluxes associated with seafloor spreading and hyperthermal events throughout Early to Middle Cenozoic would have resulted in anoxic condition of the world oceans and sulfate-reducing bacteria thrive in that setting (Burns et al., 2000), and (4) most of the ancient dolomites with negative covariant $\delta^{13}C$ and $\delta^{18}O$ values (see next section) are interpreted to be the result of dolomitization within sulfate-reducing bacterial zone (Budd, 1997; Warren, 2000).

### 5.2 $\delta^{18}O$ Composition

The $\delta^{18}O$ values for the Paleocene-Eocene dolomites range from -1.46 to 2.4‰ PDB. $\delta^{18}O$ values have a narrower range than $\delta^{13}C$ values, and show a broadly defined unimodal distribution with their highest modal class between 0 to 2‰ PDB (Fig. 79). The molar % $CaCO_3$ for samples with high calcite content, based on elemental and XRD analyses, show distinctive inverse relationship with $\delta^{18}O$ values (Fig. 80).

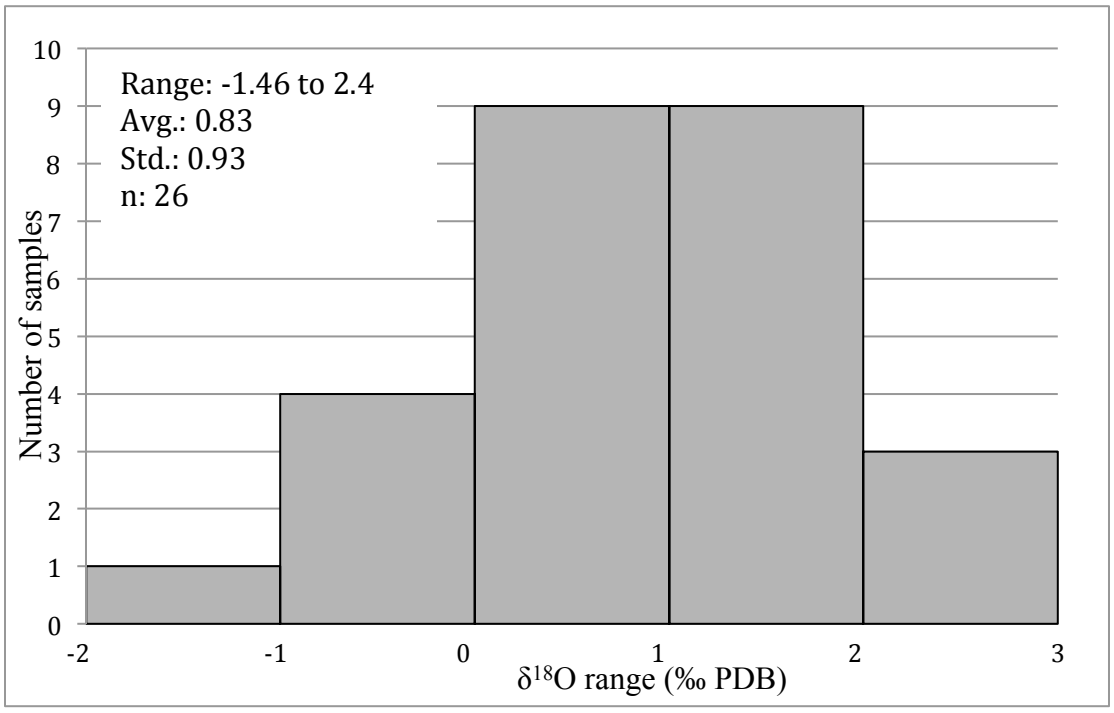


**Figure 79** Distribution of $\delta^{18}O$ values for the dolomite samples.

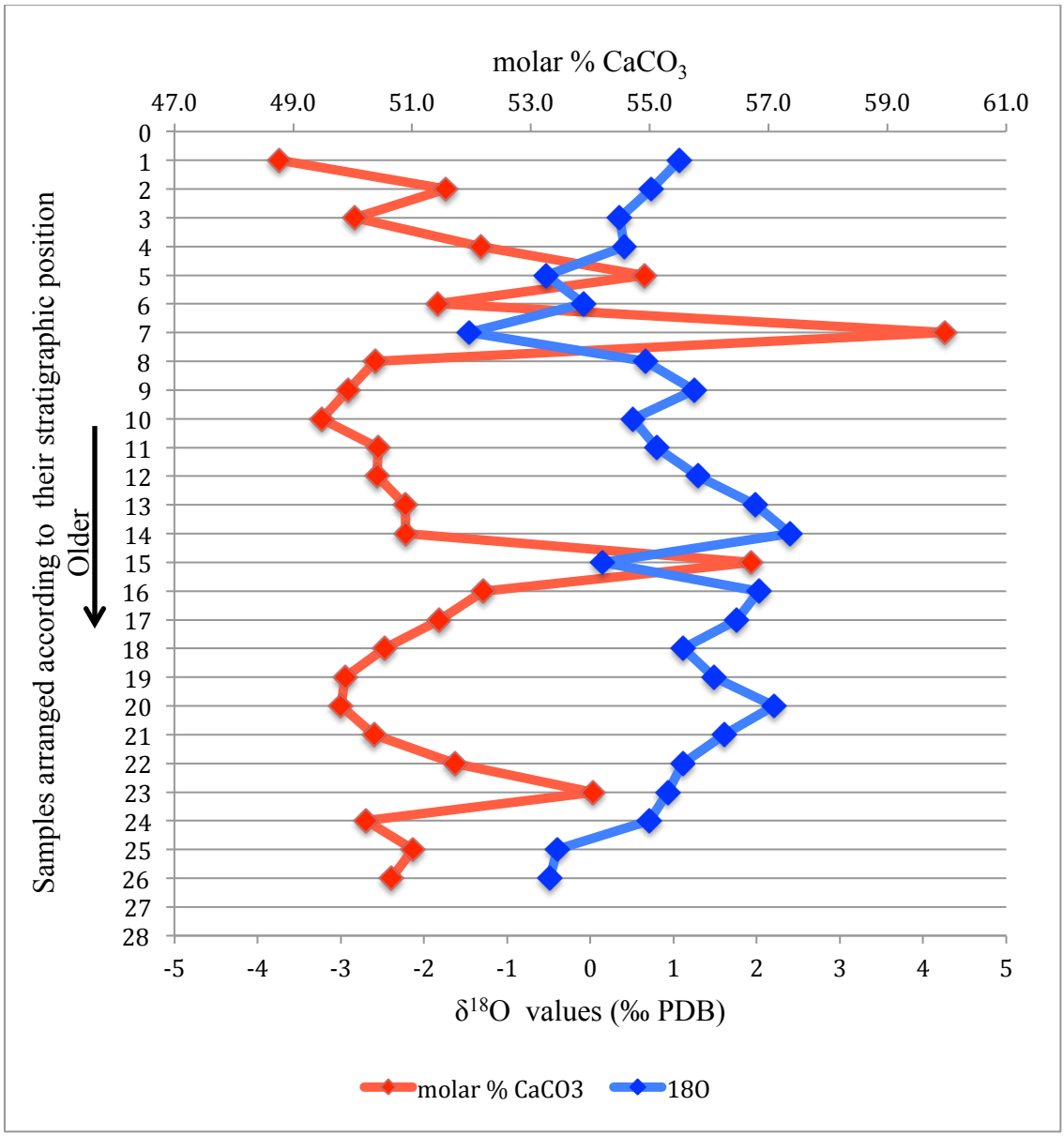


**Figure 80** A plot of $\delta^{18}O$ values and molar % $CaCO_3$ abundance for the dolomite samples. Note that samples 5, 7, and 15 show a strong inverse relationship with $\delta^{18}O$ values. This is attributed to the $^{18}O$-depleted pore-filling calcite cement. Theses three samples were also excluded from stoichiometry calculations.

The relatively low $\delta^{18}O$ values for the calcite-rich samples are probably due to the $\delta^{18}O$ of pore-filling cement. Therefore sample No.7, the lowest $\delta^{18}O$ value, does not necessarily represent the lowest value for the dolomites. Sample No.7 has also anomalously high $Na^{2+}$, $Fe^{2+}$, $Mn^{2+}$, and lowest $Sr^{2+}$ abundances. However, despite the contamination by pore-filling calcite, $\delta^{18}O$ values show the lowest standard deviation among all of the other geochemical attributes with a value of 0.93‰.

A pronounced relationship between $\delta^{18}O$ values and type of facies and crystal sizes does not exist. The majority of the Paleocene-Eocene dolomites have positive $\delta^{18}O$ values and negative $\delta^{13}C$ values (Fig. 81).

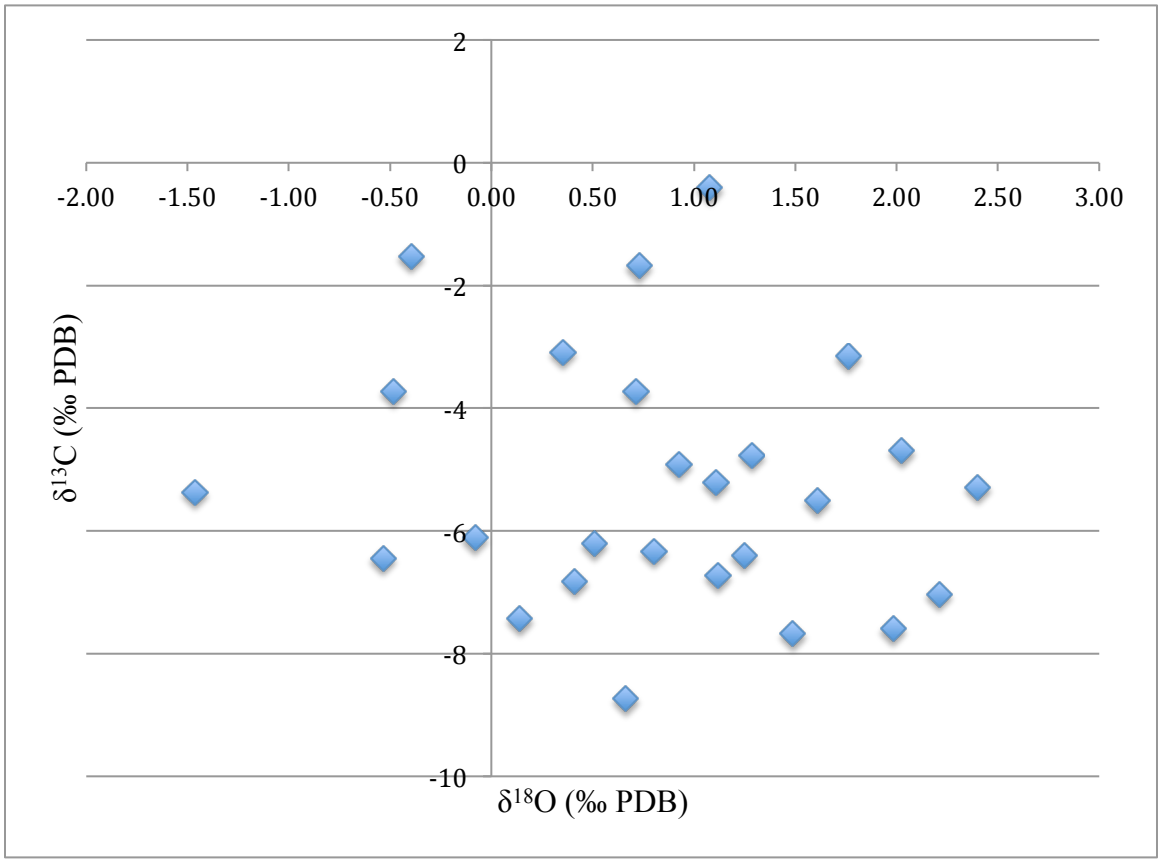


**Figure 81** A plot showing the $\delta^{18}O$ and $\delta^{13}C$ values for the Paleocene-Eocene dolomites.

### 5.2.1 $\delta^{18}O$ Discussion

Oxygen isotope composition in dolomite depends on $\delta^{18}O$ value of the diagenetic fluid and temperature in an open system; whereas $\delta^{18}O$ values of precursor carbonates influences the $\delta^{18}O$ value in dolomite in a relatively closed system, i.e., low water-rock interaction ratio. Regarding $\delta^{18}O$ content in the diagenetic fluid, regional or secular variations of normal seawater, regional or secular variations in climate (i.e., evaporation and precipitation rates), and the meteoric component in a mixed seawater-meteoric water system are important factors to be considered when interpreting $\delta^{18}O$ values (Anderson and Arthur, 1983; Budd, 1997).

On the regional scale, the range of the Paleocene-Eocene dolomites in this study (-1.46 to 2.4‰ PDB) is close to the Dammam Formation dolomites in Qatar (Middle Eocene age), with $\delta^{18}O$ values ranging from 0.4 to 2.8‰ PDB (Holail et al. 2005), and dolomites of the First Eocene reservoir (Paleocene-Eocene age) in Al-Wafra field, between Kuwait and Saudi Arabia, with $\delta^{18}O$ values from –1 to 3‰ PDB (Saller et al., 2011).

Globally, the Paleocene-Eocene witnessed secular variations in $\delta^{18}O$ values in the world-wide ocean carbonates. Oxygen isotopic values were about 0‰ PDB during the Early Eocene, and experienced an abrupt drop during PETM to reach the lowest value of around -1‰. The drop at the Paleocene-Eocene boundary was followed by a gradual increase that reached 2‰ PDB at the Eocene-Oligocene boundary (Fig. 77). These secular variations are not preserved in the dolomites of this study because the changes in the values are age-independent, i.e., $\delta^{18}O$ values for the dolomites do not correspond to secular high or low $\delta^{18}O$ values.

Marine carbonates precipitated in equilibrium with seawater commonly have $\delta^{18}O$ values close to 0‰ with about ±1‰ (Hoefs, 1997). Dolomites with $\delta^{18}O$ values less than -2‰ PDB are either formed or re-equilibrated in contact with water with low $\delta^{18}O$ values by as much as 4‰ relative to seawater, or in high temperature setting (Land, 1983). Therefore, dolomitization of the Paleocene-Eocene carbonates in contact with $^{18}O$-depleted water or in high temperature is not supported based on the high modal class between 0 to 2‰ PDB for the dolomites.

The narrow range and low standard deviation for the $\delta^{18}O$ values do not allow separation of different dolomitization fluids, and the data set does not allow further scrutinization. Yet, the oxygen and carbon isotopic composition of Paleocene-Eocene dolomites in this study overlap with evaporitic dolomite examples (Fig. 82), with their low isotopic values that are interpreted to be the result of dolomitization in contact with mixed meteoric and marine water, or within the sulfate-reducing bacterial zone.

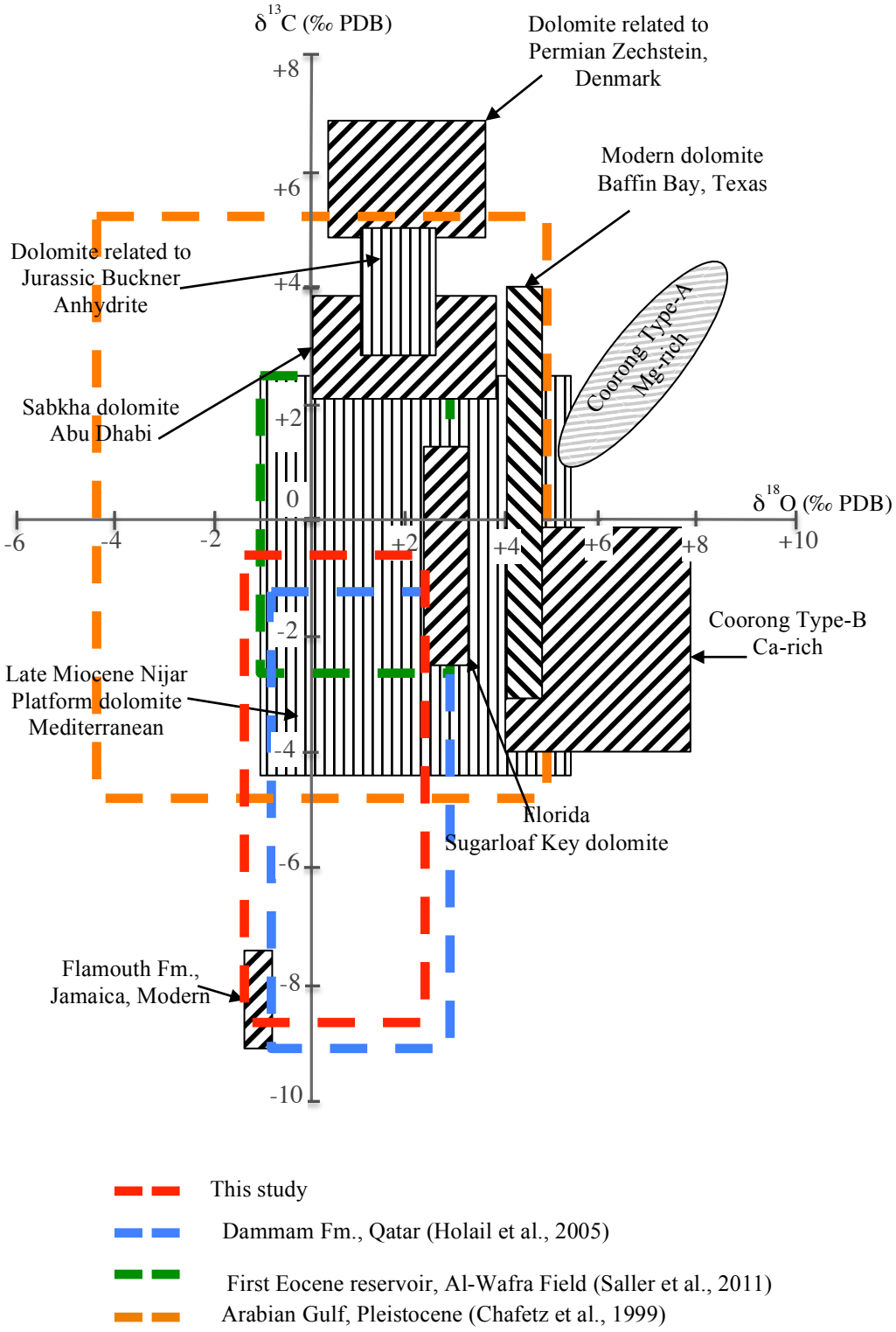


**Figure 82** $\delta^{13}C$ and $\delta^{18}O$ values for this study plotted with values from other studies (modified from Warren, 2000).

# CHAPTER 6 CONCLUSION

The Paleocene-Eocene carbonates and evaporites in southern Iraq were deposited on a shallow carbonate platform that occupied the southwestern margin of the Mesopotamian foreland basin. Tens of meters thick shallowing-upward cycles were identified based on evaporite-rich carbonates representing cycle tops. The depositional cycles are highly altered through dolomitization, and the recognizable depositional textures after dolomitization are foraminiferal biodolomicrite, sparse peloidal and foraminiferal biodolomicrite, peldolomicrite, and peloidal and foraminiferal biodolosparite.

Diagenetic processes are represented by allochem dissolution, dolomitization, evaporite precipitation and replacement, authigenic quartz precipitation, and pore-filling calcite and dolomite cementation. Dolomitization is pervasive and fabric destructive throughout the section. The dolomites have a wide spectrum of crystal sizes that range from micritic, aphanocrystalline, to 100 μm big crystals. The dolomite crystals are mainly planar-s to non-planar and they have clear syntaxial cement rims in some horizons. The dolomites are also present as pore-filling and -lining cements in different intervals throughout the section.

The molar % $CaCO_3$ for representative dolomites throughout the section range from 48.8% to 54.1% with an average of 50.8% and highest modal class between 50% and 51%. Thus, the dolomites vary between Ca-rich to Mg-rich with a nearly stoichiometric composition.

The average strontium and sodium contents in the dolomites are 102 and 600 ppm, respectively. The $Sr^{2+}$ and $Na^{+2}$ values suggest that the dolomites have probably stabilized in contact with seawater or mixed meteoric and seawater rather than hypersaline seawater. The Fe-enrichment in the dolomites, with an average of 135 ppm, indicates that dolomitizing fluids had a component of non-marine water. Dolomitization of the Paleocene-Eocene had taken place with fluids that had different chemistries and at different rock-water interaction ratios. This is inferred based on the wide range of the trace element content.

Carbon and oxygen isotopes values show an inverse relationship. The highest modal class is -6 to -7 ‰ PDB for $\delta^{13}C$ implies that dolomitization settings were enriched in organic carbon. Whereas dolomitization in contact with meteoric water can be responsible for the dominantly negative $\delta^{13}C$ values, $\delta^{18}O$ values with their highest modal class between 0 to 2 ‰ PDB disagrees with this interpretation. Therefore, the relationship between $\delta^{13}C$ and $\delta^{18}O$ values indicate that dolomitization probably occurred within the sulfate-reducing bacterial zone.

A pronounced relationship was not observed between the geochemical attributes and petrographic characteristics for the representative samples of the Paleocene-Eocene dolomites.

# References


Allan, J.R. and Matthews, R.K. (1977) Carbon and oxygen isotopes as diagenetic and stratigraphic tools: surface and subsurface data, Barbados, West Indies. Geology, 5, 16-20.

Allan, J.R. and Matthews, R.K. (1982) Isotope signature associated with early meteoric diagenesis. Sedimentology, 29, 797-897.

Allen, M. and Armstrong, H.A. (2008) Arabia–Eurasia collision and the forcing of mid-Cenozoic global cooling. Palaeogeography, Palaeoclimatology, Palaeoecology, 265, 52–58.

Alsharhan, A.S. and Nairn, A.E.M. (1995) Tertiary of the Arabian Gulf: sedimentology and hydrocarbon potential. Palaeogeography, Palaeoclimatology, Palaeoecology, 114, 369-384.

Alsharhan, A. S. and Kendall, C.G.St.C. (2003) Holocene coastal carbonates and evaporites of the southern Arabian Gulf and their ancient analogues. Earth-Science Reviews, 61, 191 – 243.

Andreson, T.F., and Arthur, M.A. (1983) Stable isotope of oxygen and carbon and their application to sedimentologic and paleo- environmental problems. In: Stable isotopes in sedimentary geology (Eds. M.A. Arthur, T.F. Anderson, I.R. Kaplan, J. Veizer and L.S. land). Soc. Econ. Paleont. Min. Short Course No.10, 1-1 to 1-151.

Andrews, J.E. (1991) Geochemical indicators of depositional and early diagenetic facies in Holocene carbonate muds, and their preservation potential during stabilization. Chemical Geology, 93, 267–289.

Bachtel, S., Toomey, N., Pollitt, D. A., Saller, A., Playton, A., Vincent Heesakkers, V. Dull, D., Montgomery, P., Archuleta, B., Anthonissen, E. and Meddaugh, M. (2011) Reservoir characterization of the Paleocene/Eocene First Eocene dolomite reservoir at Wafra Field, Partitioned Zone (Saudi Arabia and Kuwait). Amer. Ass. Petrol. Geol. Search and Discovery Article, 90124.

Banner, J. L. (1995) Applications of the trace element and isotope geochemistry of strontium to studies of carbonate diagenesis. Sedimentology, 45, 805–824.

Bathurst, R. G. C. (1975) Carbonate sediments and their diagenesis. Developments in Sedimentology 12, Elsevier (Amsterdam), 658 p.

Beydoun, Z. (1998) Arabian Plate oil and gas; why so rich and prolific?. Episodes, 21, 74-81.

Bontognali, T.R.R., Vasconcelos, C., Warthmann, R.J., Bernasconi, S.M., Dupraz, C., Strohmenger, C.J. and McKenzie, J.A. (2010) Dolomite formation within microbial mats in the coastal sabkha of Abu Dhabi (United Arab Emirates). Sedimentology, 57, 824−844.

Bosence, D., Procter, E., Aurell, M., Kahla, A., Boudagher-fadel, M., Casaglia, F., Cirilli, S., Mehdie, M., Nieto, L., Rey, J., Scherreiks, R, Soussi, M. and Waltham, D. (2009) A dominant tectonic signal in high-frequency, peritidal carbonate cycles? a regional analysis of Liassic Platforms from Western Tethys. J. Sediment. Res., 79, 389–415.

Budd, D.A. (1997) Cenozoic dolomites of carbonate islands; their attributes and origin. Earth Sci. Rev., 42, 1 – 47.

Burchette, T.P. and Wright, V.P. (1992) Carbonate ramp depositional systems. Sedimentary Geology, 79, 3 – 57.

Burns, S.J., Baker, P.A. and Showers, W.J. (1988) The factors controlling the formation and chemistry of dolomite in organic-rich sediments: Miocene Drakes Bay Formation, California. In: Sedimentology and Geochemistry of Dolostones (Eds. V. Shukla and P. A. Baker), Spec. Publ. Soc. Econ. Paleont. Mineral., 43, 41-52.

Burns, S.J., Mckenzie, J.A. and Vasconcelos, C. (2000) Dolomite formation and biogeochemical cycles in the Phanerozoic. Sedimentology, 47, 49–61.

Brand, U. and Veizer, J. (1980) Chemical diagenesis of a multi-component carbonate system: 1, Trace elements. J. Sediment. Petrol. 50, 1219-1236.

Brand, U. and Veizer, J. (1981) Chemical diagenesis of a multi-component carbonate system: 2, Stable isotopes. J. Sediment. Petrol., 51, 987-997.

Chafetz, H.S. and Rush, P.F. (1994) Diagenetically altered sabkha-type Pleistocene dolomite from the Arabian Gulf, Sedimentology, 41, 409 - 421.

Chafetz, H. S., and, Zhang, J. L. (1998) Authigenic euhedral megaquartz crystals in a quaternary dolomite. J. Sediment. Res., v.68, p. 994-1000.

Chafetz, H.S., Imerito-Tetzlaff, A.A., Zhang, J.L. (1999) Stable- isotope and elemental trends in Pleistocene sabkha dolomites: Descending meteoric water vs. sulfate reduction. J. Sediment. Res., 69, 256–266.

ÇaĞtay, M. N. (1990) Palygorskite in the Eocene rocks of the Dammam dome, Saudi Arabia, Clays and Clay Minerals, 38, 299-307.

Catuneanu, O. (2004) Basement control on flexural profiles and the distribution of foreland facies: The Dwyka Group of the Karoo Basin, South Africa. Geology, 32, 517-520.

Choquette, P.W., and Pray, L.C. (1970) Geologic nomenclature and classification of porosity in sedimentary carbonates, Amer. Ass. Petrol. Geol. Bull., 54, 107-25.

Choquette, P.W., Cox, A., Meyers, W.J. (1992) Characteristics, distribution and origin of porosity in shelf dolostones; Burling- ton-Keokuk Formation (Mississippian), U.S. Mid-Continent. J. Sediment. Petrol, 62, 167–189.

Choquette, P. W. and Hiatt, E. E. (2008) Shallow-burial dolomite cement: a major component of many ancient sucrosic dolomites. Sedimentology, 55, 423- 460.

De Benedictis, D., Bosence, D. and Waltham, D. (2007) Tectonic control on peritidal carbonate parasequence formation: an investigation using forward tectono-stratigraphic modeling. Sedimentology, 54, 587–605.

Dull, D. W. (2004) Integrating sequence stratigraphy and multiple three-dimensional geostatistical realizations in constructing a model of the Second Eocene reservoir, Partitioned Neutral Zone, Wafra field, Kuwait and Saudi Arabia. In: Integration of Outcrop and Modern Analogs in Reservoir Modeling (Eds. G. M. Grammer, P. M. Harris, and G. P. Eberli). Amer. Ass. Petrol. Geol. Memoir, 80, 309– 336.

Fischer, A.G. (1975) Tidal deposits, Dachstein Limestone of the North Alpine Triassic. In: Tidal Deposits (Ed. R.N. Ginsburg). Springer (New York), 235-242.

Folk, R.L., Land, L.S. (1975) Mg/Ca ratio and salinity: two controls on crystallization of dolomite. Am. Assoc. Petrol. Geol. Bull. 59, 60–68.

Friedman, I., and O'Neil, J.R. (1977) Compilation of stable isotope fractionation factors of geochemical interest. In: Data of Geochemistry (Ed. M., Fleischer). U.S. Geological Survey Professional Paper, 6th ed., 1-12.

Frisia, S. (1994) Mechanisms of complete dolomitization in a carbonate shelf: comparison between the Norian Dolomia Principale (Italy) and the Holocene of Abu Dhabi Sabkha. In: Dolomites – A Volume in Honour of Dolomieu (Eds. B.H. Purser, M.E. Tucker and D.H. Zenger). Int. Assoc. Sed., Spec. Publ. No. 21, 55–74.

Gao, G., and Land, L. S. (1991) Early Ordovician Cool Creek dolomite, middle Arbuckle Group, Slick Hills, SW Oklahoma: Origin and modification. Jour. Sed. Petrology, 61, 161-173.

Gao, G., Land, L. S. and Folk, R. L. (1992) Meteoric modification of early dolomite and late dolomitization by basinal fluids, Upper Arbuckle Group, Slick Hills, Southwestern Oklahoma: Am. Assoc. Petrol. Geol. Bull., 76. 1649-1664.

Gao, G., Land, L.S., and Elmore, R.D. (1995) Multiple episodes of dolomitization in the Arbuckle Group, Arbuckle Mountains, south-central Oklahoma; field, petrographic, and geochemical evidence. J. Sediment. Res., Sect. A (65) , 321–331.

Gavish, E. and G.M. Friedman (1973) Quantitative analysis of calcite and Mg-calcite by X-ray diffraction: effect of grinding on peak heights and peak area. Sedimentology, 20, 437-444.

Given, R.K. and Wilkinson, B.H. (1987) Dolomite abundance and stratigraphic age: constraints on rates and mechanisms of Phanerozoic dolostone formation. J. Sed. Petrol. 57, 1068-10787.

Goldsmith, J. R. and Graf, D. L. (1958) Structural and compositional variations in some natural dolomites. The Journal of Geology, 46, 678-693.

Goldsmith, J. R., Graf, D. L. and Heard, H. C. (1961) Lattice constant of calcium-magnesium carbonates. The American Mineralogist, 46, 453-457.

Golonka, J., Ross, M.I. and Scotese, C.R. (1994) Phanerozoicpaleogeographic and paleoclimatic modeling maps. Canadian Society of Petroleum Geologists Memoir, 17, 1-47.

Haq, B. U. and Al-Qahtani, A. (2005) Phanerozoic cycles of sea-level change on the Arabian Plate. GeoArabia, 10, 127-160.

Hardie, L.A. (1986) Stratigraphic models for carbonate tidal flat deposition. Quarterly Journal Colorado School of Mines, 81, 59-74.

Hersi, O. S. (2011) Lithologic and diagenetic attributes of the Sharwayn (Maastrichtian) and Umm Er Radhuma (Late Paleocene–Eocene) Formations and their significance to the K-T unconformity, Jabal Samhan area, Dhofar, Sultanate of Oman. Arabian Journal of Geosciences, 4, 147-160.

Higgins, J. A. and Schrag, D. P. (2008) Beyond methane: Towards a theory for the Paleocene–Eocene Thermal Maximum. Earth and Planetary Science Letters, 245, 523–537.

Hoefs, J. (1997) Stable Isotope Geochemistry, 4th ed., Springer (Berlin), 201 p.

Holail, H. M., Shaaban, M. N. Mansour, A. S. and Rifai, R. I. (2005) Diagenesis of the Middle Eocene upper Dammam subformation, Qatar: petrographic and isotopic evidence. Carbonates and Evaporites, 20, 72-81.

Homke, S., Vergés, J., Serra-kiel, J., Bernaola, G., Sharp, I., Garcés, M., Montero-verdú, I., Karpuz, R. and Goodarzi, M. H. (2009) Late Cretaceous– Paleocene formation of the proto-Zagros foreland basin, Lurestan Province, SW Iran, Geological Society of America Bulletin, 121, 963–78.

Humphrey, J.D. (1988) Late Pleistocene mixing zone dolomitization, southeastern Barbados, West Indies. Sedimentology, 35, 327-348.

Iraq Field Atlas (2003) Iraq Development Potential, unpublished report by Iraqi National Oil Company.
Irwin, H., Curtis, C. and Coleman, M. (1977) Isotopic evidence for source of diagenetic carbonates formed during burial of organic-rich sediments. Nature, 269, 209– 213.
James, N.P. (1984) Shallowing-upward sequences in carbonates. In: Facies Models (Ed. R. G. Walker). Geological association of Canada, Geosci. Canada Reprint Ser. 1, 213-228.
James, N.P. and Kendall, A.C. (1992) Introduction to carbonate and evaporite facies models. In: Facies Models: Response to Sea Level Change (Eds. R. G. Walker and N. P. James). Geological association of Canada, Geotext 1, 265-275.
Jassim, S.Z. and Budday, T. (2006) In: Geology of Iraq (Eds. S.Z. Jassim, and J.C. Goff). Publisher Dolin, Czech Republic, Brno, 352 p.
Jassim, S.Z., and Goff J.C. (2006) Geology of Iraq. Publisher Dolin, Czech Republic, Brno, 352 p.
Jones, B. (2005) Dolomite crystal architecture: genetic implications for the origin of the tertiary dolostones of the cayman islands. J. Sediment. Res., 75, 177–189.
Kaczmarek, S.E. and Sibley, D.F. (2007) A comparison of nanometer-scale growth and dissolution features on natural and synthetic dolomite crystals: implications for the origin of dolomite. J. Sediment. Res., 77, 424 - 432.
Kendall, A. C. (1992) Evaporites. In: Facies Models: Response to Sea Level Change (Eds. R. G. Walker and N. P. James) Geological association of Canada, Geotext 1, 375-409.
Kirkham, A. (1998) A Quaternary proximal foreland ramp and its continental fringe, Arabian Gulf, U.A.E. In: Carbonate Ramps (Eds. V.P. Wright and T.P. Burchette). Geological Society Special Publication No. 149, 15-42.
Kuznetsov, V. G. (2006) Cyclicity of shallow-water carbonate sediments in different climatic zones. Lithology and Mineral Resources, 41, 505–517.
Kyser, T.K., James, N.P. and Bone, Y. (2002) Shallow burial dolomitization and dedolomitization of Cenozoic cool-water limestones, southern Australia: geochemistry and origin. J. Sed. Res., 72, 146–157.
Land, L.S. and Hoops, G.K. (1973) Sodium in carbonate sediments and rocks: a possible index to the salinity of diagenetic solutions, J. Sediment. Petrol., v. 43, p. 614–617.
Land, L. S. (1983) The application of stable isotopes to studies of the origin of dolomite and to problems of diagenesis of clastic sediments. In: Stable Isotopes in Sedimentary Geology (Eds. M.A. Arthur, T.F. Anderson, I.R. Kaplan, J. Veizer and L.S. Land). Soc. Econ. Paleont. Min. Short Course No.10, 4-1 to 4-22.
Land, L. S. (1985) The origin of massive dolomite. J. Geol. Education, 33, 112-125.
Liu, C., Huang, T. and Chen, Y. (2006) High resolution bio-and sequence stratigraphy of the Zubair-3 and Zubair-1 wells in South Iraq, Biostratigraphy Report. Unpublished report by ExxonMobil Exploration Company.
Longman, M. W. (1980) Carbonate diagenetic textures from nearsurface diagenetic environments. Amer. Assoc. Petrol. Geol. Bull., 64, 461-487.
Lumsden, D.N. (1979) Discrepancy between thin section and X-ray estimates of dolomite in limestone. J. Sediment. Petrol. 49, 429-436.
Mackenzie, J. (1981) Holocene dolomitzation of calcium carbonate sediments from the coastal sabkhas of Abu Dhabi, U.A.E. J. Geol., 89, 185–198.

Machel, H.G., Krouse, H.R., and Sassen, G. (1995) Products and distinguishing criteria of bacterial and thermochemical sulfate reduction. Applied Geochemistry, 10, 373–389.
Matthews, A. and Katz, A. (1977) Oxygen isotope fractionation during dolomitization of calcium carbonate, Geochim. Cosmochim. Acta, 41, 1431-1438.
Meulenkamp, J.E. and Sissingh, W. (2003) Tertiary palaeogeography and tectonostratigraphic evolution of the Northern and Southern Peri- Tethys platforms and the intermediate domains of the African– Eurasian convergent plate boundary zone. Palaeogeography, Palaeoclimatology, Palaeoecology, 196, 209–228.
Mitchell, S. W. and Horton, R. A. (1995a) Dolomitization of modern subtidal sediments, New Providence Island, Bahamas. Geological Society of America Special Paper No. 300, 189-199.
Mitchell, S. W., and Horton, R. A. (1995b) Dolomitization of modern tidal flat, tidal creek, and lacustrine sediments, Bahamas. Geological Society of America Special Paper No. 300, 201-221.
Moore, C. H. (2001) Carbonate Reservoirs: Porosity Evolution and Diagenesis in a Sequence Stratigraphic Framework. Elsevier Science (Amesterdam), 444 p.
Murris, R.J. (1980) The Middle East: stratigraphic evolution and oil habitat. Am. Assoc. Petrol. Geol. Bull., 64, 597-618.
Mresah, M.H. (1998) The massive dolomitization of platformal and basinal sequences: proposed models from the Paleocene, Northeast Sirte Basin, Libya. Sedimentary Geology, 116, 199–226.
Nielsen, P., Swennen, R., Dickson, J.A.D., Fallick, A.E. and Keppens, E. (1997) Spheroidal dolomites in a Visean karst system — bacterial induced origin. Sedimentology, 44, 177–195.
Owen, R.M.S. and S.N. Nasr (1958) Stratigraphy of the Kuwait-Basra area. In: Habitat of Oil (Ed. L.G. Weeks). A Symposium: Amer. Ass. Petrol. Geol., 1252- 1278.
Philip, J. (2003) Peri-Tethyan neritic carbonate areas: distribution through time and driving factors. Paleo., 196, 19-37.
Pratt, B. R., James, N. P. and Cowan, C. A. (1992) Peritidal carbonates. In: Facies Models: Response to Sea Level Change (Eds. R. G. Walker and N. P. James,). Geological association of Canada, Geotext 1, 303-322.
Randazzo, A.F. and Zachos, L.G. (1984) Classification and description of dolomitic fabrics and rocks from the Florida aquifer. Sed. Geol., 37, 151–162.
Reeder, R.J. and Sheppard, C.E. (1984) Variation of lattice parameters in some sedimentary dolomites. American Mineralogist, 69, 520–527.
Saller, A., Pollitt, D. A. and Dickson, J. A. (2011) Late-stage diagenesis and bacterial sulfate reduction in the 1st Eocene reservoir, Wafra Field, Partitioned Zone, Kuwait, Amer. Ass. Petrol. Geol. Search and Discovery Article, 90124.
Sánchez-Román, M., Vasconcelos, C., Warthmann, R., Rivadeneyra, M. and McKenzie, J.A. (2009a) Microbial dolomite precipitation under aerobic conditions: results from Brejo do Espinho Lagoon (Brazil) and culture experiments. In: Perspectives in Sedimentary Geology: A Tribute to the Career of Robert Nathan Ginsburg (Eds. P.K. Swart, G.P. Eberli, and J.A. McKenzie). IAS Spec. Publ. No 41, 167–178.
Satterley, A.K., Brandner, R. (1995) The genesis of Lofer cycles of the Dachstein Limestone, Northern Calcareous Alps, Austria. Geol. Rundsch., 84, 287–292.

Sass, E. and Bein, A. (1988) Dolomites and salinity: a comparative geochemical study. In: Sedimentology and Geochemistry of Dolostones (Eds. V. Shukla and B.P. Baker). Soc. Econ. Paleont. Min., Special Publications No. 43, 223–233.

Sharland, P.R., Archer, R., Casey, D.M., Davies, R.B., Hall, S.H., Heward, A.P., Horbury, A.D. and Simmons, M.D. (2001) Arabian Plate Sequence Stratigraphy. GeoArabia Special Publication 2, Publisher Gulf PetroLink (Bahrain), 371 p.

Sibley, D.F. and Gregg, J.M. (1987) Classification of dolomite rock textures. J. Sediment. Petrol. 57, 967–975.

Sluijs, A, Brinkhuis, H., Crouch, E. M., John, C. M., Handley, L., Munsterman, D., Bohaty, S. M., Zachos, J. C. Reichart, G., Schouten, S., Pancost, R. D., Sinninghe Damste, J. S., Welters, N. L. D., Lotter, A. F. and Dickens G. R. (2008) Eustatic variations during the Paleocene-Eocene greenhouse world. Paleoceanography, 23, 1-18.

Smith, S. E. (1994) Geochemistry and Petrology of Basaltic and Plutonic from the Hayes Transform Region, Mid-Atlantic Ridge. Unpublished PhD. dissertation, University of Houston, 309 p.

Spence, G.H. and Tucker, M. E. (1999) Modelling carbonate microfacies in the context of high-frequency dynamic relative sea-level and environmental changes. J. Sediment. Res., 69, 947-961.

Sperber, C.M., Wilkinson, B.H. and Peacor, D.R. (1984) Rock composition, dolomite stoichiometry, and rock/water reactions in dolomitic carbonate rocks. J. of Geology, 92, 609–622.

Steinhauff1, D. M, Christian J. H. and Arthur E. G. (2011) The Eocene Rus anhydrite: important arabian reflector and recorder of Cenozoic history. Amer. Ass. Petrol. Geol. Search and Discovery Article, 50480.

Swart, P. K. (1983) Carbon and oxygen isotope fractionation in scleractinian corals. Earth Science Review, 19, 51-80.

Toomey, N., Montgomery, P., Meddaugh, W. S. (2011) Stratigraphy and depositional history of the First Eocene reservoir from Wafra Field, Partitioned Neutral Zone (PNZ), Saudi Arabia and Kuwait. Amer. Ass. Petrol. Geol. Search and Discovery Article, 90105.

Tucker, M.E. and Bathurst, R.C.C., (1990), Carbonate Diagenesis, LAS Reprint Series, Blackwell (Oxford), 312 p.

Tucker, M.E. and Wright, V.P. (1990) Carbonate Sedimentology, Blackwell (Oxford), 482 p.

Tucker, M. E. (1991) Sequence stratigraphy of carbonate-evaporite basins; models and application to the Upper Permian (Zechstein) of Northeast England and adjoining North Sea. Journal of the Geological Society of London, 148, 1019-1036.

Tucker, M. E. (1993) Carbonate diagenesis and sequence strstigraphy. In: Sedimentology Reviews 1 (Ed. V. P. Wright). Blackwell scientific publication, 51-72.

Vahrenkamp, V.C. and Swart, P.K. (1990) New distribution coefficient for the incorporation of strontium into dolomite and its implications for the formation of ancient dolomites. Geology, 18, 387-391.

Vahrenkamp, V.C. and Swart, P.K. (1994) Late Cenozoic dolomites of the Bahamas: metastable analogues for the genesis of ancient platform dolomites. In: Dolomites – A Volume in Honour of Dolomieu (Eds. B.H. Purser, M.E. Tucker and D.H. Zenger). Int. Assoc. Sed., Spec. Publ. No. 21, 133–154.

Vasconcelos, C. and McKenzie, J.A. (1997) Microbial mediation of modern dolomite precipitation and diagenesis under anoxic conditions (Lagoa Vermelha, Rio de Janeiro, Brazil). J. Sed. Res., 67, 378–390.

Veizer, J. (1983a) Chemical diagenesis of carbonates: Theory and application of trace element technique. In: Stable isotopes in sedimentary geology (Eds. M.A. Arthur, T.F. Anderson, I.R. Kaplan, J. Veizer and L.S. Land). Soc. Econ. Paleont. Min. Short Course No. 10, 3-1 to 3-100.

Veizer, J., Lemieux, J., Jones, B., Gibling, M. and Savelle, J. (1978) Paleosalinity and dolomitization of a lower Paleozoic carbonate sequence, Somerset and Prince of Wales Islands, Arctic Canada. Can. J. Earth Sci., 45, 1448-1461.

Veizer, J. and Hoefs, J. (1976) The nature of $O^{18}/O^{16}$ and $C^{13}/C^{12}$ secular trends in sedimentary carbonate rocks. Geochim. Cosmochim. Acta, 40, 1387-1395.

Warren, J.K. and Kendall, C.G.St.C. (1985) Comparison of sequences formed in marine sabkha (subaerial) and salina (subaqueous) settings-Modern and ancient. Amer. Assoc. Petrol. Geol. Bull., 69, 1013-1023.

Warren, J. (2000) Dolomite: occurrence, evolution and economically important associations. Earth-Science Reviews, 52, 1–81.

Wenk, H.R., Barber, D.J. and Reeder, R.J. (1983) Microstructures in carbonates. Mineral. Soc. Am., Rev. Mineral., 11, 261–301.

Wenk, H.R., Hu, M. and Frisia, S. (1993) Partially disordered dolomite: microstructural characterization of Abu Dhabi sabkha carbonates, Am. Mineral., 78, 769 - 774.

Wheeler, C.W., Aharon, P. and Ferrell, R.E. (1999) Successions of late Cenozoic platform dolomites distinguished by texture, geochemistry, and crystal chemistry: Niue, South Pacific. J. Sediment. Res., 69, 239–255.

Whitaker, F.F., Smart, P.L., Vahrenkamp, V.C., Nicholson, H. and Wogelius, R.A. (1994) Dolomitization by near-normal seawater? Field evidence from the Bahamas. In: Dolomites – A Volume in Honour of Dolomieu (Eds. B.H. Purser, M.E. Tucker and D.H. Zenger). Int. Assoc. Sed., Spec. Publ. No. 21, 111–132.

Wilson, J.L. (1975) Carbonate Facies in Geologic History. Springer (New York), 471 p.

Wright, V.P. and Burchette T.P. (1992) Carbonate Ramps, Geological Society Special Publication No. 149, 465 p.

Wright, D.T. and Wacey, D. (2005) Precipitation of dolomite using sulphate-reducing bacteria from the Coorong Region, South Australia: significance and implications. Sedimentology, 52, 987-1008.

Xia, C. (1995) Geochemistry and Petrogenesis of Mid-Ocean Ridge Basalts from $12^{o}$ to $16^{o}$, Mid-Atlantic Ridge. Unpublished PhD. dissertation, University of Houston, 325 p.

Yang, K. and Dorobek, S.L. (1995) The Permian Basin of West Texas and New Mexico: tectonic history of a "composite" foreland basin and its effects on stratigraphic development. In: Stratigraphic Evolution of Foreland Basins (Eds. S. L. Dorobek and G. M. Ross). Society for Sedimentary Geology, 52, 149-174.

Ye, Q.C. and Mazzullo, S.J. (1993) Dolomitization of Lower Permian platform facies, Wichita Formation, North Platform, Midland Basin. Carbonates and Evaporites, 8, 55–70.

Zachos, J. C., Pagani, M. and Sloan, L.C. (2001) Trends, rhythms, and aberrations in global climate 65 Ma to present. Science, 292, 686–693.

Zachos, J. C., Ro¨hl, U., Schellenberg, S. A., Sluijs, A., Hodell, D. A., Kelly, D. C., Thomas, E., Nicolo, M., Raffi, I., Lourens, L. J., McCarren, H. and Kroon, D. (2005) Rapid acidification of the ocean during the Paleocene-Eocene Thermal Maximum. Science, 308, 1611-1615.

Ziegler, M. A. (2001) Late Permian to Holocene paleofacies evolution of the Arabian Plate and its hydrocarbon occurrences. Geoarabia, 6, 445-504.

Ziveri, P., Stoll, H.M., Probert, I., Klaas, C., Geisen, M., Ganssen, G. and Young, J. (2003) Stable isotope 'vital effects' in coccolith calcite. Earth and Planetary Science Letters, 210, 137-149.

Internet references

Figure 1.
http://www.globalsecurity.org/military/world/iraq/maps-admin.htm

Figure 11.
http://www2.arnes.si/~sgszmera1/html/xrd/preparation2.html

# Appendix 1

# Appendix 1

Nahr Umr No.1 Well Microfacies Analyses

| Sample interval (ft) | | Sample interval (m) | | Microfacie | Diagenesis | Matrix, cement, and other minerals | Allochems | Porosity | Depositional Environment |
|---|---|---|---|---|---|---|---|---|---|
| Top | Bottom | Top | Bottom | | | | | | |
| Top of Dammam Formation | | | | | | | | | |
| 2445 | 2475 | 745.2 | 754.3 | Planar-s finely crystalline (20-50 μm) evaporitic dolomite | Micritization, high dissolution, dolomitization, quartz precipitation | Pore filling authigenic quartz crystals, and dolmite | Nummilites relics | High vugy and moldi porosities | Supratidal |
| 2485 | 2490 | 757.4 | 758.9 | Planar-s finely crystalline (20-50 μm) evaporitic dolomite | Micritization, high dissolution, dolomitization, quartz precipitation | Gypsum nodules, pore filling authigenic quartz crystals, and dolmite | Nummilites relics | High vugy and moldi porosities | Supratidal |
| 2490 | 2520 | 758.9 | 768.1 | Non-nplanar fine to medium crystalline (50-100 μm) evaporitic dolomite | Micritization, high dissolution, dolomitization, quartz precipitation | Gypsum and anhydrite nodules, pore filling authigenic quartz crystals, fine limpid dolomite with cloudy core in pores, and dolmite | Nummilites ultrastructure preserved by nonplanar dolomite with overgrowth | High vugy and moldi porosities | Supratidal |

| | | | | | | | | | |
|---|---|---|---|---|---|---|---|---|---|
| 2520 | 2565 | 768.1 | 781.8 | Dolomicrite | Dissolution and dolomitization | Dolomicrite. Some well developed dolomite rhombs float in the matrix, and dolomite crystals with cloudy cores in pores | N/A | Low vuggy porosity | Not identified |
| 2570 | 2645 | 783.3 | 806.2 | Evaporitic dolomicrite | Dissolution and dolomitization | Dolomicrite, and fine planar-s dolomite represent the matrix; gypsum nodules and anhydrite crystals; medium crystalline dolomite with cloudy core in some pores | N/A | Very low vuggy porosity | Supratidal |
| 2650 | 2695 | 807.7 | 821.4 | Planar-s finely crystalline (20-50 μm) dolomite | Micritization, dissolution, dolomitization, and quartz precipitation | Dolomite, micritized nummilite ultrastructure, and pore filling authigenic quartz crystals | Nummilites relics | Low vuggy and moldic porosity | Supratidal |

Nahr Umr No.1 Well Microfacies Analyses

| | | | | | | | | | |
|---|---|---|---|---|---|---|---|---|---|
| 2695 | 2725 | 821.4 | 830.5 | Non-planar finely crystalline (20-50 μm) dolomite | Micritization and dolomitization | Dolomite and micritized nummilite ultrastructure | Abundant nummilite relics | Medium moldic porosity | Intertidal |
| 2725 | 2755 | 830.5 | 839.7 | Non-planar fine to medium crystalline (50-75 μm) dolomite | Micritization and dolomitization | Dolomite, limpid dolomite with cloudy core within pore space,and micritized nummilite ultrastructure | Abundant nummilite relics | Very low moldic and vuggy porosity | Subtidal |
| 2750 | 2780 | 838.2 | 847.3 | Non-planar fine to medium crystalline (20-50 μm) evaporitic dolomite | Micritization, dissolution, dolomitization, quartz precipitation | Dolomite, micritized nummilite ultrastructure, pore filling authigenic quartz crystals within moldic pores, anhydrite nodules | Abundant nummilite relics | Very low moldic and vuggy porosity | Supratidal |

Nahr Umr No.1 Well Microfacies Analyses

| | | | | | | | | | |
|---|---|---|---|---|---|---|---|---|---|
| 2785 | 2855 | 848.8 | 870.2 | Non-planar very finely to finely crystalline (5-20 μm) dolomite | Minor dissolution and dolomitization | Dolomite and sparse gypsum in non-succcessive thin sections | N/A | Very low vuggy porosity | Not identified |
| 2865 | 2915 | 873.2 | 888.4 | Evaporitic dolomicrite | Dissolution and dolomitization | Dolomicrite. Some dolomite rhombs are scattered within the matrix, gypsum nodules and anhydrite crystals, and nummilite ultrastructure is micritized then dolomitized | A few nummilite relics | Very low moldic porosity | Supratidal |
| 2915 | 2985 | 888.4 | 909.8 | Non-planar very finely to finely crystalline (5-20 μm) dolomite | Dissolution, pore filling cement, and dolomitization | 5-20 anhedral dolomite crystals with sutured boundaries and a few well developed dolomite crystals with cloudy cores within the pores, pore-filling spar | 1-2 peloids or micritized form | No porosity | Intertidal |

Nahr Umr No.1 Well Microfacies Analyses

| | | | | | | | | | |
|---|---|---|---|---|---|---|---|---|---|
| 2985 | 3020 | 909.8 | 920.5 | Peloidal biodolomicrite | Minor dissolution, micritization of forams' outer shell, and or dolomitization | Dolomicrite | Micritized forams, and peloids | Low vuggy porosity | Subtidal |
| 3020 | 3080 | 920.5 | 938.7 | Non-planar very finely to finely crystalline (5-20 μm) dolomite | Dolomitization, quartz precipitation, and pore-filling spar | Pore filling authigenic quartz crystals and anhydrite nodules within very finely crystalline dolomite matrix, pore-filling spar | A few peloids | Very low vuggy porosity | Supratidal |
| 3080 | 3095 | 938.7 | 943.3 | Sparse peloidal dolomicrite | Minor dissolution, and dolomitization | Dolomicritic matrix with a few peloids floating in it | A few peloids | No porosity | Intertidal |
| 3110 | 3130 | 947.9 | 954.0 | Evaporitic dolomicrite | Dissolution and dolomitization | Dolomicrite and a few well developed dolomite crystals | N/A | No porosity | Not identified |

Nahr Umr No.1 Well Microfacies Analyses

| | | | | | | | | | |
|---|---|---|---|---|---|---|---|---|---|
| 3130 | 3160 | 954.0 | 963.1 | Non-planar very finely to finely crystalline (5-20 μm) dolomite | Dissolution, pore filling blocky cement, prismatic isopachous cement, and dolomitization | Micrite, altered micrite, blocky spar crystals (50-75 μm) in big vugs, isopacheous prismatic cement around a few peloids, and dolomite | A few micritized forams, and peloids | Low vuggy porosity | Intertidal |
| 3150 | 3200 | 960.1 | 975.3 | Peloidal biodolomicrite | Dissolution, micritization of forams' outer shell,dolomitization, and partial and complete pore filling cementation with blocky spar | Dolomicrite, and blocky spar crystals (50-75 μm) in big vugs, isopacheous prismatic cement around some peloids | Micritized forams, and peloids | Low vuggy porosity | Subtidal |
| 3200 | 3255 | 975.3 | 992.1 | Non-planar very finely to finely crystalline (5-20 μm) dolomite | Dissolution and partial or complete pore filling spar cement | Dolomnite and pore-filling spar | N/A | Low vuggy porosity | Not identified |

| | | | | | | | | | |
|---|---|---|---|---|---|---|---|---|---|
| 3225 | 3255 | 982.9 | 992.1 | Sparse fossiliferous dolosparite | Dissolution, micritization of forams' outer shell, dolomitization,and partial and complete pore filling cementation with equant spar | Microspar size dolomite and fine equant spar crystals linning moldic pores. | Micritized forams | Low moldic porosity | Intertidal |
| 3250 | 3260 | 990.6 | 993.6 | Evaporitic dolomicrite | Dissolution and Dolomitization | Anhydrite and dolomite partially and completely filling pores within a micrite matrix | N/A | Low vuggy porosity | Supratidal |
| 3260 | 3300 | 993.6 | 1005.8 | Non-planar medium crystalline (20-50 μm) dolomite | Dolomitization | Mainly nonplanar dolomite with some micrite pathes | Ghosts for micritized skkeletal grains | Very low porosity | Intertidal |

| | | | | | | | | | |
|---|---|---|---|---|---|---|---|---|---|
| 3300 | 3330 | 1005.8 | 1014.9 | Non-planar very finely to finely crystalline (5-20 μm) dolomite | Dissolution and dolomitization | 5-20 anhedral dolomite crystals with sutured boundaries and a few well developed dolomite crystals | Micritized forams,intraclast and/or peloids. | Very low porosity | Intertidal |
| 3330 | 3375 | 1014.9 | 1028.6 | Biodolomicrite | Dissolution, micritization,dolomitization, and partial pore filling cement | Dolomicrite and fine spar crystals linning moldic pores | Micritized forams | High moldic porosity | Subtidal |
| 3370 | 3385 | 1027.1 | 1031.7 | Non-planar very finely to finely crystalline (5-20 μm) bioclast rich dolomite | Dissolution, micritization, partial or complete pore filling dolomite crystals, dolomitization | non-planar dolomite crystals with sutured boundaries and a few well developed dolomite crystals with cloudy cores within the pores, pore-filling spar | Micritized forams (Miliolid) and green algae | Low moldic porosity | Subtidal |

Nahr Umr No.1 Well Microfacies Analyses

| | | | | | | | | | |
|---|---|---|---|---|---|---|---|---|---|
| 3385 | 3420 | 1031.7 | 1042.4 | Packed biomicrite | Dissolution, micritization, partial or complete pore filling cement, minor dolomitization | Well developed limpid dolomite rhombs in some pores,and equant pore filling spar crystals | Micritized forams (Miliolid), peloids, and green algae | Medium moldic porosity | Subtidal |
| 3415 | 3445 | 1040.8 | 1050.0 | Peloidal biodolomicrite | Dissolution, micritization, partial or complete pore filling cement, dolomitization | Well developed limpid dolomite rhombs in some pores,and equant pore filling spar crystals | Micritized forams, and peloids | Low moldic porosity | Intertidal |
| 3445 | 3460 | 1050.0 | 1054.6 | Non-planar very finely to finely crystalline (5-20 μm) evaporitic dolomite | Dissolution and Dolomitization | Anhydrite and dolomite partially and completely filling pores within very fine dolomite matrix | N/A | Low vuggy porosity | Supratidal |
| 3460 | 3465 | 1054.6 | 1056.1 | Evaporitic dolomicrite | Dolomitization | Gypsum nodules within micrite and altered micrite matrices | N/A | No porosity | Supratidal |

| | | | | | | | | | |
|---|---|---|---|---|---|---|---|---|---|
| 3510 | 3535 | 1069.8 | 1077.4 | Dolomicrite | Dolomitization and minor dissolution with the pores being filled by very finely crystalline spar | Dolomicrite and fine spar crystals filling pores | N/A | No porosity | Not identified |
| 3535 | 3545 | 1077.4 | 1080.5 | Biodolomicrite | Dissolution, partial or complete pore filling cement, and dolomitization | Dolomicrite and fine spar crystals completely or partially filling moldic pores | Relics of miliolid and other benthic forams | Medium moldic porosity | Subtidal |
| 3550 | 3580 | 1082.0 | 1091.1 | Non-planar very finely to finely crystalline (5-20 μm) evaporitic dolomite | Dissolution, micritization, partial or complete pore filling cement, dolomitization | Gypsum nodules, partial or complete pore filling cement, and dolomite | N/A | No porosity | Supratidal |

Nahr Umr No.1 Well Microfacies Analyses

| | | | | | | | | | |
|---|---|---|---|---|---|---|---|---|---|
| 3580 | 3595 | 1091.1 | 1095.7 | Sparse Peloidal dolosparite | Minor dissolution with the pores being filled by very finely crystalline spar, and dolomitization | Veryfinely crystalline spar with fine pore filling spar cement | Clotted grains look like glauconite or peloid | No porosity | Intertidal |
| Um Er Radhuma and Dammam formations contat | | | | | | | | | |
| 3595 | 3655 | 1095.7 | 1114.0 | Non-planar finely crystalline (20-50 μm) dolomite | Dissolution, partial or complete pore filling cement, and dolomitization | Dolomite, pore fiilng dolomite, and pore filling authigenic quartz crystals | Few peloids | No porosity | Intertidal |
| 3657 | 3665 | 1114.6 | 1117.0 | Planar-s finely crystalline (20-50 μm) dolomite | Dissolution, pore filling dolomite crystals, and dolomitization | Dolomite and pore filling dolomite that becomes coarser toward pore center | A few micritized forams, and peloids | | Intertidal |
| 3665 | 3705 | 1117.0 | 1129.2 | Planar-s finely crystalline (20-50 μm) dolomite | Dolomitization | Pore filling spar or dolomite cement in some vuggs, and well developed dolomite matrix | N/A | No porosity | Not identified |

Nahr Umr No.1 Well Microfacies Analyses

| | | | | | | | | | |
|---|---|---|---|---|---|---|---|---|---|
| 3700 | 3740 | 1127.7 | 1139.9 | Biodolosparite | Dissolution and pore filling spar cement | Very finely crystalline spar with medium crystalline pore filling spar cement | Relics of miliolid and other benthic forams | Medium moldic porosity | Subtidal |
| 3740 | 3765 | 1139.9 | 1147.5 | Dolomicrite | Dissolution and partial or complete pore filling spar cement | Dolomicrite and fine spar crystals filling pores | Relics of planktonic forams | Very low porosity | Not identified |
| 3760 | 3785 | 1146.0 | 1153.6 | Evaporitic dolomicrite | Dissolution, pore filling cement, and dolomitization | Dolomicrite and altered micrite, pore filling cement, and gypsum nodules | N/A | Very low vuggy porosity | Supratidal |
| 3785 | 3800 | 1153.6 | 1158.2 | Packed biodolomicrite | Dissolution, pore linning spar cement, and partial dolomitization | Dolomicrite with fine pore linning anhedral crystals | Relics of foram and/or gastropod | Medium moldic porosity | Subtidal |

| | | | | | | | | | |
|---|---|---|---|---|---|---|---|---|---|
| 3800 | 3810 | 1158.2 | 1161.2 | Biodolomicrite | Dissolution, pore linning spar cement, and dolomitization | Dolomicrite with fine pore linning anhedral crystals | Relics of foram and/or gastropod | Very low vuggy porosity | Subtidal |
| 3810 | 3830 | 1161.2 | 1167.3 | Sparse biomicrite | Dissolution, pore linning spar cement, and dolomitization | Dolomicrite with medium pore filling anhedral crystals | A few relics of rounded grains | Very low vuggy porosity | Intertidal |
| 3830 | 3870 | 1167.3 | 1179.5 | Biodolosparite | Dissolution, pore filling spar cement, and dolomitization | Very finely crystalline spar with medium crystalline pore filling spar cement | Relics of foram and/or gastropod | Very low vuggy porosity | Subtidal |
| 3870 | 3890 | 1179.5 | 1185.6 | Non-planar very finely to finely crystalline (5-20 μm) evaporitic dolomite | Dissolution, micritization, partial or complete pore filling cement, dolomitization | Mainly fine dolomite with dolomicrite patches | N/A | No porosity | Not identified |

Nahr Umr No.1 Well Microfacies Analyses

| | | | | | | | | | |
|---|---|---|---|---|---|---|---|---|---|
| 3890 | 3905 | 1185.6 | 1190.2 | Dolomicrite | Minor dissolution with the pores being filled by very finely crystalline spar cement, and dolomitization | Mainly fine dolomite with dolomicrite patches | N/A | No porosity | Not identified |
| 3905 | 3930 | 1190.2 | 1197.8 | Sparse biodolomicrite | Dissolution, pore filling spar cement, and dolomitization | Dolomicrite with fine to medium pore filling spar crystals | Relics of foram and/or gastropod | Medium moldic porosity | Subtidal |
| 3930 | 3955 | 1197.8 | 1205.4 | Evaporitic dolomicrite | Dissolution and dolomitization | Gypsum nodules within dolomicrite matrix,and as vein and vug filling cement | N/A | No porosity | Supratidal |
| 3960 | 3980 | 1206.9 | 1213.0 | Biodolomicrite | Dissolution, pore linning spar cement, and, dolomitization | Dolomicrite with fine to medium pore filling spar crystals | Relics of rounded grains | Medium moldic porosity | Subtidal |

Nahr Umr No.1 Well Microfacies Analyses

| | | | | | | | | | |
|---|---|---|---|---|---|---|---|---|---|
| 3980 | 4020 | 1213.0 | 1225.2 | Sparse biodolosparite | Dissolution, pore linning spar cement, and dolomitization | Very finely crystalline spar and fine to medium pore filling spar crystals | A few relics of rounded organisms | Low to medium moldic porosity | Intertidal |
| 4020 | 4085 | 1225.2 | 1245.0 | Non-planar finely crystalline (20-50 μm) dolomite | Mainly dolomitization although there are some dissolution vugs | 20-50 μm long subhedral dolomite crystal | N/A | Very low vuggy porosity | Not identified |
| 4085 | 4110 | 1245.0 | 1252.7 | Non-planar very finely to finely crystalline (5-20 μm) dolomite | Dissolution, pore filling cement, and dolomitization | 5-20 μm long subhedral crystals with sutured crystal boundaries and biger size pore filling crystals | N/A | No porosity | Not identified |
| 4110 | 4125 | 1252.7 | 1257.2 | Evaporitic dolomicrite | Dissolution and dolomitization | Gypsum nodules within dolomicrite matrix, and as vein and vug filling cement | N/A | No porosity | Supratidal |

Nahr Umr No.1 Well Microfacies Analyses

| | | | | | | | | | |
|---|---|---|---|---|---|---|---|---|---|
| 4125 | 4140 | 1257.2 | 1261.8 | Sparse peloidal dolosparite | Dissolution, pore filling cement, and dolomitization | Very finely crystalline spar with medium crystalline pore filling spar cement | Peloids | No porosity | Intertidal |
| 4140 | 4200 | 1261.8 | 1280.1 | Dolomicrite | Dissolution, pore filling cement, and dolomitization | Dolomicrite with medium pore filling anhedral crystals | A few peloids | No porosity | Intertidal |
| 4205 | 4260 | 1281.6 | 1298.4 | Non-planar very finely to finely crystalline (5-20 μm) peloidal dolomite | Dissolution, pore filling cement, and dolomitization | Spar crystals within pores and some well developed dolomite rhombs embedded in the matrix | A few peloids | No porosity | Intertidal |
| 4250 | 4280 | 1295.3 | 1304.5 | Peloidal biodolomicrite | Dissolution, micritization of foram shells, dolomitization, and pore filling spar | Dolomicrite and pore filling anhedral crystals | Peloids and forams | Very low vuggy porosity | Subtidal |

| | | | | | | | | | |
|---|---|---|---|---|---|---|---|---|---|
| 4280 | 4320 | 1304.5 | 1316.7 | Non-planar finely crystalline (20-50 μm) evaporitic dolomite | Dissolution and dolomitization | Dolomite, gypsum nodules ,and gypsum as vein and vug filling cement | N/A | No porosity | Supratidal |
| 4320 | 4370 | 1316.7 | 1331.9 | Peloidal biodolomicrite | Dissolution, micritization of foram shells, dolomitization, and pore filling spar | Micrite, pore filling spar crystals, and a few rhombic dolomite | Peloids and forams | Very low vuggy porosity | Subtidal |
| 4390 | 4520 | 1338.0 | 1377.6 | Evaporitic dolomicrite | Dissolution, pore filling cement, and dolomitization | Gypsum and ahydrite within dolomicrite matrix | N/A | Very low vuggy porosity | Supratidal |
| 4510 | 4560 | 1374.6 | 1389.8 | Sparse peloidal dolosparite | Dissolution, pore filling cement, and dolomitization | Very finely crystalline spar and well-developed dolomite rhombs clusturing in some part | Few peloids | Very low vuggy porosity | Intertidal |

| | | | | | | | | | |
|---|---|---|---|---|---|---|---|---|---|
| 4560 | 4640 | 1389.8 | 1414.2 | Evaporitic dolomicrite | Dolomitization | Gypsum nodules within dolomicrite matrix | N/A | No porosity | Supratidal |
| 4640 | 4670 | 1414.2 | 1423.3 | Non-planar very finely to finely crystalline (5-20 μm) dolomite | Dolomitization | 5-20 μm nonplanar dolomite crystals with sutured crystal boundaries | N/A | No porosity | Not identified |
| 4674 | 4700 | 1424.6 | 1432.5 | Dolomicrite | Dolomitization | Dolomicrite | N/A | No porosity | Not identified |
| 4705 | 4720 | 1434.0 | 1438.6 | Dolomicrite | Dissolution, dolomitization, and pore filling spar cement | Dolomicrite and fine spar crystals filling pores | N/A | Very low vuggy porosity | Not identified |
| 4710 | 4750 | 1435.5 | 1447.7 | Planar-s finely crystalline (20-50 μm) dolomite | Dissolution, pore filling crystals, and dolomitization | Dolomite and pore-filling and-lining cement | A few peloids | Very low vuggy porosity | Intertidal |

Zubair No.1 Well Microfacies Analysis

| Sample interval (ft) | | Sample interval (m) | | Microfacie | Diagenesis | Matrix, cement, and other minerals | Allochems | Porosity | Depositional Environment |
|---|---|---|---|---|---|---|---|---|---|
| Top | Bottom | Top | Bottom | | | | | | |
| Top of Dammam Formation | | | | | | | | | |
| 2000 | 2120 | 609.6 | 646.1 | Sparse biodolomicrite | Dissolution, dolomitization, and pore linning spar cement | Dolomicrite and fine pore linning spar cenment | A few relics of forams | Medium porosity | Intertidal |
| 2120 | 2180 | 646.1 | 664.4 | Non-planar finely crystalline (5-20 µm long)evaporitic dolomite | Dissolution and dolomitization | Dolomite | Relics of forams | low porosity | Shallow lagoons |
| 2180 | 2240 | 664.4 | 682.7 | Biodolomicrite | Dissolution, dolomitization, and pore linning spar cement | Dolomicrite and fine pore linning spar cenment | Relics of forams | Medium porosity | Shallow lagoons |
| 2240 | 2370 | 682.7 | 722.3 | Planar-s finely to medium crystalline (50-75 µm long) dolomite | Dolomitization | Dolomite | N/A | No porosity | Not identified |
| Missing interval | | | | | | | | | |

Zubair No.1 Well Microfacies Analysis

| | | | | | | | | | |
|---|---|---|---|---|---|---|---|---|---|
| 2430 | 2440 | 740.6 | 743.7 | Planar-s finely to medium crystalline (50-75 µm long) dolomite | Dolomitization | Dolomite | N/A | No porosity | Not identified |
| Missing interval | | | | | | | | | |
| Contact between Dammam and Rus formations is at 824 m (2638 ft) | | | | | | | | | |
| 2917 | 2995 | 889.1 | 912.8 | Peloidal biodolomicrite | Dolomitization and minor dissolution | Dolomicrite | Peloids and micritized benthic forams | No porosity | Intertidal |
| 3000 | 3090 | 914.4 | 941.8 | Packed biodolomicrite | Dissolution | Dolomicrite | Micritized miliolid and other benthic forams | No porosity | Subtidal |
| The contact between Rus and Um Er Radhuma formations | | | | | | | | | |
| 3050 | 3145 | 929.6 | 958.5 | Evaporitic dolomicrite | Dissolution and dolomitization | Dolomicrite and gypsum nodules and anhydrite crystals | A few foram relics | Low porosity | Supratidal |

Zubair No.1 Well Microfacies Analysis

| | | | | | | | | | |
|---|---|---|---|---|---|---|---|---|---|
| 3100 | 3200 | 944.8 | 975.3 | Planar-s finely crystalline(5-20 μm long) evaporitic dolomite | Dissolution and dolomitization | Dolomite and anhydrite nodules and crystals | Few micritized formas, and peloids | Low porosity | Supratidal |
| 3200 | 3250 | 975.3 | 990.6 | Dolomicrite | Dissolution, dolomitization, and cementation | Dolomicrite and very finely crystalline pore filling cement | N/A | No porosity | Not identified |
| 3250 | 3400 | 990.6 | 1036.3 | Non-planar finely crystalline(5-20 μm long) evaporitic dolomite | Dissolution, quartz precipitation, and dolomitization | Micrite, microspar, and gypsum nodules, anhydrite crystals, and authigenic quartz | N/A | Low porosity | Supratidal |
| 3400 | 3650 | 1036.3 | 1112.5 | Evaporitic dolomicrite | Dissolution and dolomitization | Dolomicrite and gypsum nodules and anhydrite crystals | A few foram relics | Low porosity | Supratidal |

| | | | | | | | | | |
|---|---|---|---|---|---|---|---|---|---|
| 3650 | 3820 | 1112.5 | 1164.3 | Non-planar finely crystalline(5-20 µm long) evaporitic dolomite | Dissolution and dolomitization | Micrite, altered micrite, few dolomite rhombs, and gypsum and anhydrite nodules and anhydrite crystals | N/A | Low porosity | Supratidal |
| 3830 | 3900 | 1167.3 | 1188.7 | Planar-s finely crystalline(20-50 µm long) evaporitic dolomite | Dissolution and dolomitization | Dolomite and anhydrite nodules and crystals | A few micritized formas | Low porosity | Supratidal |
| 3900 | 3950 | 1188.7 | 1203.9 | Non-planar finely crystalline(20-50 µm long) evaporitic dolomite | Dissolution, silica precipitation, and dolomitization | Dolomite,authigenic quartz, anhydrite crystals | N/A | Low porosity | Supratidal |
| 3950 | 3970 | 1203.9 | 1210.0 | Sparse biodolosparite | Dissolution, pore filling spar cement, and dolomitization | Very finely crystalline spar with fine to medium pore filling anhedral crystals | Relics of foram and/or gastropod | Medium moldic porosity | Intertidal |

Zubair No.1 Well Microfacies Analysis

| | | | | | | | | | |
|---|---|---|---|---|---|---|---|---|---|
| 3970 | 4020 | 1210.0 | 1225.2 | Dolomicrite | Dissolution, pore filling spar cement, and dolomitization | Dolomicrite and fine subhedral spar crystals linning pores | A few foram relics | Low moldic porosity | Not identified |
| 4020 | 4060 | 1225.2 | 1237.4 | Evaporitic dolomicrite | Dissolution and dolomitization | Dolomicrite and gypsum nodules and anhydrite crystals | N/A | Low porosity | Supratidal |
| 4060 | 4070 | 1237.4 | 1240.5 | Biodolomicrite | Dissolution, complete and partial pore filling cement, and dolomitization | Dolomicrite and fine pore linning spar cenment | Relics of miliolid and other benthic forams | Medium moldic porosity | Subtidal |
| 4080 | 4090 | 1243.5 | 1246.6 | Sparse biodolosparite | Dissolution, pore filling spar cement, and dolomitization | Very finely crystalline spar with fine to medium pore filling anhedral crystals | Relics of foram and/or gastropod | Medium moldic porosity | Intertidal |
| Missing interval | | | | | | | | | |
| 4190 | 4200 | 1277.0 | 1280.1 | Biodolomicrite | Dissolution, complete and partial pore filling cement | Dolomicrite | Relics of miliolid and other benthic forams | Medium moldic porosity | Subtidal |

| | | | | | | | | | |
|---|---|---|---|---|---|---|---|---|---|
| 4200 | 4220 | 1280.1 | 1286.2 | Evaporitic dolomicrite | Dissolution and dolomitization | Dolomicrite, gypsum nodules, and anhydrite crystals | N/A | Low porosity | Supratidal |
| 4223 | 4235 | 1287.1 | 1290.8 | Dolomicrite | Dissolution, partial or complete pore filling spar cement, and dolomitization | 5-10 μm subhedral spar crystals with sutured crystal boundaries and biger size pore filling spar crystals | A few foram relics | Low moldic porosity | Subtidal |
| 4235 | 4250 | 1290.8 | 1295.3 | Evaporitic dolomicrite | Dissolution and dolomitization | Dolomicrite, gypsum nodules, and anhydrite crystals | N/A | Low porosity | Supratidal |
| 4260 | 4328 | 1298.4 | 1319.1 | Biodolomicrite | Dissolution, dolomitization, and complete and partial pore filling cement | Dolomicrite | Relics of miliolid and other benthic forams | Medium moldic porosity | Lagoon |
| 4328 | 4336 | 1319.1 | 1321.5 | Evaporitic dolomicrite | Dissolution, quartz precipitation, and dolomitization | Dolomicrite, gypsum nodules, anhydrite crystals, and authigenic quartz | N/A | Low porosity | Supratidal |

| | | | | | | | | | |
|---|---|---|---|---|---|---|---|---|---|
| 4336 | 4365 | 1321.5 | 1330.4 | Sparse biodolosparite | Dissolution, pore filling spar crystals, and dolomitization | Very finely crystalline spar with fine to medium pore filling anhedral crystals | Relics of foram and/or gastropod | Medium moldic porosity | Intertidal |
| 4375 | 4461 | 1333.4 | 1359.6 | Non-planar finely crystalline(20-50 μm long) evaporitic dolomite | Dissolution and dolomitization | Nonplanar dolomite, micrite patches, and anhydrite | N/A | No porosity | Supratidal |
| Bottom of Um Er Radhuma Formation at 1391 m | | | | | | | | | |